Stony Brook University

Polymer Layered Silicate Nanocomposites:
Structure, Morphology, and Properties

A Dissertation Presented

by

Pranav Nawani

to

The Graduate School

in Partial Fulfillment of the

Requirements

for the Degree of

Doctor of Philosophy

in

Chemistry

Stony Brook University

May 2008

Stony Brook University

The Graduate School

Pranav Nawani

We, the dissertation Committee for the above candidate for the Doctor of Philosophy degree, hereby recommend acceptance of this dissertation.

Benjamin S Hsiao, Dissertation Advisor
Professor, Department of Chemistry

Benjamin Chu, Chairperson of Defense
Distinguished Professor, Department of Chemistry

Dilip Gersappe, Third Member
Professor, Department of Material Science and Engineering

Dr. Andy H Tsou, External Member
Exxon Mobil Chemical Company

The dissertation is accepted by the Graduate School.

Lawrence Martin
Dean of the Graduate School

Abstract of the Dissertation

Polymer Layered Silicate Nanocomposites: Structure, Morphology, and Properties

by

Pranav Nawani

Doctor of Philosophy

in

Chemistry

Stony Brook University

2008

Layered silicates are important fillers for improving various mechanical, flame retardant, and barrier properties of polymers, which can be attributed to their sheet-like morphology. Layered silicates can be modified with organic surfactants to render them compatible with polymer matrices. Organically modified silicates (organoclays) having large surface areas are very cost-efficient non-toxic nanofillers effective at very low loads and are readily available. Upon amalgamation of organoclays with polymer matrix nanocomposites, polymer chains can penetrate in between the silicate layers and result in an intercalated structure where the clay stack remains intact but the interlayer spacing is increased. When penetration becomes more severe, disintegration of clay stacks can occur, resulting in an exfoliated structure. It has often been observed that exfoliation is not complete down to the level of isolated silicate layers; rather, the large clay stacks are broken up into shorter stacks termed 'tactoids' together with a few individual silicate layers, resulting in a kind of mixed intercalated-exfoliated

structure. Organoclay particles are mostly intercalated, having a preferred orientation with the clay gallery planes being preferentially parallel to the plane of the pressed film. Preferential orientation of organoclays affects the barrier properties of polymer membranes. Additional fillers like carbon black can induce a change in the orientation of organoclays. The effect of carbon black on the orientation of organoclays was elucidated and a relationship between orientation and permeability of air through such membranes was established.

We have also investigated the flammability properties of a series of polymer nanocomposites, containing various Transition Metal Ion (TMI) modified organoclays. The improved fire retardation in nanocomposites with TMI-modified organoclays can be attributed to enhanced carbonaceous char formation during combustion, i.e., charring promoted by the presence of catalytically active TMI. Polymer nanocomposite materials depend not only on the properties of individual components but also on their morphology and interfacial interactions. In polymer nanocomposites, the interfacial interactions are maximized due to the large surface area of the filler particles exposed to the polymer matrix, resulting in unique anisotropic properties. Thus, it will be of great importance to achieve exfoliation of the lamellar stacks prior to mixing with the polymer matrix, in the dry powder state or in a solution state. In layered silicates the lamellar stacks are held by electrostatic interactions between the basal charges and ions present within the basal spacing. Lamellar stacks of layered silicates can be exfoliated if the amount of energy gained by them is higher than the electrostatic energy required to hold the lamellar stacks together. Using 'Microwave radiation', exfoliation of organoclays was achieved. Various characterization techniques were used to evaluate structure, morphology and properties of fillers and polymer nanocomposites.

Table of Contents

List of Figures

Acknowledgments

First of all, I would like to thank my advisor, Professor Benjamin S. Hsiao, for providing me the opportunity to work on very interesting projects, and in a stimulating environment at the Polymer Science Lab in the Chemistry department. With his unrelenting ways of tackling problems, he has spurred me to scale new challenges in each and every project. A high standard he sets through example has always inspired me. He has been a source of ideas throughout my reseach, and discussions with him always leave me with new directions to ponder. I am indebted to him for supporting me through the course of my doctoral studies at Stony Brook. My dissertation committee includes, Distinguished Professor Benjamin Chu (Chemistry Department) and Professor Dilip Gersappe (Material Science Department) at Stony Brook University, and Dr. Andy H. Tsou from Exxon Mobil, New Jersey. Through my Ph.D. program I am thankful to Dr. Tsou who has helped me with useful insights starting from the beginning years of my PhD. Professor Dilip Gersappe has been extremely co-operative to being my third member on the committee. I would like to specially thank my collaborators at NIST, Dr. J.W Gilman, and Drs. Andy Tsou and Weiqing Weng, at Exxon through my Ph.D. research. I would like to specially thank Drs. Mikhail Gelfer, Lixia Rong, Igors Sics, Christian Burger, and Professor C. Krishnan, who have been of great help during my Ph.D. years. I would also like to thank Hongwen Zhou for his discussions and all other lab members for their cooperation. Special thanks to Jane Wainio, Diane Godden, Katherine M. Hughes from the Chemistry Department staff. There are several other people in Stony Brook and outside whose support and presence was invaluable to me during the course of my Ph.D., which includes Ajay Gupta, Pradipta De, Diptikalyan Saha, Rahul Agarwal, Gajendra Pandey, Sunita

Mukhi, Hyunsoo Park, Prashant Jha, Samrat Chawda, Puneet Kohli, Navdeepak Singh, Abhishek Datta, Lucienne Buannic, Gina Sporleder, David Sporleder, Meng Jiang, Jennifer Szlosek, Supradeep Narayanan. A special note of thanks to Amber Carr and Kellie Morgan for proof reading my thesis report and Anand Kashyap for heping me with latex. A note of thanks to my friends across the world: Sangeeta Parashar, Monish Singhal, Sandeep Modi, Abu Bucker, Arif Khurshed, Anil Sharma, Deepak Sharma, Sanjay Sharma, Prashant Agarwal, Helena Oneill, Rubeena Agarwal, Desiree Schliwa, Rossana Iervolino, Naoko Yamakawa, Abhijeet Sengupta, Ranjeev Sinha, Prasanna Apranji, Tripti Jakhmola, who kept me motivated throught my Ph.D research. A special note of thanks to my brother Pratyush Nawani and sister in law Swati Nawani, my sister, Jyoti Pokhriyal, and brother-in-law Sandeep Pokhriyal who are the most important people and they stood by me when it was most needed. Finally, I owe a great deal of this achievement to my parents who have been a never-ending source of support for me. They have been there for me in all the troubled times with their encouragement and advice.

Chapter 1

Introduction

1.1 General

Hybrid materials containing organic and inorganic components blended together, either occurring naturally or prepared synthetically, have gained much interest in industry and research communities [1-7]. Polymers are commonly used materials and over periods of time their applications have increased in our lives. Therefore, it is imperative to develop new polymeric materials with improved properties to address the growing number of applications. The maximum benefits of nanoscience can be harnessed by developing materials providing multiple advantageous properties, and designing such materials by incorporating various properties is therefore vital. Polymer nanocomposite materials are a particular kind of synthetic hybrid material, which shows multiple unique properties [5, 8-18]. To enhance the properties of a polymer, fillers are often added to obtain a homogeneous mixture called a composite. If one of the dimensions of the filler particles is in the nanometer range then these composite materials are termed as polymer nanocomposites. The transition of length scale from micrometer to nanometer yields dramatic changes in physical properties as nanoscale particles have a large surface area for a given volume. Usually fillers used are inorganic in nature, and act as reinforcing material. The role of the matrix is to adhere and to bind fillers. The resulting material will have properties which will be a combination of the individual properties of polymer and filler particles. The properties of polymer nanocomposites depend not only on the properties of individual components but also on their morphology and interfacial interactions

[6, 19]. The effective properties of polymer nanocomposites are dependent on various filler properties, such as their size, area, aggregate structure, surface chemistry, and interactions with the polymer matrix, all of which will affect the dispersion of inorganic fillers in the polymer matrix [20, 21]. Due to its extreme utility and importance both in research and industry, it becomes imperative to understand the relationship between the microstructure and the macroscopic properties that are of interest. To achieve maximum property enhancement a homogeneous dispersion of nanoscale fillers is highly desired [21]. As a result there is a need to understand the design of nanometer scale architecture and factors affecting such structures and how they can affect the final properties of materials. Often these improvements in properties may occur at the expense of other useful polymeric properties, such as toughness and crack resistance, or may render high toxicity [22-24]. Consequently it is highly desirable to be able to use fillers which can improve properties and reduce toxicity, but not at the cost of polymeric properties. Common nanoscale particles with various geometries (spherical, fiber and sheet) are shown in Figure 1.1 and their respective surface area-to-volume ratios are given [25, 26].

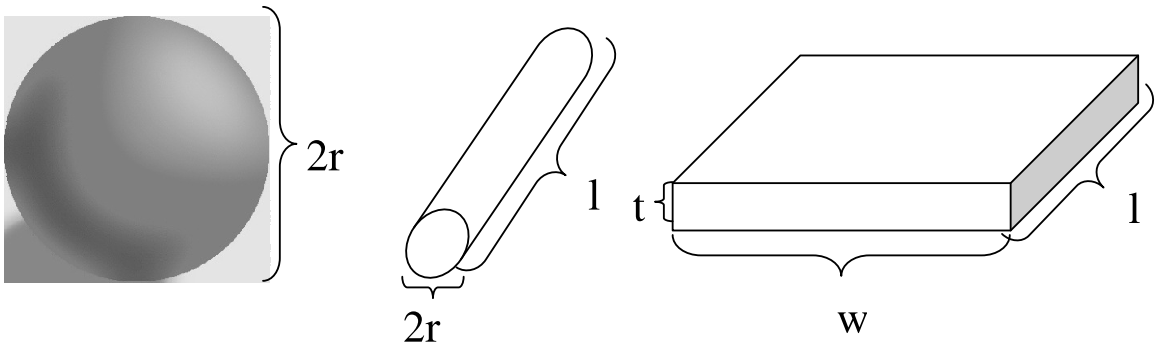

Figure 1.1: Commonly used nanoscale particles with various geometries (spherical, fiber and sheet). Surface area to volume ratios: Sphere: 3/r, where r is radius of sphere. Fiber: 2/r + 2/l, where r is radius of cylinder and l is length. Sheet: 2/t + 2/l +2/w, where t is thickness, w is width and l is length of the sheet .

It can be said that the smaller the diameter, the greater the surface area per unit volume [27]. A change in particle diameter, layer thickness, or fibrous material

diameter from the micrometer to the nanometer range will affect the surface area-to-volume ratio thereby affecting surface interactions and thus final properties [25].

1.2 Layered Silicates

Sheet-like materials are often preferred for enhancement of polymeric properties including barrier, mechanical and flame retardation. Clay minerals are made up of sheets of silicate layers which are approximately 1 nm thick and several hundred nanometers in the lateral direction [28]. Clay is made of several sheets of silicates stacked together as shown in Figure 1.2. Clay minerals offer high effective surface

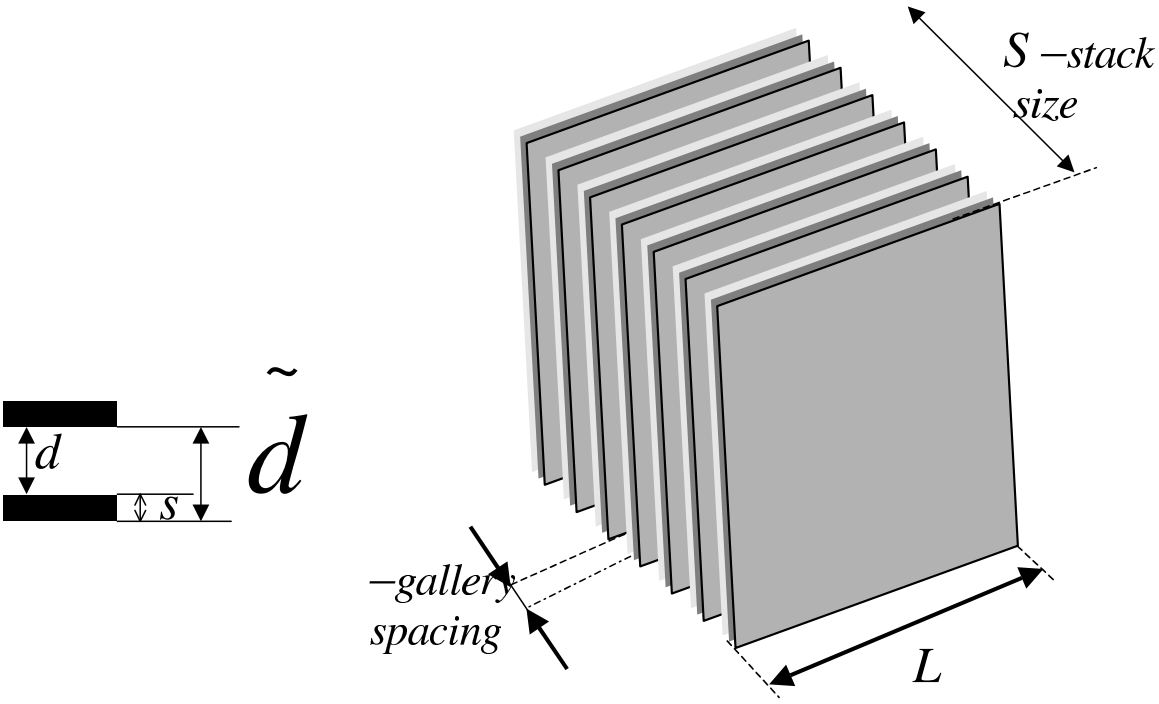

Figure 1.2: The sheet-like morphology of clay stacks as shown is particularly efficient.

area and have desired surface properties, because these advantageous and intrinsic surface characteristics can be used successfully to improve upon properties of existing polymers, they are the most commonly used sheet-like fillers [29]. In polymer clay nanocomposites, the interfacial interactions are maximized due to the large surface

area of the filler particles exposed to the polymer matrix, which results in unique anisotropic properties. Smectites are the most commonly used fillers among layered silicates and over the years they have shown a wide range of applications in modified electrode [30-33], catalysis [34-35], and polymer nanocomposites [1-20, 36, 37]. Smectites classified as phyllosillicate minerals have a layered structure made up of two dimensional sheets with the details of the structure of clays being discussed in Chapter 2. Clays are hydrophilic in nature and to make clays compatible with a polymeric matrix, the surface characteristics need to be changed to hydrophobic. To do this, inter-layer ions are exchanged with organic surfactants and such clays are often termed organoclays. The intercalated organoclays formed by electrostatic interactions between layered silicates and surfactants have long been an active research subject in the mineralogy community [38-44].

In recent years, interest in organoclays has also expanded into the polymer community. A broad variety of organoclays has been synthesized and characterized with the intent to prepare new kinds of polymer composites. [28, 29 45, 46] The complex structure of organoclays can be partially attributed to the pronounced structural and energetic heterogeneity in mineral clays [47]. On the basis of calorimetric data and adsorption measurements, it has been shown that clay minerals always contain several types of adsorption sites with different interaction energies [47, 48]. The energies associated with the basal and lateral surfaces in clay layers can differ greatly from each other and therefore result in different adsorption properties. The surface energy alone on the basal space may also vary at different locations. As a result, when mineral clay is intercalated by small molecules such as water, the distribution of layer thickness can be quite non-uniform [47-49]. If the long-chain cationic surfactants are used to complex with the clay surface, the non-uniformity in the distribution of layer thickness may be even more severe.

The cationic surfactants can be adsorbed on the clay surface by two mechanisms: (1) cation exchange and (2) hydrophobic bonding [38, 47, and 50]. As a result, the amount of adsorbed surfactant may significantly exceed the ion exchange capacity [51-53]. The excessive surfactant may be located either in the vicinity of the clay surface or between the adsorbed organic layers. Conformation of the hydrocarbon chains in the surfactant depends on the grafting density, the type of ion exchange process, and the thermal history utilized during the preparation of organoclays. [38, 39, 41] FTIR and solid-state NMR measurements have confirmed that varying chain conformations with different trans-gauche ratios can coexist in the intercalated clay complexes [45,54-56]. As the surfactant content approaches the overall ion exchange capacity of the clay, the hydrocarbon tails belonging to surfactant molecules adsorbed at opposing sides of the silicate gallery can interpenetrate [38, 39]. The extent of the penetration will affect the thickness of the organic layers. As a result, a few types of distinct layers with different thicknesses may coexist in organoclays [50, 57-58], which is characteristic for the so-called interstratified systems [49, 59-60]. In this work, we have paid special attention to organoclays having relatively high content of a long-chain surfactant (C16-C18), as these systems are often used for the preparation of polymer-clay nanocomposites by the melt-blending process. It has been shown that the surfactant component can promote the exfoliation of layered silicates in the polymer matrix and create a 'nanocomposite', which can result in superior thermal stability, barrier, and mechanical properties when compared to the unfilled polymer matrix [61-64]. However, the extent of clay exfoliation often depends on the dispersion method used. The method of melt mixing is the most practical way to compound polymer nanocomposites, however organoclay dispersion may be limited because phase segregation can occur. Phase segregation is caused by thermal degradation and desorption of an organic component in organoclay [60]. Melt mixing is performed at an elevated temperatures (above 150°C), where thermally induced structural changes frequently occur

in organoclays. Understanding thermally induced structural changes in the organoclay can thus enable us to improve the control of clay dispersion in the polymer matrix via melt mixing. Therefore it is of interest to study the structural changes induced in organoclays at elevated temperatures. Systematic investigations of the thermal behavior and temperature dependence of structural changes organoclays is reported in this work. In previous research on the temperature dependence of the morphology of organoclays [41, 65] it was found that the complexes are formed by, montmorillonite-like, bedellite and nontronite clays with n-tetra-decyl-ammonium ions containing 8 to 22 CH_2 groups. Based on the X-ray diffraction (XRD) analysis data, it was concluded that organoclays could undergo a phase transition at higher temperatures, which resulted in a decrease in the inter-layer spacing (*d*-spacing). It was suggested that the observed changes in the *d*-spacing of organoclays during the phase transition could be attributed to the formation of well-ordered gauche block structures rather than the simple melting-like order-disorder transition. Another research group [66] attributed the decrease in *d*-spacing in the alkanol/calcium montmorillonite complex to a melting-like order-disorder phase transition. Yui et. al. and Okahata et. al. [53, 67] suggested a different argument of such change in *d*-spacing, as according to them the thermally induced transitions observed in layered silicate-surfactant complexes below 100°C might be due to the changes from highly ordered pseudo-crystalline structure of adsorbed surfactant bi-layers to less ordered liquid crystal-like conformation. Previous high-temperature behavior of organoclays was investigated via FTIR [28, 29, 68, and 70] and the results indicated that a higher gauche content in the hydrocarbon tails of dimethyl di-hydro tallow ammonium chloride present in thermally treated organoclay (Cloisite 20A) might be attributed to the surfactant loss at elevated temperatures [68]. The onset of degradation might occur at a temperature as low as 130-150°C. However, the maximum weight loss corresponding to the decomposition of surfactant usually occurred above 250°C. Combined TGA/mass spectrometry results suggested that the

thermal degradation of "excessive" surfactant molecules residing between the surfactant layers adsorbed on the mineral surfaces might occur at the same or even higher temperatures than that of bound surfactant [29, 68]. This is because the degradation of bound surfactant can be facilitated by the proximity to the catalytically active aluminosilicate sites. As organoclays are layered silicates intercalated with organic surfactants, the silicate layers can be considered rigid and inert in the temperature range of the experiment. Therefore, we can assume that all observable structures have the form of lamellar stacks; as a result, the SAXS treatment can be reduced to the consideration of 1D projection of the lamellar system onto its lamella normal (in the limit of sufficiently large lateral layer extensions). Furthermore, the silicate layers can be considered perfectly monodisperse (with a thickness about 1 nm) so that all thickness variations of the lamellar system are generated by the organic layers.

1.3 Nanocomposites

In the past decade, usage of layered materials for enhancing the properties of polymeric material have been of great interest due to the fact that the property enhancement is achieved at low load levels of fillers often less than 5 weight % [3, 69-71] as compared to 30-50 wt% for conventional fillers. They also show a great improvement in properties over composites formed using many other conventional filler particles, which is possibly due to their sheet like layered structure. Even though polymer clay composites are reported in the literature as early as the 1950s [36, 72], extensive study of polymer clay nanocomposites, based on various clays and polymer matrices, was performed only after polymer clay nanocomposites were developed by Toyota [9, 69, 73-79]. The Toyota polymer clay nanocomposite contained nylon and montmorillonite clays [69]. Polymer nanocomposites incorporating organoclay can be obtained by various methods like *in-situ* polymerization, [80-82] melt compounding, [78] solution mixing, [83] and emulsion processing [84] discussed in more details in Chapter

2. The hydrophobic groups present between the layers of organoclays render them compatible with polymers and hence are responsible for their miscibility with the polymer matrix. Polymers are able to penetrate the inter-layer spaces of the organoclays and the mixing of organoclays with polymer may result in different morphologies, depending upon various factors related to the structure, interaction and processing. When polymer chains penetrate the inter-layer spaces with the organoclay stack intact, while it exhibits an increase in inter-layer or *d*-spacing, the resultant morphology is termed as "intercalated" structure.

The other possibility is that upon introduction of the polymer chain, the electrostatic barrier holding the clay layers together may be overcome and the clay stack separates into individual layers in a process called "exfoliation". The uniqueness of the properties in polymer nanocomposites arises due to the length scale of component phases [4,-6, 19, 85]. Layered organoclay can be broken down into their nano-scale building blocks, that is individual platelets, which is known as exfoliated organoclay, these will be good alternatives for preparation of polymer nanocomposites. Exfoliation of clay has been reported to have been achieved while polymer nanocomposites are formed [1, 3, 4, 9, 66, 86-87]. Exfoliated clay layers have a high aspect ratio (in the range of 50 to 2000), hence possessing better reinforcement properties compared to other inorganic fillers. In exfoliated-intercalated polymer-organoclay nanocomposites great property enhancement is achieved due to the high aspect ratio of clay fillers as well as the huge specific surface area of clays (600-800 m^2/g) which allow for an efficient filler-matrix contact. While intercalated nanocomposites show improvement in the properties, a higher degree of improvement is expected if the clay is exfoliated in the polymer matrix. Therefore exfoliated morphology is the most desired. The property enhancement of these nanocomposites will mostly depend on the state of nanofiller dispersion and this has long been an essential issue, affecting many physical properties. The process of clay dispersion often results in the disintegration of large

silicate stacks into short stacks known as primary "tactoid" [88-90]. Alternatively a few layers may disintegrate from the stack or leave behind a single independent layer [66, 86-87], thus increasing the effective specific surface area. In such cases, a partially exfoliated morphology is observed and enhancement in properties is achieved by a better interaction of the polymer matrix with the rigid fillers. Such nanostructures show notable enhancement of properties in bulk counterpart/matrix such as modulus, toughness, flame retardation and barrier properties can be simultaneously achieved in the final products [2, 8-18, 66, 86-89]. Even without complete exfoliation and in their tactoid state, these organosilicates are still unique fillers that have a sub-micron size (200 nm by 10 nm) and a moderate aspect ratio of 20. Mica has an aspect ratio of 30 to 100 with a particle size of 5 to 20 μm, whereas talc has an aspect ratio of 5 to 20 and is 5 - 8 μm in size. Another commonly used filler,Kaolin has an aspect ratio of 4 to 12 with its particle size of 1-2 μm [91]. For polymer composite applications, small sub-micron fillers, such as carbon black and silica, are essential for manipulating fatigue resistances, fracture toughness, and tensile strengths of these composites since larger size fillers (those greater than a micron) act as stress concentrators and defect initiators. Therefore, even tactoid organosilicates could be very useful fillers in polymer nanocomposites.

1.4 Permeability

In polymer nanocomposites containing impermeable inorganic sheet like filler particles, the available free volume to the permeant molecule is reduced, while the average random walk like path that the permeant molecule has to travel within the polymer matrix also known as tortuosity is increased, which reduces the permeability of polymer matrices. Permeating molecules can wiggle around in a tortuous path created by presence of organoclays, or they can diffuse between the layers if there is interaction of the permeating molecules with the surfactants. Hence, the permeation

of a molecule in the polymer matrix is dependent on the tortuosity of the path for the traveling molecule [12]. In polymer nanocomposites with intercalated-exfoliated morphologies the permeation of molecules depends strongly on the extent of dispersion, exfoliation, and preferred orientation of organoclay stacks. The presence of oriented organoclay layers increases the tortuosity for the permeating molecule, and the random walk path traveled by permeating molecule is longer. If the clays are partially exfoliated, their surface area increases, and so does the tortuosity. Consequently, a good dispersion of fillers enhances the barrier properties. In contrast, a formation of aggregates of the filler particles results in a deterioration of barrier properties. The shape of filler particles may affect the tortuosity and have a strong effect on the barrier properties of a filled material. The sheet-like morphology as shown in Figure 1.2 is particularly efficient for better barrier properties [12, 92]. In order to achieve maximum possible tortuosity to the permeating molecules the sheets of filler particles should be preferentially oriented as shown in Figure 1.3, in the direction parallel to the plane of the polymer surface.

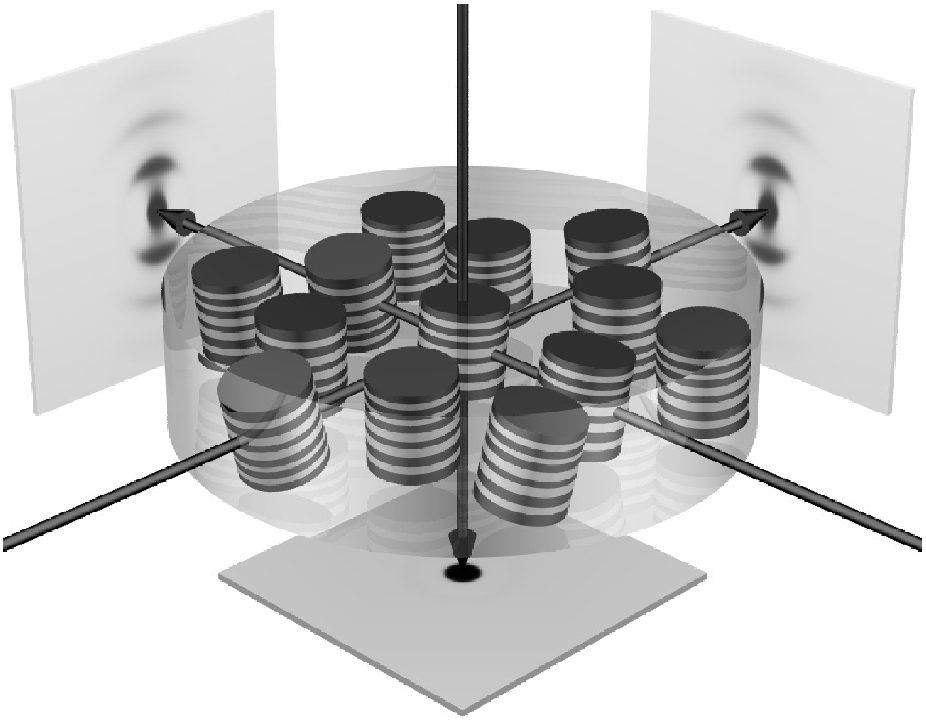

Figure 1.3: Directional SAXS simulation from nanoclays with cylindrical symmetry and preferred orientation.

The higher the degree of exfoliation and preferred orientation, the lesser will be the permeation of gas molecules. In the case of improper dispersion, i.e. a formation of aggregates of inorganic filler particles, the permeating molecules are allowed to diffuse faster. Commercial organoclays based on montmorillonites are effective agglomerates of smaller, primary particles consisting of 10-20 layers in a coplanar orientation. Those primary particles are usually referred to as the tactoids. The first step of melt mixing is to break up the agglomerates of organoclays to their primary particles through diffusion of polymer chains into the layer spacing of stack. This, in turn, will provide fillers from micron in size with aspect ratios of about 1 to fillers of sub-micron, 0.1 to 0.2 nm, with aspect ratios of about 10 - 30, depending on the type of clay. The ultimate goal during formation of polymer organoclay nanocomposite is to diffuse polymers into the silicate galleries to completely exfoliate organosilicates leading to fillers 1-nm thick with aspect ratios of about 200nm or more. Combination of exfoliation and preferred orientation of clays in polymer nanocomposites can explain various property enhancements in polymer nanocomposites. If the organoclay platelets are oriented parallel to the polymer film the properties of polymer film increases [19].

Additional filler carbon black In order to enhance the property of rubber, clay particles have been used as filler. [77, 78, 93-96] However, due to marked inhomogeneity of rubber clay nanocomposite arising from a high aspect ratio of clays, there is a large portion in the nanocomposite that is un-reinforced matrix. As a higher load of clay makes it difficult to achieve good dispersion, additional filler particle is thus desired to be added in order to achieve further property enhancement. Carbon black has been used in industry as filler material for various composite materials such as tubing and tires, and can be used as additional filler alongside organoclay to enhance the property of polymer matrix. Carbon black, when dispersed in polymer matrix, forms a strong network of nanostructure in polymer matrix which is connected with the polymer in a three dimensional network that will have similar properties to that of a gel [97]. This

structure can be defined on the basis of long range connectivity of carbon black taking place by percolation theory resulting in enhancement of various polymer properties and thus carbon black can be used as an additional filler [98]. The volume at which this effect occurs is called the percolation threshold. The origin of percolation theory can be traced back to Flory's theory [99] for polymer gelation and the first known literature on percolation theory is attributed to Thansely [100, 101] in 1957. Percolation theory defines how random sites in a system can be interconnected, which is helpful to estimate a property change in a two phase system. The low percolation threshold concentration requires an optimum amount of filler particles which is necessary to retain desirable properties of polymer. This may be sensitive to filler properties such as aggregation and size distribution, and can be affected by visco-elasticity of polymer matrix [102] and processing route [103-104]. Carbon black is available in various particle sizes having different morphologies [105] and due to their small particle size (as low as < 50 nm) [106] they have excellent reinforcing effect on the polymer matrix [107-108]. The production of carbon black dates back to the ancient Chinese practice of using soot from lamp oil for ink and dyes. Currently carbon black is being used in sensors [109], dyes [110], electrodes [111] and composites [1-20, 36, 37, 66, 86-89, 112] due to its various ideal properties in such applications. The introduction of carbon black in rubber vulcanizes it as well as improves its tensile properties, tear abrasion resistance, hardness and, overall, produces a rubber exhibiting outstanding mechanical properties. These physical properties such as viscoelastic shear and low modulus in polymer nanocomposites are dependent on the adhesion between carbon black particle and polymer matrix, therefore interfacial interaction plays a vital role in property enhancement [113-116]. Hence to understand the structure and morphology of nanocomposites, it is very important to estimate change in the properties of polymer. Transmission electron microscopy (TEM) studies of polymer clay nanocomposites have evidenced [92, 93, 117-118] that clay breaks into smaller tactoids

that could disintegrate into single layers giving exfoliated intercalated mixed morphology for dispersed clay. In the case of polymer nanocomposite containing carbon black, TEM micrographs have evidenced the aggregation of carbon black particles fused into concentric graphitic layers. These aggregates of finely dispersed particles form agglomerates which have an average size of a few microns [98, 114-115]. In both cases (polymer clay and polymer carbon black) physical factors of mixing can influence morphology of composites. Therefore, control of the sample microstructure and its resultant physio-chemical properties can be controlled by judicious manipulation of the mixture condition. In the past, the combined effect of clay and carbon black on properties of polymer matrix has been reported [119]. In this study we present the inductive effect of carbon black particles on the orientation of organoclay particles dispersed in polymer and a synergistic effect of organoclay and carbon black on the permeability of polymer. The property enhancement of polymer nanocomposites is, for the most part, governed by the dispersed nanofillers and their morphological state. Due to the overlap of features at many length scales, the detailed morphology of nanocomposite remains a mystery. In the presence of irregularly and allotropically shaped particles, the polymer melt could have significant influence on the development and morphological characteristic of matrix resulting in preferential orientation [120] of polymer chains. In order to fully understand why the enhancement in polymer properties occurs upon addition of nanofillers and to establish a relationship between the two, it is imperative to characterize the structure of polymer nanocomposite as well as the morphology of dispersed nanofillers. Studying the dispersion state and the orientation of such particles in polymer nanocomposite will give us better insight into property enhancement. It is shown that the permeation properties of nanocomposites strongly depend on the extent of clay exfoliation as well as the orientation of organoclays.

1.5 Flame Retardation

Additives that increase the amount of chars formed during combustion cycles are very effective fire retardants [9, 66, 121], and organoclays have been frequently mentioned as effective fire retardant agents, though their fire retardation (FR) properties are not sufficiently high [122]. In Chapter 4.4 we will discuss our efforts to reduce flammability of polymer by promoting char formation in polymer nanocomposites. The FR activity of organoclay is usually attributed to its ability to drastically enhance the melt viscosity of filled materials, thus slowing down the diffusion of highly combustible products and promoting the formation of silica-rich carbonaceous char to starve the flame of fuel [15, 65, 122-123]. Charred material also acts as a barrier by physically delaying the volatilization of decomposed products and transfer of volatile gas within the system. The physical structure of char plays important role in reducing the flammability of polymer, as system where formation of thick foamy char is formed have shown reduced flammability as compared to thin brittle char formed [122]. Charring is an important mechanism of the FR activity, yet it is not well understood in great detail. To be an effective flame retarding nanofiller, the charring process in polymer nanocomposite should occur rapidly at a temperature above polymer nanocomposite but below gasification temperature (details of combustion of polymer is given in Chapter 2). It was suggested that charring in nanocomposites could be partially attributed to their catalytic activity, facilitating the processes such as oxidative dehydrogenation and aromatization [15, 34, 123, 124-126]. In this study, we hypothesize that the catalytic efficiency of organoclays based on Montmorillonite mineral can be improved by incorporation of common transition metal ions (TMI), such as Cu or Fe. This is because the addition of TMI complexes to polymers has been proven to enhance the corresponding fire retardancy [127-128]. It appears that the presence of TMI ions promotes cross-linking of various polymers, enhances char-

ring, and slows down thermal degradation. On the other hand, TMI may also catalyze chain scission, thus making polymers more volatile and degradable.

Recently, we demonstrated that organoclays modified with TMI can significantly improve the thermal stability, reduce the release rate of volatile products from thermal degradation, and increase the content of solid residue of organoclays upon heating at 900°C in air [129]. These characteristics suggest that TMI-modified organoclays may also improve the fire retardation properties of corresponding nanocomposites. Currently, as the FR activity of organoclay is insufficient to replace conventional FR additives, they are often used in combination with other FR agents such as hydrated alumina ($Al_20_3H_2O$), conventional FR additives or carbon nanotubes [130-132]. Insufficient FR activity of organoclays can be attributed to thermal degradation of surfactant components via Hoffman elimination [29], resulting in the emission of combustible volatile products. We hypothesize that the TMI-modified organoclays can at least partially overcome this problem. We suggest that the TMI modification of organoclays, taking advantage of the unique surface chemistry and adsorption capacity of organoclays, may lead to effective fire retardant materials. In our previous study [129] it was indicated that TMI modified organoclays have higher thermal stability shown by TGA. The higher thermal stability of TMI-modified organoclays can be attributed to the charring processes, facilitated by the presence of catalytically active TMIs. In addition, the TGA data showed that washing of organoclays by methanol may slightly increase the thermal properties which can be accounted for by the loss of loosely held surfactant and organic contaminants. A drastic enhancement of thermal stability of organoclays can therefore be accomplished by the introduction of TMIs, and the higher thermal stability of TMI-modified organoclays suggests their use as more effective FR agents. In particular, we expect TMI-modified organoclays to have dual physico-chemical mechanisms of fire retardancy [129]. In the physical mechanism, organoclays can act as barriers for gas diffusion and physical cross-links

that hamper the flow of polymer melt, resulting in flammability reduction [9, 15, 66, 122-123]. In the chemical mechanism, TMI-modified organoclays can promote a variety of reactions during combustion, thus facilitating the formation of carbonaceous char. These reactions may include oxidative dehydrogenation, olefin dimerization and aromatization [34, 65, 124-125]. TMIs may form aggregates within the organic layer, resulting in a pillar-like structure and decreased *d*-spacing, but enhanced thermal stability. SAXS results, as discussed in [129], indicated that the layer structure of TMI-modified organoclays persisted at temperatures above the degradation temperature of conventional organoclays. In our previous work we have demonstrated that the TMI-modified organoclays can remain compatible with the polymer matrix, similar to unmodified organoclays. This is usually not the case for conventional FR agents [129, 133]. We have elucidated the status of TMI in clay using EXAFS and demonstrated rheological properties of polymer clay nanocomposites. It has been shown in previous work by our group that the introduction of C20A into the EVA matrix would result in physical gelation of EVA [134], whereas the rheological behavior of pure EVA is typical of high polymer melts.

It was also shown that miscibility between EVA and clays decreases as temperature increases in the 120-240°C range so EVA-organoclay systems show a tendency to undergo phase segregation at elevated temperatures. Phase segregation results in a formation of a network of clay tactoids in the polymer matrix essentially in a thermally induced physical gelation. Due to the formation of a tactoid network, rheology of EVA-clay nanocomposites is determined by viscoelastic properties of organomineral aggregates rather than by a relaxation behavior of a polymer matrix. Hence the temperature dependence of viscoelastic properties in EVA-organoclay system is rather weak as compared to an unfilled polymer matrix, which may be beneficial for FR properties, as it essentially causes physical gelation of polymer matrices at high temperatures and thus reduces spreading of fire by dripping polymer. However, overall

FR performance will depend on the whole spectrum of physico-chemical properties of tested composites.

1.6 Characterization

Layers of clays have a lamellar structure and X-ray scattering is the most powerful technique to quantitatively characterize the stacking behavior of organoclays, as well as most polymer nanocomposites in general. The large density difference between the mineral silicate and the organic component in organoclays has made SAXS a natural technique to characterize the structures of organoclays [38, 39, 29, 45] at room temperature and higher temperatures. It has been shown that the degree of delamination between the layered silicates and the distribution of inter-layer distance in organoclays can be determined from the SAXS data [59-60]. In chapter 4.1 we have discussed the structure of various organoclays, where we have primarily used X-ray scattering to evaluate the structure of clays at room temperature and to study thermally induced effects we performed in-situ X-ray scattering. In Chapter 4.1 we have also discussed effect of solvent and microwave on the exfoliation of organoclays using X-ray scattering. This information is particularly useful for the analysis of nanocomposites because one can study the affinity between the polymer chains and the organoclays based on the changes in the SAXS profiles from organoclays to composites [9, 65]. However, if one wishes to determine quantitative information about the state of intercalation and exfoliation in organoclays from the SAXS data, the task becomes much more difficult. This is because there are many factors, including the defects in organic-layered silicate complexes and the heterogeneous distribution of inter-layer periodicity. The differences in the packing density of the organic components, interstratifications of different possible arrangements and variations in distributions in alkyl chain lengths of surfactants used can lead to the broadening or/and shifting of scattering peaks [56, 60]. Disappearance of X-ray scattering peaks is often misin-

terpreted as exfoliation of the organoclay stack [42] while there can be other factors which can cause scattering peaks to disappear like loss in the periodicity of the clays. Hence X-ray analysis using Bragg's peak remains true only for the structures where the periodicity of the organoclays is still intact. Thus it becomes imperative to consider all the conditions while collecting and analyzing the X-ray data.

Evaluating structure of organoclays in polymer nanocomposites becomes more complicated. Curiously and somewhat confusingly, two different schemes to characterize the spatially dimensional geometry of heterogeneous nanostructured materials are in common use. The first scheme depends on the geometry of the individual domains of the minority component and characterizes layered systems as two-dimensional (2D) and systems containing long rods or needles as one-dimensional (1D). The other scheme depends on the spatial geometry of the arrangement of the domains, i.e., the geometry of the lattice for periodically ordered systems, and characterizes stacks of layers or lamellae as 1D systems, whereas bundles of long cylinders are 2D systems, often approaching a 2D hexagonal packing order. Systems having compact (e.g., spherical) domains and also continuously connected network structures are classified as 3D in both schemes. The second scheme is usually dominant for systems with a higher degree of periodic order, e.g., block copolymers, while the first scheme is often used for less ordered (including random) systems, or to emphasize the spatial nature of specific properties, e.g., 1D electrical conduction in nano-wires. For the nanocomposites studied in this report, both schemes would be applicable, and to avoid confusion, we will refer to them as layered or lamellar rather than as 1D or 2D. Studies in the past, where the X-ray data is collected by tilting the surface of polymer nanocomposite films at different diffraction angles [135-136] show that the organoclays are not fully exfoliated in polymer matrix. Various studies have been done in the past using SAXS, WAXD and small angle neutron scattering (SANS) where it was shown that the clays dispersed in polymer matrix are preferentially ori-

ented in the polymer matrix [136-139]. In Chapter 4.2 preferred orientations of the organoclays can be observed in X-ray scattering patterns recorded with 2D position sensitive detectors. The SAXS of intercalated nanocomposites is dominated by usually equidistant reflections due to the gallery spacing in intercalated stacks. From the reflections obtained, the orientation of the scattering stacks can be inferred. X-ray measurements can provide detailed information on the structure of organoclays and their polymer nanocomposites but a proper analysis may not be an easy task. TEM is an alternative technique to study the spatial distribution of organoclays dispersed in the polymer matrix. TEM images can reveal real space information about exfoliated composites, and the individual layers can be seen as hair-like structure in the cross section. Also in organoclay stacks, which may not be intercalated or exfoliated by polymer chains, if any, can be revealed by TEM usually in form of dark regions. Hence, a combination of TEM and X-ray techniques provides detailed information on the morphology of polymer nanocomposites. As discussed in Chapter 4.2 and 4.3, clay tactoids and single silicate layers are often aligned in the direction parallel to the in-plane direction of the polymer film. Three dimensional(3D) TEM and directional X-ray diffraction techniques have been used to demonstrate and to provide quantitative and complimentary structural information on clay orientation in polymer nanocomposites with and without carbon black as additional filler. Quantitative analysis of TEM has been shown to be capable of evaluating the extent of silicate exfoliation in polymer matrices. In Chapters 4.2 and 4.3 we present characterization of morphology and calculate the orientation of organoclays in a series of nanocomposite, containing ethyl vinyl acetate, or butyl polymers containing either organoclays and / or carbon black, using X-ray scattering and TEM. In Chapter 4.3 the effect of carbon black on the morphology of polymer nanocomposite and the orientation of organoclays was calculated and can be accounted for by the availability of less free volume for organoclays and strong association of carbon black and clay, leading to decrease in

orientation of particles. In Chapter 4.4 we discuss the overall purpose of TMI modification on the flame retardancy property of polymers. We have determined the effect of TMI-modified organoclays on the structure, thermal stability and fire retardation properties of EVA-based nanocomposites. For this purpose, all nanocomposites were investigated using small-angle X-ray scattering (SAXS), scanning and transmission electron microscopy (SEM/TEM), thermal gravimetric analysis (TGA), and standard fire testing techniques (UL-94 flame test and limited oxygen index). The specific goal of this study was to verify the effect of catalytically active TMI on the thermal stability and char formation of EVA-organoclay nanocomposites.

1.7 Scope of thesis

Even though the organosilicates are considered good additives for fire retardation, their high temperature use is restricted due to organic surfactants. However, not much has been done to fully explore the possibility of improving thermal stability of such organoclays. In recent years great progress has already been achieved related to development and characterization of polymer nanocomposites, but still their properties are not yet optimal and the upper limits for their properties have not been explored. Understanding the key reason why property enhancement takes place and the physical meaning of polymer filler interactions is still not explored completely. Correlation of particle matrix interaction, nanostructure formed, and its effect on various properties is not completely defined. Synergistic effects of nanofillers with other conventional fillers to obtain enhanced properties has not been fully scaled. Furthermore, most advances have been achieved only on a laboratory scale, since the optimal synthetic route for these composites has not been reached. The main focus of this research project is to establish a complete understanding of organoclays as nano-fillers and polymer organosillicate nanocomposites. In order to achieve higher surface area of nanofillers for property enhancement, exfoliation of clay in nascent

stage was achieved by two methods: 1) irradiating organoclays by microwave, 2) dispersing organoclays in various solvents. The project focused on the synthesis of layered silicate with improved thermal stability by introducing transition metal ions, as well as developing an understanding of the role of organoclay orientation on improving the gas barrier properties. We have established a relationship between the orientations of organoclays dispersed the weight fraction of organoclays and permeability of polymer and effect of TMI-modified clays on FR properties of polymer nanocomposites.

Chapter 2

Research Background

2.1 Structure of clay minerals

Clay minerals are the basic component for the preparation of organoclays, one of the most common types of nanofillers. Essentially, clay minerals may be defined as hydrous-layered silicates. Mineral layer-forming clays consist of two types of continuous sheet-like structural units. One is a tetrahedral sheet of silica, which is arranged as a hexagonal network in which the tips of all the tetrahedral units point in one direction, shown in Figure 2.1. The other structural unit (octahedral sheet) consists

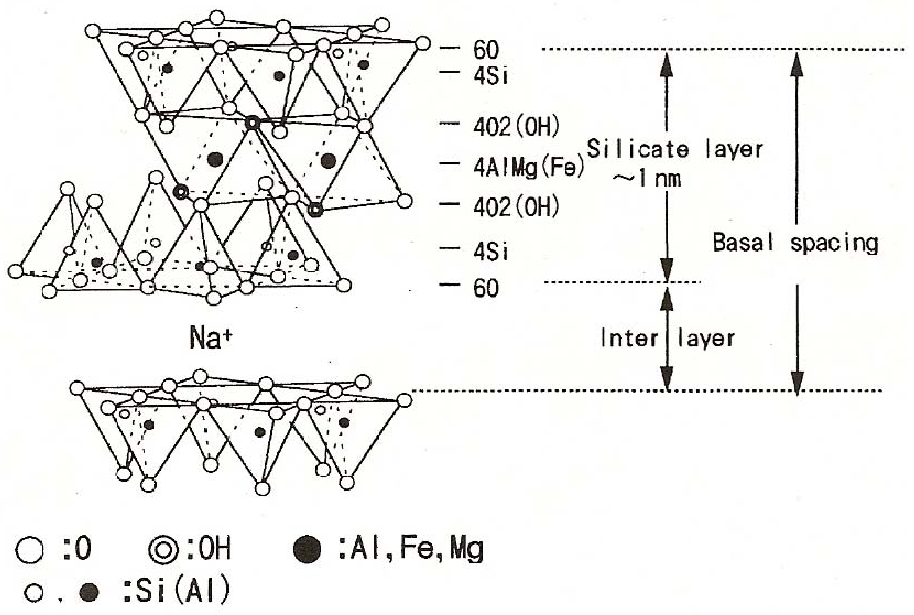

Figure 2.1: The structural unit of clay [182].

of two layers of closely packed oxygen or hydroxyl groups in which aluminum, iron or

magnesium atoms are embedded at an equidistance from oxygen or hydroxyl group Figure 2.1. Stacking of the layers leads to a regular van der Waals gap between the layers called the inter-layer space or silicate gallery, shown in Figure 1.2. Isomorphic substitution within the layers (i.e. of Si by Al or of Si by Mg) generates negative charges at layer surfaces that for some clays may be counterbalanced by monovalent cations, such as Na^+, K^+, Li^+ residing in the inter-layer space. For certain classes of clays (i.e. smectites) such cations may be exchanged for other metal or organic cations. The ability to exchange cations is an important feature of clay minerals.

Indeed, for polymers to form a nanocomposite with layered silicates, compatibility is the most important feature. Organic polymers are usually hydrophobic in nature while silicates are generally hydrophilic. Hence, to make clays compatible with polymers they must be modified by organic coupling agents such as surfactants, to make them hydrophilic and therefore making them compatible with the polymer matrix [140]. Exchanging of inter-layer cations (hydrated Na^+ or K^+) with various organic cations (i.e. quaternary ammonia) renders the normally hydrophilic silicate surface organophilic. It was suggested that the organic cations lower the surface energy of the silicate surface and improve its wetting with the polymer matrix, which makes an organosilicate compatible with polymer system [1]. The layered silicate used in this study belongs to phyllosilicate class. Two different phyllosilicates were used, 2:1 smectite and 1:1 flourohectorite.

Montmorillonite clay minerals $[(M_y nH_2O)(Al_{2-y}Mg_y)Si_4O_{10}(OH)_2]$ with this general formula are classified as 2:1 smectite belonging to the pristine family. These clays can be described as a 2:1 system as shown in Figure 2.1, which means that individual silicate layers in Montmorillonite (also known as Wyoming Cloisite, provided by Southern Clay Products Wyoming) are formed by two tetrahedral and one octahedral sheet which are connected with a 2:1 oxygen framework. The oxy-anion layer consists of two inverted silicate tetrahedral sheets, sharing their apical oxygen with

an octahedral sheet, with a regular repetition of these sheets in the layer. In general the coordination cations in tetrahedral sheets contain Si and Al alternatively and an octahedral sheet contains Mg, Al and Li [62, 141]. Due to their non-stoichiometric isomorphic substitution, the net surface charge is negative and depends on the precise chemical composition of the clay. The surface charge of layered smectite is intermediate and varies 0.4 to 1.2 e^- per Si_8O_{20} unit [142, 143]. This charge is balanced by the hydrated cations like Na^+, K^+, Ca^{2+} etc, intercalated between the layers. These cations are exchangeable and can be exchanged by other inorganic cations [144-145] or organic surfactants [146-148] to render the hydrophobic character necessary to the clay for polymer nanocomposite formation. The number of exchangeable cations per formula unit defines the cation exchange capacity (CEC) of the clay and is in the range of 0.3 to 0.4 eq. CEC can be determined via exchange with organic cations [160].

In smectite minerals the octahedral sites may be occupied by magnesium, iron or small metal ions as well as by aluminum. Relatively high surface area (>800 m^2/g) and high surface charge resulting in considerable (90 mEq/100g) ion exchange capacity make Cloisite a very popular material for preparation of organoclays used in synthesis of nanocomposites [149-150]. Among other advantages of Montmorillonite is the small particle size of stack-like clay tactoids (<2mm), resulting easy diffusion of organic modifier into these particles. The thickness of mineral layers is on the order of Angstroms while the diameter of a single crystal varies from few nanometers to several micrometers. Individual silicate layers possess high aspect ratios (100-2000), which result in an increase in modulus in nanocomposites containing intercalated and exfoliated organoclays.

The other mineral clay that has been used in this study is the synthetic clay mineral Somasif (SME100) manufactured by Unico (Japan) using the undisclosed proprietary solution-precipitation process followed by a high-temperature thermal

treatment. According to the manufacturer, Somasif has a general chemical composition of $(Na)_{2x}(Mg)_{3-x}(Si_4O_{10})$ $(F_aOH_{1-a})2$*n H−2O, where 0.15<x<0.5; 0.8<a<1.0. According to Unico, structurally SME100 is smectite-like mineral, which is similar to naturally occurring Montmorillonite minerals, which has a general composition of $(Na_y)(Al_{2-y},Mg_y)(Si_4O_10)(OH)^{-2}$-*n.$H_2O$; 0.25<y<0.6), Somasif does not contain catalytically active aluminum ions as a substitute in the octahedral position within the mineral layers. Another difference is its partial substitution of apical hydroxyl groups with fluorine.

2.2 Mechanism of clay exfoliation

The extent of exfoliation can be estimated by the ability of the system to overcome attractive forces holding the stack together. Layers of silicates are held together by electrostatic attraction between negatively charged basal spacing and positively charged cations (surfactants if organoclays) present in the basal space. Other forces could be van der Waals forces of attraction which keep these layers together. The exfoliation of clay tactoids dispersed in polymer requires a driving force to overcome the attractive force between silicate layers and gallery cations. In the literature evidence of exfoliation of clay in polymer nanocomposites is given [66, 86, 87]. The mechanism explained is that the surfactant within the layer will be in a certain conformation with certain entropy that is counterbalanced by elastic forces and which, if overcome, allow attractive forces adjacent clay layers to move apart. If the conformation of surfactant can be changed, than this can overcome the attractive forces. The inner layers in the clay stacks will also have higher binding energy as compared to the surface layers; hence a surface layer will come off easily as compared to the layer in between. One of the ways to bring a change in conformation of surfactants is thermal energy, where change in conformations of surfactants results in the increase of gallery spacing between silicate layers.

The structural heterogeneity in clays due to random variation of chemical constituents often causes variation of the ion exchange capacity between individual layers, resulting in complicated characteristics of intercalation in corresponding layered structures. In order to bring change in conformation of surfactants, uniform heating is desired otherwise heating will have multiple effects on the structure of clay. The Microwaves can be used as a source of thermal energy for rapid and uniform heating of materials. In this work we have used two approaches for exfoliating the clay particles: one irradiating organoclays with Microwave and another dispersing them in solvent (results of which are discussed in chapter 4.1). Here, basic insights into fundamentals of Microwave heating and its effects on the structure of clays are discussed.

Microwaves are non-ionizing electromagnetic waves of a particular wavelength (1nm to 300nm) which can be used as a source of thermal energy in both domestic and industrial processes. Recently, Microwaves have attracted the attention of chemists and are being used for rapid synthesis and chemical reactions which would otherwise require several days to prepare under conventional thermal conditions [151-155]. Some benefits of using Microwave as source of heat over conventional method is that Microwaves have a homogeneous thermal effect on the system, the capacity to suppress undesired phases, and cause rapid and simultaneous heating. In addition, the time required for heating is less, [156] hence making Microwaves a better source of thermal energy. If there is at least one component in the system that can interact with Microwaves, it can lead to desired heating results depending on other physical conditions. Dielectric materials, are the ones which contain either permanent or induced dipoles, show desired heating effects when exposed to Microwaves, and the energy transfer takes place via resonance or relaxation of the interacting molecule. Microwaves contain electric and magnetic components, and the electric field applies force on the charged particles which results in particle polarization. Energy transfer from Microwave to material is believed to occur either through resonance or

relaxation, resulting in rapid heating. Polarization is the phenomenon responsible for the majority of Microwave heating effects in dielectric materials. In the presence of Microwaves, the application of an electric field to the dielectric material results in the rotation of molecular dipoles or displacement of charges, by which the distribution of electron cloud within the molecule is distorted. Dielectric materials, where permanent dipoles already exist either due to charged particles or due to differences in electronegativity, undergo a reorientation of their dipoles in the presence of Microwaves. As the dipole reorients itself with the field, there is a phase difference between orientation and dipole which causes energy losses due to random collisions of molecules, resulting in heating. The ability of the dipole to respond to the field is critical, as in the case of low frequency region, where dipoles will remain in phase with the applied field and a very small amount of energy will be gained or lost resulting in very small heating effect. In the case of a very high frequency region, the dipole will not have sufficient time to respond and hence no heating will observed. The Microwave region is in between these two extremes of frequency. The Microwave frequency is low enough that the dipoles have time to respond the alternating field and therefore to rotate, but the frequency is also high enough that the rotation does not precisely follow the field. The extent of Microwave heating for a material will depend on its relative permittivity and dielectric loss. In this study we hypothesize that organoclays, being dielectric in nature, and which have polar organic surfactants as dipoles, will have a drastic effect on the structure of clays. The surfactants within the clays are present in particular conformations. Upon Microwave heating these surfactants will change their conformation from random coil to stretched conformation and this can lead to the exfoliation of clays.

2.3 Nanocomposite

A heterogeneous mixture of two homogeneous phases when combined together in such a way that these phases are not visibly distinguishable in final form is known as a composite. The continuous phase is called the matrix, while the dispersed phase may be defined as filler. Composites thus formed often have superior properties as compared to properties of individual materials. Conventionally, inorganic materials have been used as fillers and polymers as matrix for improving various properties of polymer systems, such as strength, stiffness, and thermal stability. When one dimension of the filler particles is on the nanometer scale such composite systems are termed as nanocomposites consisting of polymer matrix and nanofillers. Organically modified layered silicates or organoclays are the widely used as nanofillers. Useful properties of organoclays fillers are attributed to high surface areas, high aspect ratios and high strengths.

Nanocomposites formed by the polymer and organically modified layered silicates were first reported by Blumstein in 1960's but the real exploitation of this technology started in the 1990s. Nanofillers, when properly dispersed, are efficient at far lower loads than conventional micrometer-size fillers and may improve the properties of polymers without decreasing their toughness [16, 66].

2.3.1 Preparation of Polymer - Clay Nanocomposites

The three most common techniques for manufacturing of the polymer organoclay nanocomposites may be summarized as follows.

- Solvent based: In the solvent-based synthesis, both the organically modified layered silicate and the polymer are dissolved in same solvent system and then two solutions are mixed. The solvent is then allowed to evaporate at an appropriate

rate. For example: mixing a polystyrene-toluene solution and organoclay dispersed in toluene and then evaporating the solvent we can obtain polystyrene organoclay nanocomposite.

- In-situ polymerization: When the polymerization reaction is carried out in the presence of organically modified layered silicate, it is known as *in-situ* polymerization. For example, polystyrene organoclay nanocomposites can be prepared by the polymerization of styrene in the presence of organoclay.

- Melt blending synthesis: In this process, organically modified layered silicate is dispersed in polymer matrix under shear at a temperature above the softening point of the polymer used. During mixing, the polymer chain diffuses from bulk polymer melt into the galleries between silicate layers. Melt mixing occurs at elevated temperatures under the influence of high shear (shear rates as high as 10-100 $s^{-}1$). Melt-mixing allows for highest throughput among mentioned techniques thus being attractive from the industrial point of view, on the other hand it requires sufficient thermal stability of all involved components.

2.3.2 Morphology

When layered nanofillers are dispersed in polymer matrix three different types of morphological structures may be formed which may or may not coexist in a system.

i) Phase segregated structure: Clay stacks are dispersed in a polymer matrix, however, the polymer does not penetrate inter-layer space (silicate gallery)as shown in Figure 2.2. The structure and properties of resulting composites are not strongly different from conventional filled systems. This is characteristic for poor compatibility between polymer and organoclay.

ii) Intercalated structure: The individual polymer chain penetrates the inter-layer spaces of organoclay stacks without layered structures being completely destroyed, forming multilayered organomineral structures [5,157] Intercalated systems given in

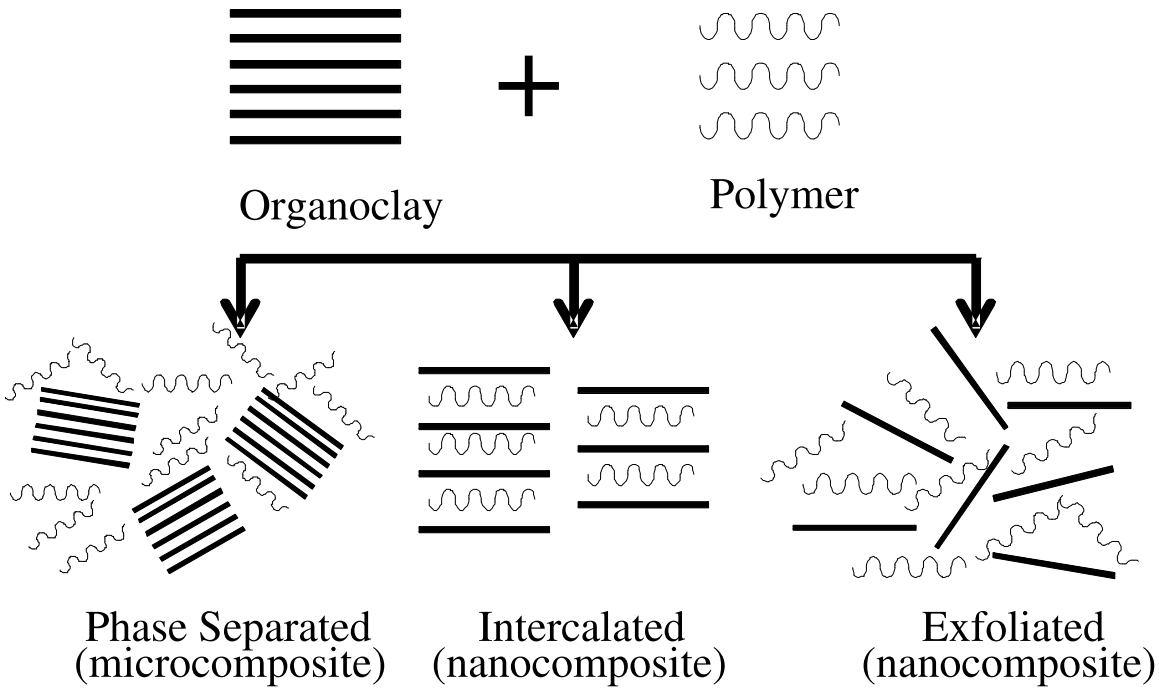

Figure 2.2: Various possible polymeer nanocomposite morphologies a) Phase segregated structure, b) Intercalated structure, c) Exfoliated structure.

Figure 2.2 are usually formed when organoclay is partially compatible with polymer matrix. Mechanical properties (modulus) are drastically improved as compared to phase-segregated system.

iii) Exfoliated or delaminated structure - The polymer chain enters the layered structure resulting in delamination or exfoliation shown in Figure 2.2 of clay stacks so that individual clay layers are dispersed in a polymer matrix and their positions are no longer correlated. The exfoliated structure can be partially ordered (i.e. by drawing), where the silicate layers are more or less oriented in one direction, or disordered, where dispersed layers are oriented randomly [158]. Exfoliated systems are characteristic for good organoclay-matrix compatibility and usually have the best mechanical properties. Formation of these morphological structures depends on various parameters.

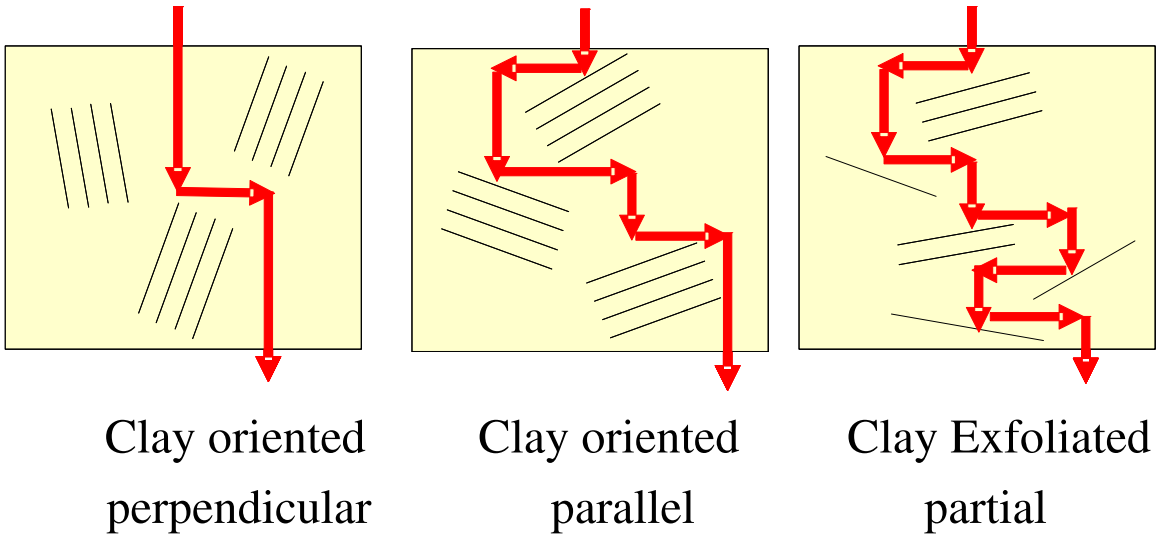

Figure 2.3: The random tortuous path adopted by the permeating molecule as shown,through the polymer nanocomposite membrane containing high aspect ratio clay platelets..

2.4 Barrier Properties of Polymers

Permeation of a molecule through a neat polymeric film will depend on the absorption and desorption rates of the molecule at the surface of the polymer. Once inorganic sheet-like fillers are introduced in the polymer matrix, the polymer nanocomposite will exhibit improved barrier properties. The random tortuous path adopted by the permeating molecule as shown in Figure 2.3, through the composite containing high aspect ratio platelets [159], will lead to lower rates of permeation due to higher tortuosity. The path of gas molecules through a polymer matrix follows 'the solution diffusion model'. Figure 2.4 shows schematic illustration of the time-dependence of the integrated flux of a gas transport across a membrane. It is a three-step process: 1. Adsorption and dissolution of gas at the polymer-membrane interface. 2. Diffusion of the gas into and through the bulk polymer. 3. Desorption of gas into the external phase.

The model assumes that the pressure within a membrane is uniform and the chemical potential gradient across the membrane is expressed only as a concentration

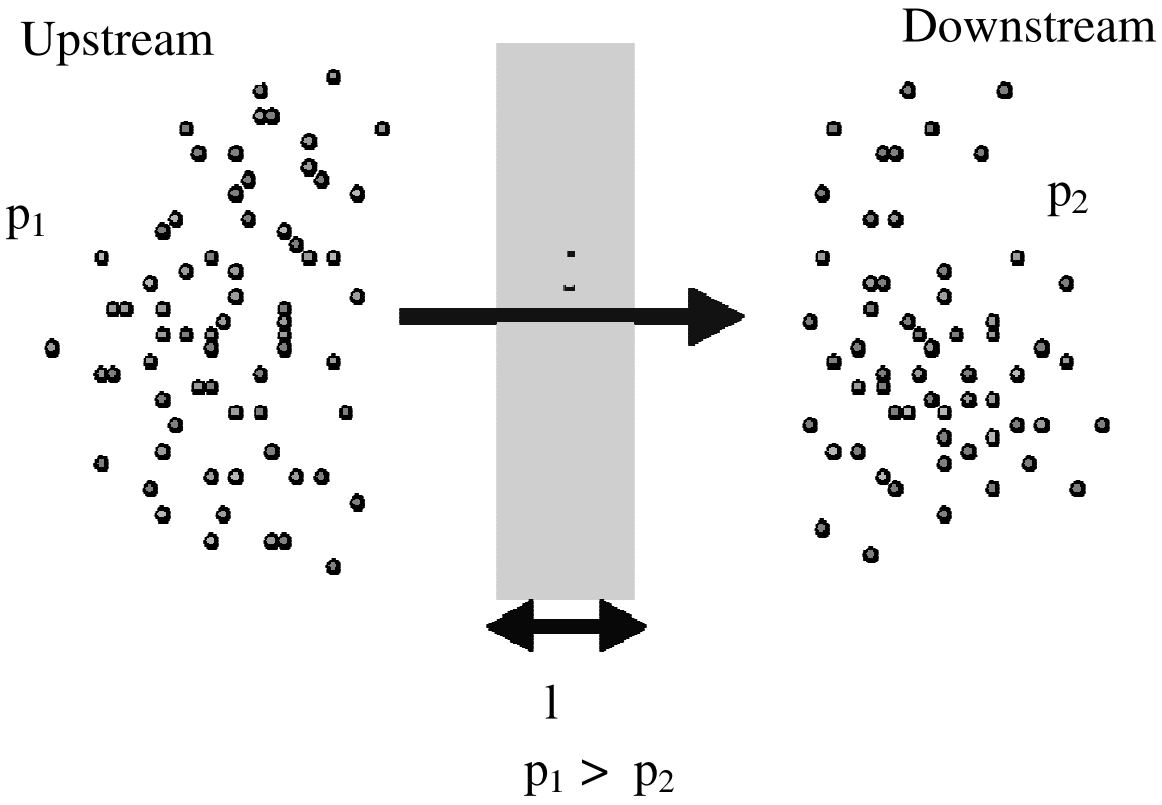

Figure 2.4: The solution diffusion model showing diffusion of molecules across the barrier of width 'l'.

gradient. The upstream gas has a pressure of p_1 and it comes in contact with the membrane interface with a driving force hence creating a flux, which is dependent on concentration and is given by Fick's law in equation 2.1:

$$J = -D(dC/dl) \tag{2.1}$$

where J is the flux created due to the potential gradient, D is the diffusion coefficient, and dC/dl is the concentration gradient created by the permeant molecules across the membrane, and l is the thickness of the membrane. When the solubility of the permeant gas in the polymer matrix is sufficiently low, the concentration is proportional to the vapor pressure and is given by Henry's Law in equation 2.2:

$$C = S * p \tag{2.2}$$

where S is the solubility coefficient and p is the pressure of permeant. Neilsen [160] suggested one of the first models to describe the permeation of gases through polymer nanocomposites that predicts the reduction of the permeability coefficient. The model was based on the tortuosity of the pathway for the permeating molecule through the polymer nanocomposite, as shown in Figure 2.3. This model doesn't account for the Brownian motion of the permeating molecules and assumes that the filler particles are oriented in the direction parallel to the plane of the film. Another solution was provided by Gusev et al.[161] which is based on the finite element analysis. According to this theory polymer nanocomposites containing sheet-like filler particles show an exponential decay of the permeability which depends on the filler volume fraction and aspect ratio. The ratio of the permeability coefficient for randomly orientated platelets and perfect aligned platelets will vary with the average aspect ratio of system. With the increasing aspect ratio, the effect of misalignment becomes larger and the decrease in permeability due to misalignment will approach a constant value. Other theoretical approaches for predicting barrier properties have been discussed in the literature [100, 162-163].

2.4.1 Polymer Structure's effect on permeability:

The compact structure and the ability of polymers to pack efficiently make them a good barrier of permeation. Permeability of polymers is affected by local molecular mobility, with higher molecular mobility facilitating diffusion of gas through the polymer matrix. For instance, in semicrystalline polymers above T_g (glass transition temperature) of amorphous component, gas molecules predominantly travel through the rubber-like amorphous domain [164]. The phenoxy-type polymer matrix has strong cohesion among chains due to strong hydrogen bonding and compact backbone structure, which impedes the permeation of molecules through the polymer matrix [165], resulting in a low permeability in these systems. In a polymer system the decrease in permeability is the result of an increase in permeant size with the decrease

in the free volume of the polymer. Thus glassy polymers are less permeable than rubbers. Consequently, the increase in the degree of crystallinity of a polymer, the chain order, the degree of cross-linking, the degree of hydrogen bonding, the packing density and the compact morphology of the polymer are all structural factors decreasing permeability and enhancing the barrier properties of a polymer [164, 166]. Polymers that can interact with permeating molecules will have poor barrier properties, while those interacting poorly will demonstrate improved barrier properties [166]. The diffusion of a permeating molecule in polymer matrix is dependent on how tortuous is the path for permeating molecule[12]. The tortuosity factor 'τ' is defined as the ratio of the actual distance a molecule must travel to get through the film (l') to the thickness of the permeating membrane (l) in equation 2.3:

$$\tau = (l'/l) \tag{2.3}$$

In polymer composites containing impermeable inorganic filler particles the available free volume to the permeant molecule is reduced as shown in equation 2.4, while the average path it has to travel within the polymer matrix is increased, which reduces the gas permeability. Obviously, good dispersion of filler enhances barrier properties; in contrast formation of aggregates of filler particles results in the deterioration of barrier properties. The shape of filler particles may affect the tortuosity factor and have a strong effect on barrier properties of a filled material. The sheet-like morphology as shown in the Figure 1.2 and Figure 2.3 is particularly efficient for better barrier properties [12, 100, 180].

$$P_f/P_u = \phi_p/\tau \tag{2.4}$$

In order to give maximum possible tortousity factor to the permeant molecules the sheets of filler particles should be oriented in the direction parallel to the plane of polymer surface. The tortousity factor changes to the following equation 2.5:.

$$\tau = 1 + (L/2W)\phi_f \tag{2.5}$$

In the above equation, L is the length and W is the width of the filler particle, and this ratio is also referred to as the aspect ratio (L/W) and is the volume fraction of filler particles ϕf: Combination of Equation 2.3 and Equation 2.5 gives equation 2.9, which shows the dependence of permeation on the aspect ratio of filler particles; hence aspect ratio plays an important role in improving the permeability of polymers.

$$P_f/P_u = \phi_p/[1 + (L/2W)\phi_f \tag{2.6}$$

The higher the aspect ratio the less is the permeation. This relation remains valid when the filler particles are oriented in a direction parallel to the polymer surface. If the orientation of these particles is perpendicular, the ratio changes to (W/L) and according to this relation the permeation will increase with a decrease of aspect ratio, hence yielding poor barrier property [100, 167, 180F].The diffusion of permeating molecules in polymer nanocomposites can adopt three different routes: diffusing through the polymer, the interfacial part or the bulk polymer. In the presence of silicates, which are impermeable, permeation can occur through either the interfacial part, which will lead to a tortuous path, or through the bulk polymer. In the case of improper dispersion there is a formation of aggregates of inorganic filler particles, which will allow molecules to diffuse faster, otherwise they adopt a tortuous path created by the presence of filler particles. In the presence of the filler particles the flux J can be rewritten as equation 2.7

$$J_o = -D[W/L * (dC/dl)] \tag{2.7}$$

When the layered silicates have N number of layers the expression for the flux can be redefined as equation 2.8[100]

$$J_o/J_N = 1 + \sigma\alpha\phi + \alpha^2(\phi^2/1 - \phi) \tag{2.8}$$

This relation predicts that the diffusion of flux can vary with layered silicates loading in two ways. It can either wiggle through the tortuous path created due to

the presence of layered fillers, or diffuse between two silicate gaps which is the slower path. The tortuosity factor will hence depend on the aspect ratio, orientation, and volume fraction of the filler particles.

2.4.2 Permeability in polymer-organoclay composites:

Clays as such are usually incompatible with most organic polymers, hence to make them dispersive they are modified with organic surfactant molecules. The content of surfactants used can be as high as 40-50 % by weight. Most of the surfactants currently used are the halide of long chain alkyl amines, and they replace the sodium ions present in the inter-layer gallery spacing of layered silicates. Typically, polymer-organoclay composites can have intercalated or exfoliated morphology as shown in Figure 2.2. In the intercalated system the polymer chain penetrates between the layers, however stack-like structures remain intact. In the case where exfoliation occurs, the layered stacks are completely broken. Obviously, exfoliation of clay stacks results in an increase of the aspect ratio. For layers of the organosilicate to be completely exfoliated in the polymer nanocomposites, two important factors are maximal coverage of clay surface by a surfactant and large *d*-spacing of Aluminosilicate layers. Larger surfactant size can lead to increased *d*-spacing in layered silicates hence facilitating exfoliation [168-169]. Broad particle size distribution of the clay leads to the mixture of layers and tactoids of varying thickness. Hence, in reality the polymer system has mixed morphologies, and the average aspect ratio determined by a character of stack size distribution should therefore be taken into consideration [169, 170]. Partial exfoliation can increase the average aspect ratio and lead to better barrier properties [100, 171, 180]. If there are few individual layers in polymer nanocomposites that are exfoliated from the clay stack then permeation will decrease drastically, as the layers will provide a tortuous path for diffusion. Hence the mineral sheets present in the polymer matrix force the diffusing molecules to make long detours

around the exfoliated layers, and the local permeability is affected by the presence of impermeable silicates in polymer system [172].

2.4.3 Effect of pressure on permeability:

Four typical patterns of response are observed in permeability versus pressure relationships: (a)Diffusion coefficient being independent of gas pressure (i.e., low sorbing penetrants, such as He or N2 in rubbery or glassy polymers). (b) Increase of permeability with increasing pressure. This relation often describes the permeability of an organic vapor into a rubbery polymer. (c) A decreasing trend of permeability with increasing pressure. This is typically observed with highly soluble gases such as CO2 in glassy polymers. (d) A combination of (b) and (c) is typical of a plasticizing penetrant such as organic vapor in a glassy polymer. If the pressure of permeating molecules is continuously increased there is a point when there is a sudden increase of permeance across the membrane and this pressure is called the plasticization pressure 'p' given in the equation 2.9;

$$p = p_0 exp^{-E_P/RT} \tag{2.9}$$

At this pressure the polymer chain packing is disrupted and the polymer matrix swells, increasing the segmental mobility of the polymer chain. This results in an increase in gas diffusivity and induces permeability increases [173]. This behavior is explained by the free volume theory. Free volume theory of diffusion suggests that molecules can only diffuse through free volume in a molecule matrix. Diffusion in a rubbery polymer is the result of redistribution of free volume within a matrix and migration of the permeant molecules among these volumes. Previously researchers have summarized the permeability equations derived based on the free volume approach to model the gas transport in plasticized polymer matrices.

2.5 Combustion of polymers

Combustion is a chemical reaction which occurs in the presence of fuel and oxygen and results in the release of a large quantity of heat energy. Any substance which can be burned to release energy can be viewed as fuel. On the basis of combustion, solids can be classified into two categories: charring and non-charring. Charring solids are those which leave behind a residue when applied to flame, while non-charring materials burn out completely. Thermoplastic polymers such as polyethylene, polypropylene, ethylene-vinyl acetate (EVA) can be classified in non-charring group of solids. When a polymer is exposed to heat, combustion and pyrolysis takes place. Burning of a polymer occurs in several stages. Upon heating the polymer breaks into a combustible substance which acts as a fuel, and part of this fuel is fully combusted in the flame by combining with the stoichiometric amount of atmospheric oxygen. The remaining part of this generated combustible fuel can be combusted by drastic means, e.g. in the presence of a catalyst and by an excess of oxygen which leads to more severe burning of polymer system. During the combustion, a part of heat released is fed back into the system (also referred to as thermal feedback), while the other part is lost to the environment. A schematic representation of polymer combustion cycle is shown in Figure 2.5. Hence without FR treatment polymeric materials can be described as hazardous in the event of fire.

Conventionally used fire-retarding (FR) agents were halogenated organic compounds (such as hexa-bromo-cyclo-dodecane, tetra-bromo bis-phenol, tri-bromophenol allyl ether, bis tri-bromophenoxy ethane, chlorinated paraffin etc.). Organic phosphorous and nitrogen-based compounds such as melamine, melamine cyanurate, melamine phosphates, ammonium polyphosphate-pentaerythryol or ethylene-urea formaldehyde, guanidine phosphates for textiles, and guanidine sulphamate and the mineral additives (i.e. aluminum and magnesium hydroxides). These FR agents have been classified according to the mechanism of their fire retardation in two broad

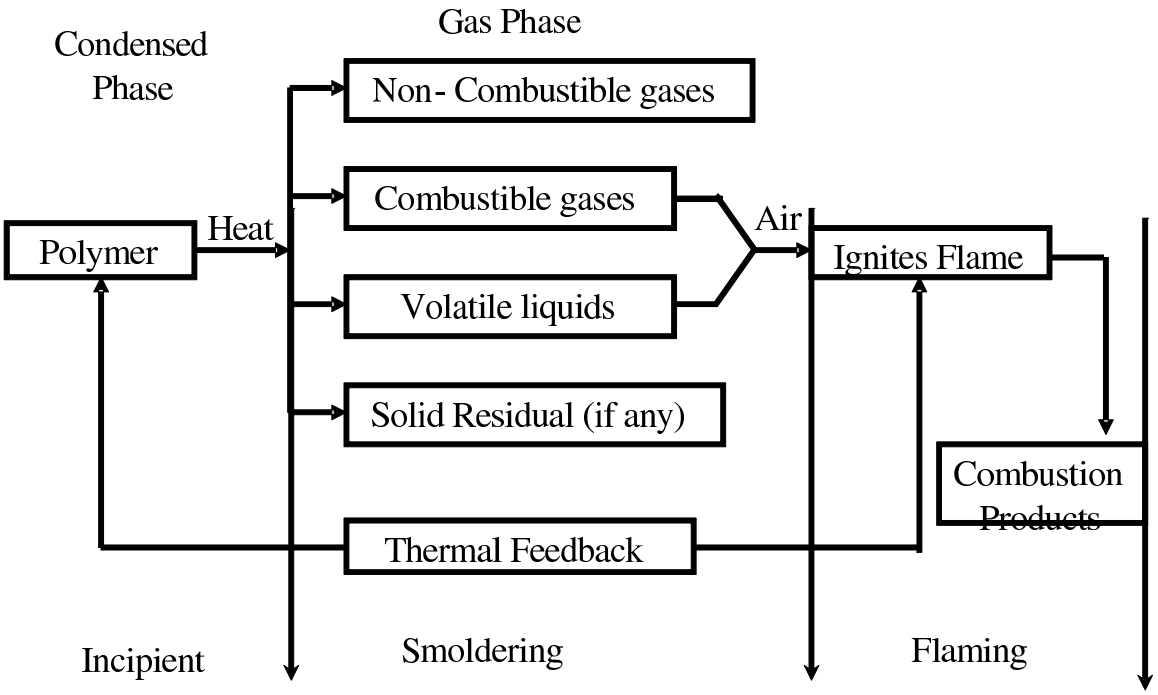

Figure 2.5: The Polymer combustion cycle.

categories (1) Those which are active in gas phase and (2) Those which are active in condensed phase (formation of char and release of water upon heating). i) The halogenated compounds are active in the gas phase. Vapors of halogenated compounds react with the free radicals produced during combustion of polymer, and the trapping of these radicals in a gas phase leads to inhibition of fire. Halogenated FR agents have many disadvantages, the major one being high toxicity. Indeed, there is the possibility of formation of halogenated dioxins and bi-benzofurans during thermal degradation of halogenated organic derivatives [1, 140-141]. ii) The FR activity of organo-phosphorous additives and compounds containing nitrogen is mostly based on FR technology known as intumescence. Intumescence may be defined as the ability of FR agents added to otherwise flammable material to induce foaming upon heating resulting in the formation of foamed char acting as an insulating barrier [174-175]. Though intumescence-inducing FR agents were shown to be rather effective and non-toxic in nature they have several disadvantages such as water solubility, brushing

problems, relatively high cost and relatively low thermal stability [176-179]. For achieving of sufficient fire retarding properties in a polymer system, these additives are required to be added to the system during processing, which usually takes place at higher temperature. Thus, poor thermal stability of intumescent systems creates problems. iii) Mineral additives such as aluminum and magnesium hydroxide release water in the event of fire and hence they act as a cooling agent, which suppresses fire and decreases the temperature of the burning material.

Chapter 3

Experimental

3.1 Material used

Natural clays used: Naturally occurring mineral clay montmorillonite and its organically modified Cloisite 20A (C20A) used in this study were manufactured by the Southern Clay company. Montmorillonite's general composition is $(Na_y)(Al_2 - y,Mg_y)(Si_4O_{10})(OH)_{2-}$*n H_2O; 0.25<y<0.6) and based on the data provided by Southern Clay C20A contains the Montmorillonite mineral clay and di-methyl di-hydrogenated tallow quaternary ammonium chloride (DMDTA) shown below in Figure 3.1. The content of the surfactant in C20A organoclay was 35-wt%. DMDTA

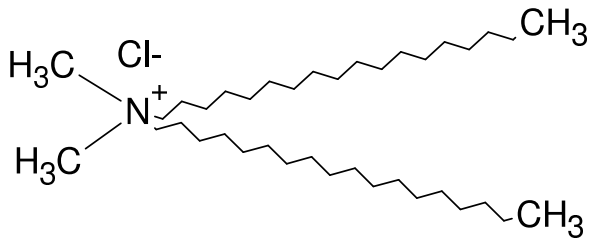

Figure 3.1: Chemical structure of the surfactant, di-methyl-di-hydrogenated-talloammonium chloride, present in the purchased organoclays Cloisite C20A and Somasif MAE .

is a blend of surfactants prepared from natural products by Akzo Nobel. According to Akzo Nobel, the major component in this blend is di-methyl di-octadecyl-ammonia chloride (DMDOA); minor components included (in the order of decreasing content) di-methyl octadecyl - hexadecylammonia chloride, di-methyl di-hexadecyl ammonium chloride, and a small (<3 wt%) amount of tertiary ammonium chlorides (such

as di-methyl octadecyl ammonium chloride and di-methyl - hexadecyl ammonium chloride). Both clays were received in the form of a dry powder and were used as received. Synthetic clays used: Among synthetic clays used the chosen Somasif sample (SME100) was a mineral clay manufactured by Unico (Japan) using the undisclosed proprietary solution-precipitation process followed by a high-temperature thermal treatment. According to the manufacturer Somasif has a general chemical composition of $(Na)_{2x}(Mg)_{3-x}(Si_4O_{10})$ $(F_aOH_{1-a})2$ *n H_2O, where 0.15<x<0.5; 0.8<a<1.0. According to Unico, structurally SME100 is smectite-like mineral, which is similar to naturally occurring Montmorillonite minerals, such as Cloisite. However, in contrast to montmorillonite, somasif does not contain catalytically active aluminum ions as a substitute in the octahedral position within the mineral layers. Another difference is its partial substitution of hydroxyl groups within the silicate layers with fluorine. It is known that Cloisite minerals can undergo dehydroxyllation above 600°C, losing apical OH groups and transforming into an anhydrite form. Obviously, dehydroxylation process will be hindered in fluorinated Somasif mineral. Synthetic organoclays used was Somasif-MAE (SMAE) manufactured by Co-Op Chemical Co., Japan. This organoclay contained Somasif SME100 mineral and di-methyl-di-hydrogenated-talloammonium chloride (DMDTA)Figure 3.1 surfactant (ca. 42 wt%). DMDTA was a blend of surfactants prepared from natural products by Akzo Nobel. The major component in this blend was dimethyldioctadecyl ammonia chloride (DMDOA); minor components included (in the order of decreasing content) dimethyloctadecylhexadecyl ammonia chloride, dimethyldihexadecyl ammonia chloride and a small (< 3 wt%) amount of tertiary ammonia chlorides (such as dimethyloctadecyl ammonia chloride and dimethylhexadecyl ammonia chloride). Hydrogenated tallow is a product consisting of a distribution of hydrocarbon chains with approximate composition 65% C18; 30% C16; 5% C14. Structure of surfactant contained in Cloisite C20A and Somasif MAE is shown in Figure 3.1. Synthesized organoclay: Montmorillonite min-

eral clay was modified with phosphonium surfactant, purchased from Fluka (Fisher. Surfactant used for modification was a quaternary organic compound containing tri-butyl-hexa-decyl-phosphonium bromide (TBHDP Br) where the molecular formula was $C_{28}H_60BrP$. Figure 3.2 shows the structure of surfactants TBHDP Br used to synthesize the organoclay from montmorillonite .

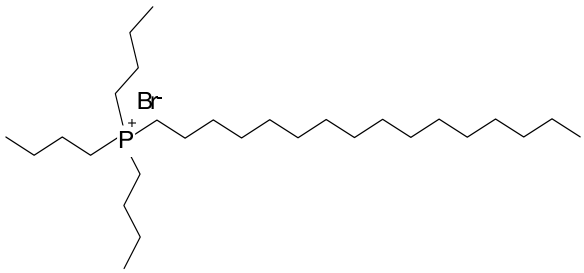

Figure 3.2: Chemical structure of the surfactant tri-butyl hexa-decyl-phosphonium bromide used in the synthesized organoclays TBHDP Br.

Carbon black used: Furnace carbon black used in this work was N660 and is commercially available standard ASTM grades. Primary particle diameter is 46 nm and surface area is 37 m2/gram.

Ethylene Vinyl Acetate (EVA) Co-Polymer: Ethylene-co-vinyl acetate (EVA) copolymers used were the plastic material examined and were received from E. I. du Pont de Nemours and Company. Elvax 350 has 25 wt % (8 mole %) vinyl acetate and melt index of 19 (ASTM D1238) whereas Elvax 770 has 9.5 wt % (3 mole %) vinyl acetate and 0.8 melt index. Both EVA materials are structurally similar to a low-density polyethylene (LDPE) with many long chain branches and their density values are approximately 0.94 g/cm^3. Structure of EVA is given in Figure 3.3. Brominated isobutylene p-methyl styrene (BIMS): Another elastomer material evaluated in this study is brominated poly (isobutylene-co-p-methylstyrene), or BIMS, which is one of the lowest permeability elastomer available commercially. This copolymers is industrial grade and is proprietary of Exxon Mobil and is named as ExxproTM specialty elastomer. BIMS of ExxproTM 3745 from ExxonMobil Chemical, which

is the commercial grade having the highest PMS content of 7.5 wt % and highest BrPMS content of 1.2 mole %, was used. Two different surfactants tri ethylamine and containing dia benzoic acid were used to functionalize BIMS. Miscellaneous: The compounds $AgNO_3$ and $FeCl_3 \cdot 6H_2O$ were purchased from Fisher Scientific Company; $CuCl_2 \cdot 2H_2O$ was purchased from J. T. Baker Chemical Company. Sodium borohydride (NaBH4, 98%) was purchased from Sigma-Aldrich. Ethanol and methanol were purchased from Fisher Scientific Company. All solvents, salts and transition metal salts used in our study were used as received unless specified.

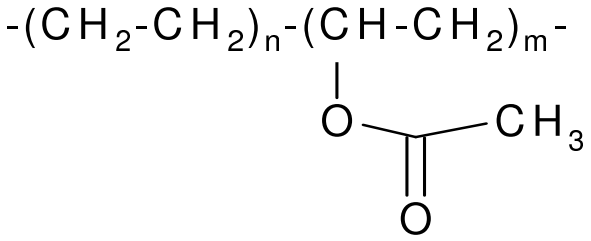

Figure 3.3: Chemical structure of Ethylene Vinyl Acetate (EVA) co-polymer.

3.2 Sample Preparation

Irradiation of clays under Microwaves: For Microwave irradiation: Mineral clays Montmorillonite and Somasif MEE and their organic counterparts Cloisite C20A and Somasif MAE finely powdered and pre dried in vacuum oven were used. A pre-weighed sample of 0.5 grams of each of mineral clays and organoclays were placed in 6 different vials and each vial was placed individually in domestic Microwave equipment for certain period of time(0 to 78s). After irradiating each sample vial for a pre specified time(0 to 78s), under similar conditions, these vials were removed and sealed for further tests. The domestic Microwave used for this study was manufactured by Sharp Electronics.

Clay dispersed in solvent samples: Organoclay/solvent blends (1 wt % organoclay) for the dispersion index study were prepared as follows. In a glass bottle vial with

a cap, the organoclay and the solvent were mixed. The suspension was stirred for a minimum time period of 12 hrs. Occasionally it was further shaken vigorously by hand. Finally, it was sonicated at room temperature for 20 min. The samples were then visually examined after standing for 2-3 hrs and 3-7 days at two different times. Organoclay/solvent suspensions for the SAXS study were prepared as follows. Organoclay C20A was weighed and varied according to the desired wt %, and it was dispersed in various organic solvents. Upon mixing organoclay and solvent, a colloidal suspension was formed. This suspension was further stirred for 20 mins. using a Fisher Scientific's tissuemiser homogenizer at 5000 RPM and then sonicated at room temperature for 20 mins. Depending on the wt % of organoclay in the suspension, different visual results were obtained. Organoclay C20A was weighed and dispersed in various organic solvents and the weight was varied according to the desired weight percent. On mixing organoclay and solvent a colloidal suspension was formed. This suspension was first tissumised (vigorous mechanical stirring) for 20mins. at 5000 RPM and was then sonicated at room temperature for 20 mins. Depending on the weight percent of organoclay in mixture we obtained different results, which were visually different.

Modification of clays: 1)Synthesis of Organoclays from Mineral Clays: All reagents were used as received unless otherwise indicated. N, N, N,-tributyl-N-hexadecyl phosphonium bromide (95% TBHDP, Fluka/Fisher) was received as fine crystalline white solid. In dealing with the exchange of cations in clay materials, the parameter "cation exchange capacity" (CEC), which represents the retention capacity for cations of the clay, was used. The CEC value of an adsorbent is formally defined as the sum total of the exchangeable cations that the adsorbent can uptake. Generally, a negatively-charged adsorbent such as clay will attempt to take up enough cations in order to become neutral in overall charge. The CEC value is thus a measure of this tendency. Every type of clay has its own characteristic CEC value. The amount of TMI extracted

from a modified sample of clay can correlate closely to the CEC value of that clay. As stated in Table 1, the CEC value of Montmorillonite is 92.6 mmol of exchangeable sites per 100g. In order to synthesize an organoclay from mineral clay, the CEC value of the mineral clay must be considered. To determine how much organic surfactant to incorporate into a certain mass of montmorillonite, the following equation was used:

Weight of Surfactant Needed = (Desired % of surfactant) x (CEC of MMT) x (MW of surfactant) x (starting mass of clay)

The percentage value is the desired amount of surfactant in co-ordinance with the CEC value of the clay; in this work, a value of 125% above the CEC (numerically expressed as 1.25) was used for the chosen clay. The CEC value of Montmorillonite (MMT) was numerically expressed as 92.6 x 10-5 mol/g. The respective molecular weight of TBHDP Br was 507.67 g/mol. Prior to clay treatment, the surfactants were dissolved in de-ionized water (approximately 3.0 g each in 100.0 mL H_2O) at 65 +/- 2 °C while gently agitating for six hours using a magnetic stirrer. Sodium Montmorillonite (Na-MMT), also known as Wyoming Cloisite, was provided by Southern Clay Products. Modification of clay minerals by surfactants was done in a 3.0 weight-% aqueous slurry using 5.0 g of clay and 160.0 mL of de-ionized H_2O. Na-MMT has a cation exchange capacity (CEC) value of 92 mmol of exchangeable sites per 100 g. A technique adapted from Davis et al [180] was used for the synthesis of the organoclays. The 3.0 wt-% Na-MMT aqueous slurry was diluted with de-ionized water to give a 1.5 mass-% Na-MMT slurry, and then stirred at 65 °C +/- 1 °C for twenty-four hours at a high mixing speed (3000RPM). The heated aqueous surfactant solution was then added to the heated Na-MMT aqueous solution, which was followed by dilution with an additional 165.0 mL of de-ionized water. The exchange reaction continued for twenty-four hours at 65°C and at 3000RPM. After twenty-four hours had elapsed, the temperature was kept at 65°C, and the clay-surfactant mixture was filtered. The resulting organoclays were vacuum filtered using a medium-grade filter. Throughout

the filtering process, the organoclay was lightly agitated using a spatula. The filtered organoclay was washed with 65°C de-ionized water. A portion of the washed organoclay was then washed with ethanol and another with methanol. All samples were then vacuum dried at 100°C. 2)Modification of Organoclay Samples by TMI: The organoclay sample (Cloisite 20A or C20A) used in this study was manufactured by the Southern Clay Company. The maximum amount of cations per unit mass that can be exchanged by clay is defined as its cation exchange capacity (CEC). The clay layers are negatively charged due to presence of unsatisfied O^{2-} on the surface (from silicates), uncompensated internal charges, loss of inter-layer cations and OH dissociation. When clay particles are suspended in ionic solution sites, the cations in solution may replace the inter-layer exchangeable cations. The exchange of ions involves adsorption and desorption and it is an equilibrium process. Typically when clay is placed in a solution of given electrolyte, an exchange occurs between the ions of the clay (Y) and ions of electrolyte ($X_a q^{n+}$) as given in the following reaction Equation :

$$X_{aq}^{n+} + (M_y^+ nH_2O)(Al_{2-y}Mg_y)Si_4O_10(OH)_2 \rightarrow (X_{y/2}^{+2} nH_2O)(Al_{2-y}Mg_y)Si_4O_10(OH)_2] + yNa_{aq}^+ \tag{3.1}$$

At typical reaction that might have occurred in inorganic clays is as follows

$$X_{aq}^{+2} + 2RN_s^+(clay) \rightarrow X_s^{+2}(clay) + 2RN_{aq}^+ \tag{3.2}$$

where $R_1R_2R_3R_4N^+$ is the quaternary ammonium surfactant present in commercial organoclays Figure 3.1 and phosphonium present in organoclay synthesized in lab Figure 3.2. The direction of the reaction can be controlled, as it depends on the nature of TMI, ions of the clay, and their concentration. The reaction can move to the right by increasing the concentration of TMI in solution. Absorption takes place because of the attraction of positively charged ions to the negatively charged layers of clays. Depending on the charge of cation the number of cations adsorbed varies. If

a monovalent cation is exchanged with a divalent or trivalent cation, then 2 monovalent cations are exchanged for a divalent and three monovalent are exchanged for a trivalent cation. Ion exchange is also pH dependent, as cationic exchange takes place at higher pH. Solvents and transition metal salts used in this study were purchased from Aldrich Chemicals. These salts were acquired in their hydrated forms as $CuCl_2 \cdot 2H_20$ and $FeCl_3 \cdot 6H_2O$. Modified organoclays were prepared by treating the organoclay suspensions in alcohol (ethanol or methanol) by a TMI solution using the same solvent. All organoclay samples were dried in a vacuum oven at 110°C for several days. Organoclays: Washed and dried samples of each of the organoclay were placed in separate beakers. 40.0 mL of 0.30 M TMI salt solution in methanol was added to organoclays washed with methanol. 40mL of 0.30 M TMI salt solution in ethanol was added to organo clays washed with ethanol. 40.0 mL of 0.30 M TMI salt solution in dioxane was added to organoclays washed with dioxane. These were then kept for vigorous stirring for 36 hours using a magnetic stirrer. To prevent the solvent from evaporation these beakers were tightly wrapped with parafilm and then in aluminum foil. The mixture was filtered (see step c) and dried in vaccum oven for 12 hours at 80°C. These modified clays turned to various colors from the original off white. Washed or TMI-doped clays were filtered using 100mL filtration funnel with fine pore size using water pump vacuum. Aliquot from the beakers was transferred to the funnel and a vaccum was applied. Continuous stirring was performed during the filtration using a glass rod. These clays were then washed with 40.0 mL pure solvent (the choice of solvent for washing was dependent upon copper solution that will be used for exchange). Once clays were washed and filter dried they were dried in the vacuum oven at 80°C for approximately 12 hours. 3)Reduction and Drying of Modified Clay Samples: The reduction procedure for the transition metal deposits within the clays was performed as follows. 1.0 g of modified clay was subjected to washing in 20.0mL ethanol for twenty-four hours in order to remove any residual

traces of modification solution. Meanwhile, 1.0 g of $NaBH_4$ (98%, Sigma-Aldrich) was pre-dissolved in 50.0mL ethanol. After the twenty-four hour period, the modified clay was filtered, left to air-dry for another twenty-four hours, and then combined with the $NaBH_4$ solution. The reaction mixture was then left to stir for twenty-four hours. After twenty-four hours had elapsed, the reaction mixture was filtered. The filtered clay, now reduced, was then filter-washed with excess de-ionized water and then with ethanol. The washed reduced clay was then left to air dry for twenty-four hours and then vacuum dried at 100°C.

Preparing polymer nanocomposite: 1)Nanocomposites were prepared by melt blending of EVA copolymer with organoclays using a micro-processor (DACA, US). The combined weight of TMI-modified organoclay and polymer was 3.0 g per load. Mixing was performed at 170°C at 200 RPM under the flow of nitrogen. To achieve complete dispersion the mixing time was 10 min. After mixing, the polymer nanocomposite was extruded and subsequently pressed by a carver pressing apparatus at 170°C and 4000-psi pressure. Samples were left for annealing for 30 min at 170°C and were allowed to cool down to the room temperature. 2)Nanocomposites were prepared by melt blending copolymer BIMS and functionalized BIMS with the organoclay C20A only, carbon black only, C20A and carbon black together, using a Brabender micro-processor. The combined weight of organoclay and polymer was 3.0 g per load. Mixing was performed at 150°C at 40 RPM under the flow of nitrogen. The mixture was further mixed with the curatives package (stearic acid, Kadox 911, and MBTS) at 40°C and 40 RPM for 3 minutes. To achieve complete dispersion the mixing time was 10 min. Compression molding: After mixing, the polymer nanocomposite was extruded and subsequently pressed by a carver pressing apparatus at 170°C and 4000-psi pressure. Samples were left to anneal for 30 min at 170°C and were allowed to cool down to the room temperature to provide defect-free pads. Typical thickness of a compression molded pad was around 0.38 mm. For various tests different

sample dimensions were prepared. Polymer nanocomposite samples used for X-ray measurements were cuboid shaped of 4 mm x 4 mm x 1 mm dimension. The dimension of polymer nanocomposite samples used for permeability measurements were 5 mm diameter disks with thickness of 1mm, and punched out from molded pads. The Polymer nanocomposite samples used for UL- 94 flame test were cuboid-shaped samples of 127 mm x 12.7 mm x 12.7 mm dimension. The Polymer nanocomposite samples used for Limited Oxygen Index test were cuboid-shaped samples of 100.0 mm x 6.5 mm x 3.0 mm dimension.

3.3 Characterization

3.3.1 Elemental Analysis:

Element analysis for carbon, hydrogen and nitrogen was performed by Schwarzkopf Microanalytical Lab, Inc., (Queens, NY).

3.3.2 Scanning electron microscopy (SEM):

Images of clays/organoclays samples before and after modification were taken on a Jeol SEM microscope (JSU-5300). All clay samples were in the form of a fine powder and sputter-coated with gold. SEM images were taken using a back-scattering detector

3.3.3 2D and 3D Transmission Electron Microscopy (TEM):

All nanocomposite samples were cryo-microtomed at -150°C using a diamond knife to obtain sections of 100nm thickness for transmission electron microscopy (TEM). No staining was applied. 2D TEM images were acquired on a JEOL 2000FX TEM instrument at 160 kV accelerating voltage. Multiple images from various locations at different magnifications were collected to provide an overall assessment of dispersion uniformity. For 3D TEM, a FEI Tecnai TEM instrument (G2 F20 Super Twin TMP) was used. All samples were run on the scanning transmission electron microscopy

high-angle annular dark field (STEM-HAADF) mode to minimize the sample damage while maximizing the contrast. The image acquired in such a way is also known as STEM-HAADF tomography. During the measurements, the sample was tilted from a 0 degree angle to 60 degrees, which took about 90 min, and the samples were tilted back from 0 to 60 degrees, which took another 90 min. The total exposure time was 3 hrs. The images were reconstructed using the Voltex 3D volume rendering software.

3.3.4 Thermal Properties:

Thermal gravimetric analysis (TGA) measurements were performed using a TA 7 thermal analyzer, manufactured by Perkin Elmer. All measurements were carried out in the temperature range of 40°C to 900°C and at a heating rate of 20°C/min. Data collection for TGA for all nanocomposite samples were taken under identical conditions.

3.3.5 Synchrotron X-ray Scattering/Diffraction:

SAXS (small-angle X-ray scattering) measurements were performed using 1D linear position sensitive detectors (EBML, Grenoble, France) at beamline X27C in the National Synchrotron Light Source (NSLS), Brookhaven National Laboratory (BNL). The chosen X-ray wavelength was 1.371 $\AA$. For SAXS measurement, the sample to detector distance was fixed at 800-820 mm and the scattering angle in SAXS was calibrated using silver behenate. X-ray measurements for all nanocomposite samples were taken under the same conditions by changing the orientation of the film with respect to the beam at two different angles. The direction of the beam hitting the sample, normal to the plane of film has been called "face-on" direction and if parallel with respect to plane of the film is called "edge-on" as shown in Figure 3.4. Two-dimensional X-ray patterns were acquired using imaging plates manufactured by Fuji Company. 1-D patterns were then obtained by integrating 2D images using the Polar software developed at Stony Brook Technology and Applied Research (Stony Brook,

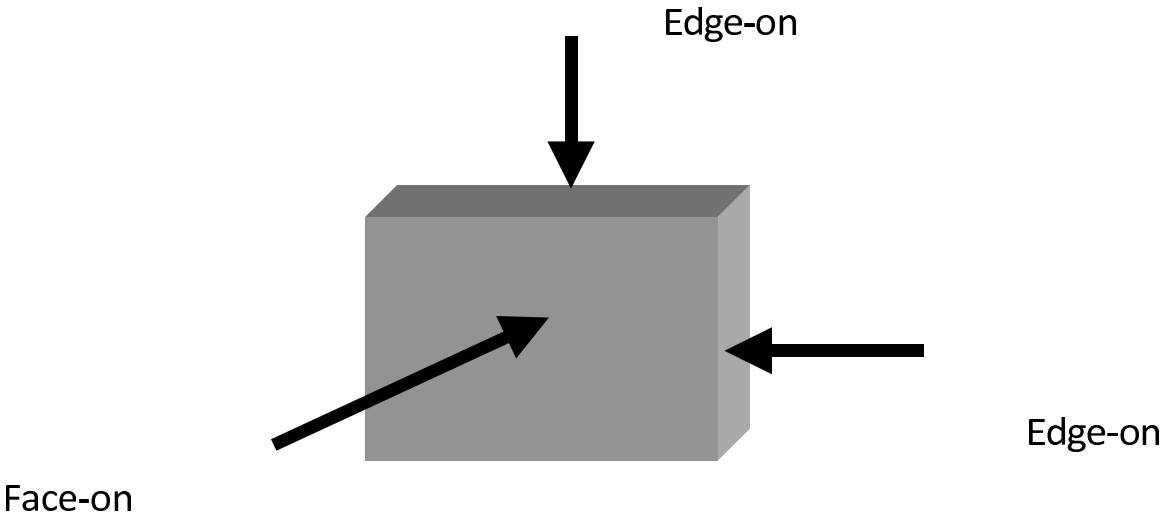

Figure 3.4: Shows beam position with respect to the plane of the sample, edge-on and face on.

NY). To collect X-ray data while *in-situ* heating, an indigenously-built oven was used to heat samples to desired temperatures.

3.3.6 Permeability Tests:

EVA nanocomposites were compression molded into films at 150°C and cured. Five-centimeter diameter disks were punched out from these cured pads and compression-molded films and conditioned in a vacuum oven at 40 or 60°C overnight prior to the permeability measurements. Oxygen permeation values at 60°C for elastomer cured pads and at 40°C for polymer nanocomposite films were acquired using a Mocon OX-TRAN 2/61 permeability tester. Due to the relative higher permeability values of polymer nanocomposites, a lower temperature was employed for better sensitivity of the permeability measurement. Five-centimeter diameter disks of various nanocomposites containing either clay, carbon black, or both were conditioned overnight prior to the permeability measurements. Disks were tested for oxygen permeation measurements were performed on using a MOCON OX-TRAN 2/61 permeability tester at 40°C with nitrogen on one side of the disk at 0.07 MPa(g) (10 psig) and 0.07 MPa(g)

(10 psig) oxygen on the other. The time required for oxygen to permeate through the disk, or for oxygen concentration on the nitrogen side to reach a constant value, was recorded and used to determine the oxygen permeability. Due to the relative higher permeability values of polymer nanocomposites, a lower temperature was employed for permeability measurement for better sensitivity.

3.3.7 UL-94 Vertical flame test:

As per the UL-94 guidelines, ASTM D 3801 standard samples were prepared and were stored in a desiccator for approximately 48 hours. UL- 94 flame tests were performed as per the standard guidelines. The temperature of the room in which the samples were held was 24 C and the humidity range of the room was determined to be 45-75% at that particular time. Samples were immediately tested after being removed from the desiccator. There was no air draft in experimental chamber and flame was calibrated before applying to samples. The vertical burning test was carried out for each sample. To ignite the bunsen burner purified methane was used and the methane gas flow rate was maintained at 105 ml/min throughout the experiment. The flame of bunsen burner was calibrated and the height of the blue flame was maintained at 20 mm, in accordance with UL standards. For each of polymer nanocomposite sample, five samples were suspended vertically over surgical cotton and were ignited by a pre-calibrated flame of the bunsen burner. The calibrated flame was applied twice to the lower end of the specimen for 10 s. After the flame tests were performed, the nanocomposites could be then classified as V-0, V-1, or V-2 materials, described later.

3.3.8 Limited Oxygen Index (L.O.I.):

The L.O.I. test to find the lowest oxygen concentration was performed in a standard chamber designed according to the standard ASTMD 2863-97. Standard samples were prepared and were stored in a dessicator approximately 48 hours before tests.She sample was supported vertically in a controlled atmosphere, with a mixture of oxygen

and nitrogen flowing upwards through a transparent chimney. A bunsen burner was used to ignite the upper end of sample bars in the pre known concentration of Nitrogen and Oxygen and the flame was removed upon the ignition of sample. The concentration of oxygen in L.O.I. machine was raised if the specimen extinguished either before burning, for 3 minutes or 5 cm in length. The oxygen content was adjusted until the limiting concentration was determined. The inflow of gases were maintained at a constant pressure and any reduction in the partial pressure (concentration) of oxygen is balanced by a corresponding increase in the partial pressure (concentration) of nitrogen. L.O.I. is more commonly reported as a percentage rather than fraction and the values were calculated following the scheme given in ASTMD 2863-97.

Chapter 4

Results and Discussion

In following chapters we will discuss in detail the various results based on our experimental findings. These results have been discussed in various sections, each concentrating on different aspects of fillers and polymer nanocomposites.

Section 4.1 will detail the results of structural analysis of various cays.Also the effect of various environments on the structure of different kind of clays was evaluated.

Section 4.2 will discuss results of the orientation of clay dispersed in the polymer matrix and the effect of various weight percents of clay added to the polymer on orientation of clay. We will also discuss the relationship of clay orientation and the permeability of polymer matrix.

Section 4.3 will discuss the results of inductive effect of carbon black on the morphology and orientation of clay, as well as the synergistic effect of the two fillers on the permeability of polymer matrix.

Section 4.4 will in discuss in detail the thermal stability of organoclay and transition ion modified organoclays, and the effect of modified organoclays on the flame retardant properties of polymers.

4.1 Structure of clay

In this study we have evaluated structure of two organoclays Cloisite 20A and Somasif MAE which we have used to make polymer nanocomposites in our further study. We have utilized a variety of experimental techniques including, thermal gravimetric analysis (TGA), scanning electron microscopy (SEM), and small-angle X-ray scattering

(SAXS), to elucidate the structure of organoclays and their thermal behavior. We have also evaluated the effect of microwave and solvent on the structure of clay, using small angle X-ray scattering.

4.1.1 Element Analysis

The results of elemental analysis of organoclays are listed in Figure 4.1 (Table). It was observed that montmorillonite (MMT) mineral contains a significant amount of Fe which is present as structural iron. This is attributed to the fact that MMT was pre-treated by the manufacturer to remove exchangeable ion contaminant. We thus suggest that iron present in MMT mineral exists in the ionic form within the clay lattice (structural iron). On the other hand, Fe content in Cloisite 20A (C20A) organoclay tested as received from manufacturer is even higher than in the original mineral. This unexpected result suggests that C20A traps additional iron during processing. Somasif MEE 100 (SME100) and Somasif MAE (SMAE) contain less than 0.2% of Iron and Aluminum. Magnesium is replaced by Aluminum which is present in the lattice of MMT and also the apical hydroxides are of MMT are replaced by Fluoride in Somasif based clays. The overall surfactant content (calculated from combined C, H and N concentrations) in Organoclays C20A and SMAE systems corresponds to the value calculated for di-methy di hydrogenated tallow quaternary amine chloride (DMDHTA) surfactant. This suggests DMDHTA as the major organic component in modified organoclays. This value of DMDHTA in organoclays C20A and SMAE is more than the cation exchange capacity of their mineral clay counterpart MMT and SME100 respectively, which suggest that there is an excess of unbound surfactant molecules attached via van der Waals forces.

4.1.2 Scanning Electron Microscopy (SEM)

In MMT and C20A, there is abundant octahedral Al and limited tetrahedral charge is there. The SEM images of both clays as shown in Figure 4.2 and Figure 4.3, depict

Material Analyzed	MMT	C20A	SME 100	SMAE
Carbon	0.36	28.89	0.2	32.25
Hydrogen	1.18	5.82	0.92	5.66
Nitrogen	<0.01	0.95	<0.01	1.03
Aluminum	3.03	4.39	0.08	0.18
Iron	0.90	1.20	<0.01	<0.01
Magnesium	1.22	0.82	9.69	9.77
Fluoride	0.00	0.00	5.58	5.59

Figure 4.1: Elemental Analysis results for C20, Washed C20, Cu & Fe modified C20

thin transparent flakes with warped edges The 'house of cards' morphology along with the sharp edges distinguishes MMT based clays. Smectites also forms typical honeycomb, cornflakes or rose-like textures.

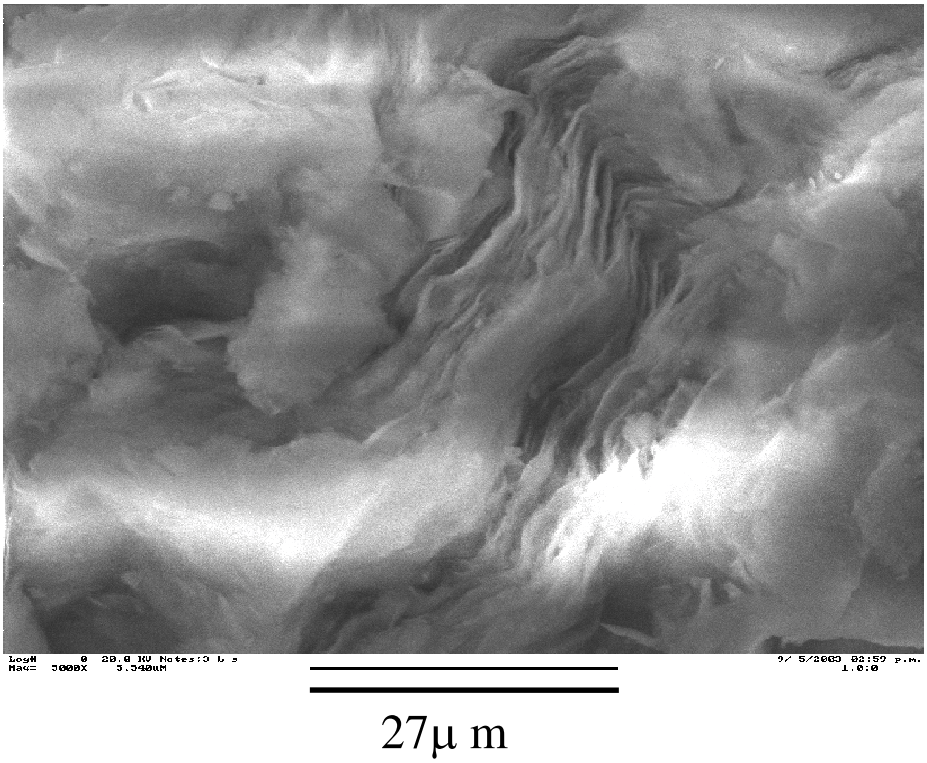

Figure 4.2: SEM images of mineral clay Montmorrillonite.

In SEM results, Somasif based clays can be distinguished by the presence of tubular structures as shown in Figure 4.4 and Figure 4.5. SME100 and SMAE exhibited a significant amount of needle-like tubular structures along with clay platelets. These tubules were 200-300 nm in diameter and 3-10 nm in length. We hypothesize that the tubular structures may be formed as a by-product of the SME100 synthesis and can be considered as the synthetic analogs of naturally occurring tubular chrysotile minerals, $Mg_3Si_2O_5(OH)_4$.

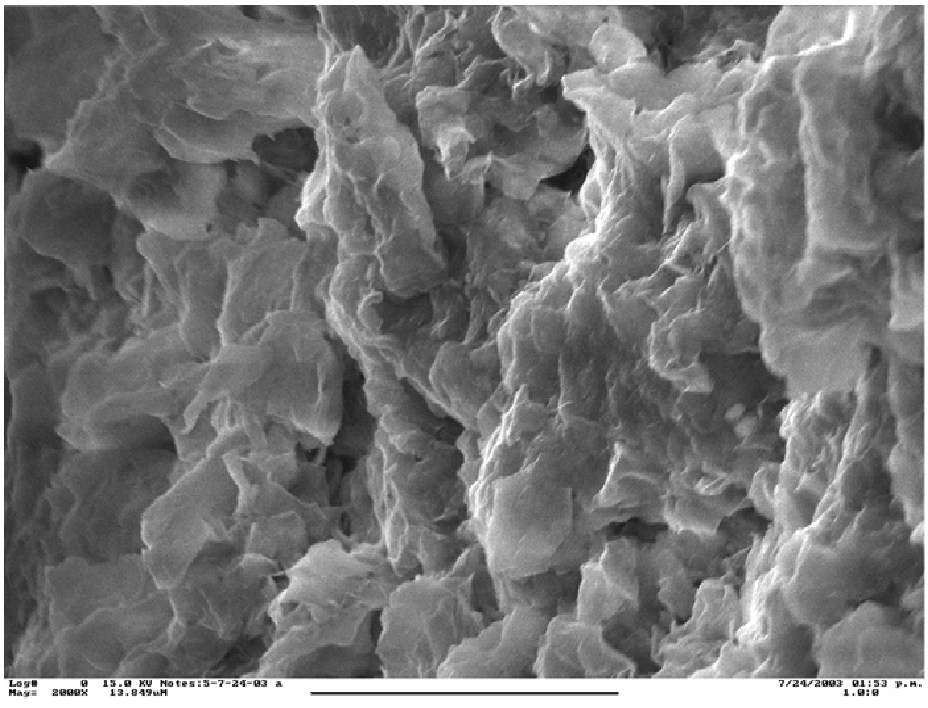

Figure 4.3: SEM images of organoclay Cloisite C20A.

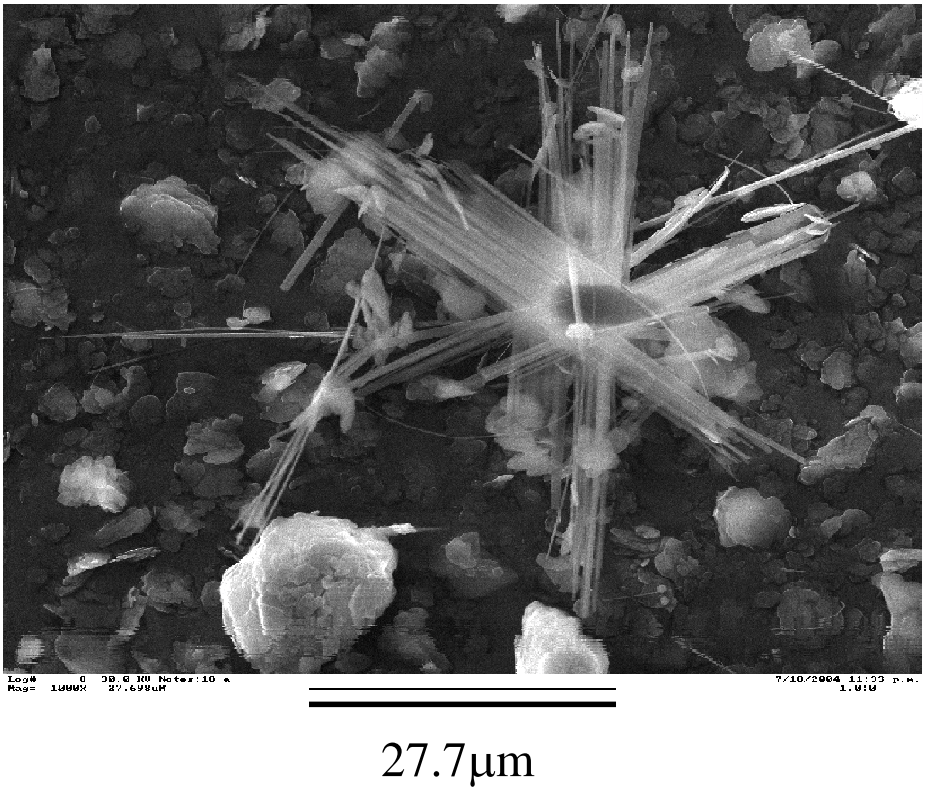

Figure 4.4: SEM images of mineral clay Somasif (SMEE).

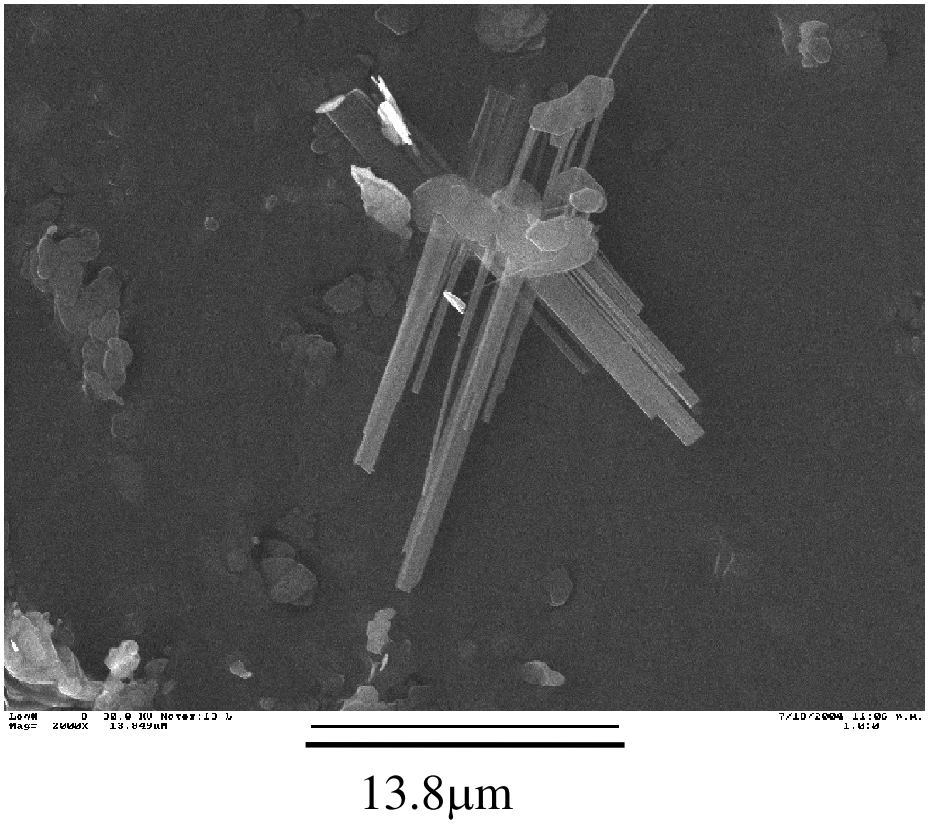

Figure 4.5: SEM images of organoclay Somasif MAE.

4.1.3 Thermo Gravimetrical Analysis (TGA)

Figure 4.6 illustrates the TGA thermograms of mineral clays (MMT and SME100), corresponding modified organoclays (C20A and SMAE), and surfactant DMDTA, used for modification of these clays. TGA thermograms were collected under the flow of nitrogen. It is seen that a small but distinct weight loss below 100^{o}C exists in all TGA profiles, which can be attributed to the desorption of residual water molecules present in the clays and it is evident from thermograms that MMT and C20A contain more residual water. This can be attributed to the apical hydroxide groups present which undergoes extensive hydrogen bonding to retain water in their structure. In ramping TGA thermograms, the behavior of weight loss below 200°C in air is similar for all clays.

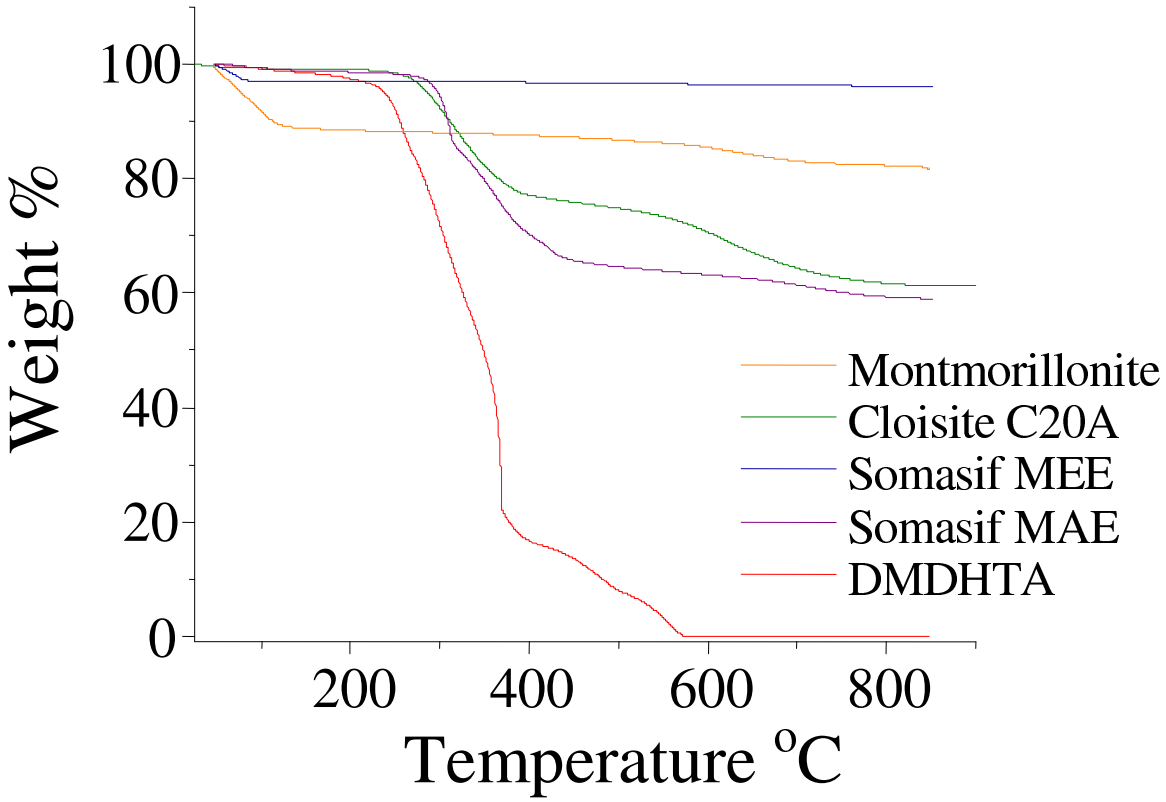

Figure 4.6: TGA thermo gram of organoclays and surfactant present in the organoclays.

The relative weight loss below 250°C increases with the overall surfactant content (SMAE > C20A), which is consistent with the higher content of excess (adsorbed above CEC) surfactant. It is interesting to note that the rate of weight loss is in the temperature range 400°C < T < 500°C and this may be related to the charring resulting from the oxidative dehydrogenation of the organic phase, promoted by the catalytic properties of the clay surface. The reaction can result in the formation of a thermally stable carbonaceous char from the organic component in organoclays. From TGA thermograms shown in Figure 4.6 we can say that the major loss of surfactant begins at about 250°C, indicating the escape of some of the free surfactant molecules. At 320°C, all tested organoclays exhibited a weight loss accounting for 30-35 wt % of organic component (or 10-17 wt % total). This finding can be attributed to the escape of surfactant molecules due to the dissociation of electrostatic complex formed between surfactant molecules and clay surfaces and/or the thermal and oxidative degradation of surfactant molecules. It is interesting to see that SME100 did not undergo structural dehydroxylation above 600°C, in contrast to MMT. The observed high-temperature stability in SME100 may be attributed to the substitution of hydroxyl groups for fluoride, as a result MMT will hold more residual hydrogen-bonded water molecules and desorption of strongly bound water takes place at a higher temperatures. We hypothesize that water may be located around cationic head groups of organic components present in organoclays SMAE. The water adsorption phenomenon was also consistent with the small weight loss in the region of 140-200°C for all Somasif samples.

4.1.4 Structure and morphology by X-ray scattering

Figure 4.7 and Figure 4.9 exhibits selected integrated SAXS profiles collected at various temperatures of two different organoclays C20A and SMAE, respectively. It is interesting to see that the SAXS profiles acquired at room temperature in these samples bear a similar trait of multiple peaks. In C20A the lamellar peaks in SAXS

profile do not appear at equidistant positions on the s scale as shown in Figure 4.7, which is the characteristic of the so-called interstratified system, where multiple layers of different thicknesses can coexist in the same clay stack. SAXS profile of SMAE showed distinct scattering peaks Figure 4.9, which were very different from those observed in cloisite-based organoclays. At first sight, the scattering profiles of the SMAE organoclay appear to be complicated mixtures of different structures. In following section we will discuss SAXS analysis for these two organoclays at high temperature by analyzing their thermally resolved *in-situ* X-ray data.

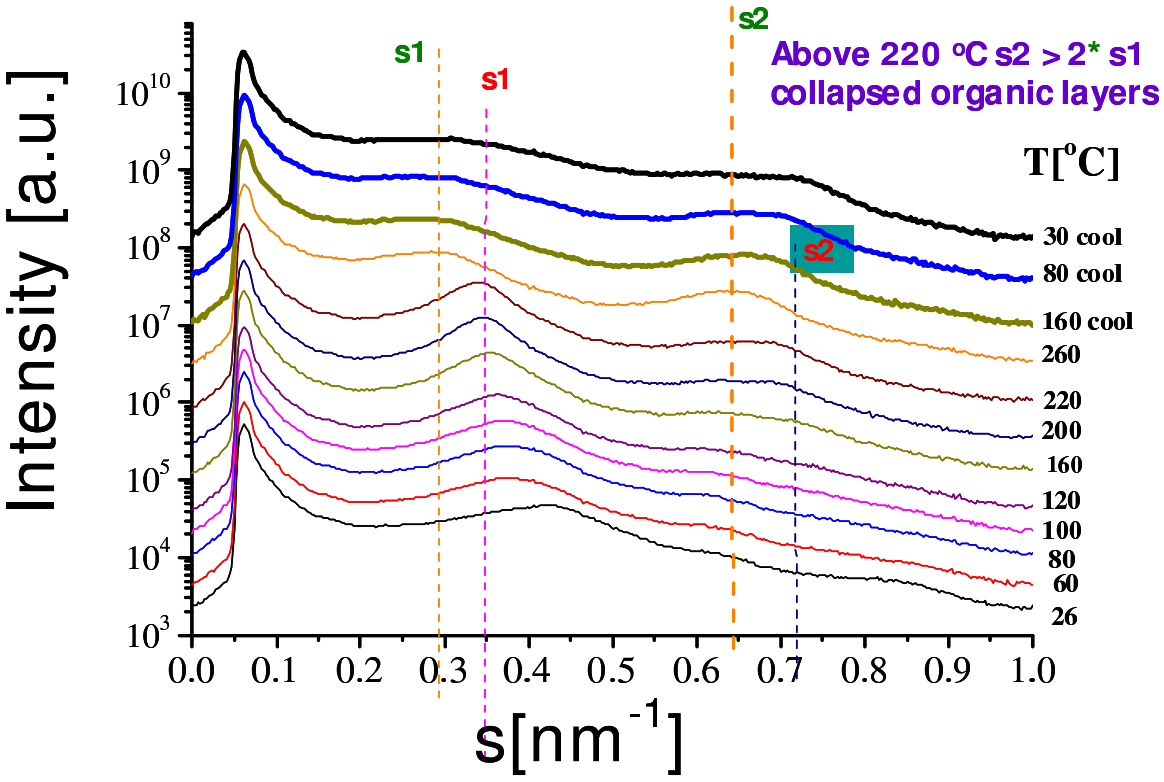

Figure 4.7: Thermally resolved integrated SAXS profiles of Cloisite C20A organoclay.

With the increase in temperature, SAXS profile of C20A undergoes a drastic change (Figure 4.7) and the exact nature of this change depends on the surfactant content. In the *in-situ* X-ray profiles of C20A we can identify three different temperature zones Figure 4.7: (1) A low-temperature (room temperature) curve, where

s2 < 2s1; SAXS peaks are not equidistant on the s scale. To be more specific, the position of the second scattering peak at s2 is less than twice of the position of the first scattering peak s1 (s2 < 2s1). Also it is seen that at ambient temperatures in C20A thinner and thicker organic layers coexist with fused mineral layers. This may be attributed to the structural heterogeneity of MMT. Indeed, while the overall surfactant content in C20A corresponds to 100% of cation exchange capacity in MMT, the structural heterogeneity of a mineral may result in coexistence of non intercalated mineral layers with layers having excessive surfactant content. (2) In the zone two within the temperature range of 40 -180°C, the scattering peaks become narrow and the positions of the peaks shift toward equidistant (s2 = 2s1). For two intermediate temperature curves (collected at a temperature 60 and 160°C) in (2), where s2 = 2s1, a unimodal layer thickness distribution is observed for C20A organoclays, while scattering peaks shift toward equidistant position, s2 remains less than 2s1. (3) In the zone three within the temperature range of 180-260°C, significant surfactant loss is observed. In this zone the scattering peaks broaden and become non-equidistant again. However, in this case, the position of the second peak (s2) shifts toward higher s values than twice that of the position of the first scattering peak s1 (s2 > 2s1). Furthermore, the corresponding layer thickness distributions may be described as bimodal, consisting of a single Gaussian mode for the surfactant-intercalated layers and a delta thickness distribution (from the fused tactoid). It is interesting to see that the fractions of the fused tactoid becomes 35% for C20A at 260°C, which is consistent with the corresponding weight losses detected in the staged TGA thermograms (Figure 4.6. It is interesting to see that upon cooling from 260 to 30°C (as in Figure 4.7), the scattering peaks remain nonequidistant on the s scale, with s2 > 2s1 which indicates that the original layer structure in organoclays is permanently lost. In as-received C20A organoclay, the scattering peaks are non-equidistant at the s scale, indicating the existence of dual thickness distributions of organomineral

layers, where some layers overloaded with surfactant above the average CEC coexist with layers of lower surfactant content in the same stacks. In agreement with the TGA results, temperature-resolved SAXS profiles showed that the as-received C20A organoclay underwent rapid degradation above 200°C, which manifested itself by the broadening and shifting of the scattering peaks (Figure 4.7). Results of our SAXS modeling detailed elsewhere [7] suggests the coexistence of two distinct populations of organic layers, having various thicknesses in different temperature zone 1 where the thinner layer represents the structure of a monolayer of surfactant molecules bound to the adjacent mineral surfaces (Figure 4.8). The monolayer structure is due to the hydrophobic aggregation of surfactant tails in the organic layers. The thicker organic layer consists of two monolayers of surfactant molecules (we termed it, the double-layer structure) with only about half of them bound to the mineral surfaces (Figure 4.8). The free (nonbound) surfactant molecules are held in the silicate gallery by van der Waals forces through aggregations of their hydrophobic tails. In temperature zone 2, the collapse of the double-layer structure leads to the formation of a unimodal thickness distribution in organic layers. This mechanism can be accounted for by the fact that electrostatic interactions between the surfactants and clay surface are much stronger than the van der Waals forces between the surfactant layers. Thus, the complexation between the surfactant and clay surface should be much more thermally stable than the layer-layer interactions. Thermal stability of individual organic layer in organoclays may vary significantly due to the structural heterogeneity of MMT mineral. Consequently, thermally less stable layers may be degraded and deplete the organic component significantly than the remainder of the material. It is interesting to see that upon cooling from 260 to 30°C (as in Figure 4.7), the scattering peaks remain non-equidistant on the s scale, with $s2 > 2s1$, which indicates that the original layer structure in organoclays is permanently lost. From the X-ray profile of SMAE as shown in Figure 4.9, the most striking feature is the presence of a weak scattering

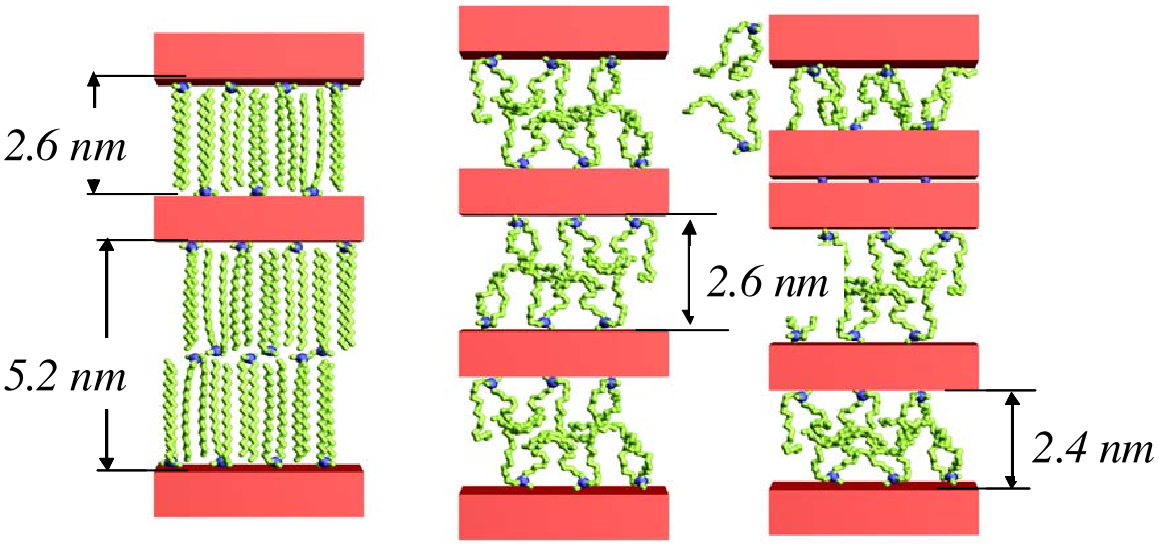

Figure 4.8: Bimodal thickness distribution for the surfactant layers in organoclays where both interdigitated and non-interdigitated surfactant layers were found within the same stack [7].

maximum (marked by an asterisk) at around one half (and also at three halves) of the position of the intense peak associated with the lamellar long spacing. Such a peak is located at s = 0.15 nm^{-1} for SMAE. Since the silicate layers are assumed rigid and inert (i.e., not undergoing any conformational change, chemical transformation or density change), the most likely explanation for the occurrence of this peak is a small translational displacement of neighboring layers, leading to the formation of loosely coupled pairs. This structure is similar to the "Peierls effect". in solid state physics (of course, the origin of the classical Peierls effect is quite different from the one observed here, but we still refer to the phenomenon in this study as "Peierls-like" for its striking similarity). In other words, the presence of the above unique scattering peak indicates a breaking of translational symmetry and a doubling of the repeat period in the 1D lattice, spanning over two basal spacings.

A possible explanation for the Peierls-like lamellar structure is that in a stack of organoclay, we assume each silicate layer has two different surfaces, visualized as dark and light in Figure 4.10. The stack contains alternating surfaces so that light

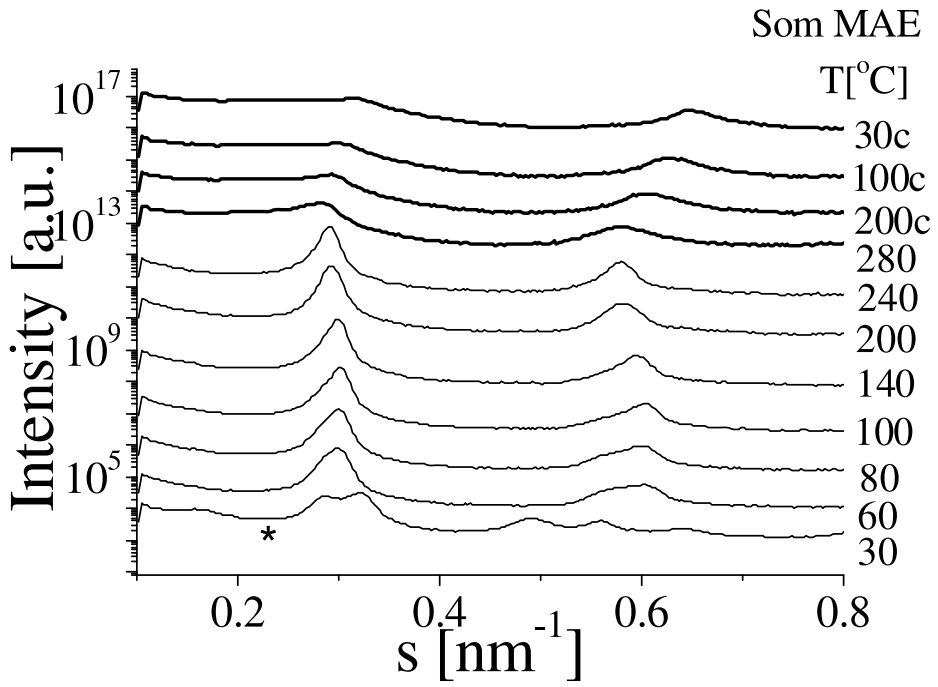

Figure 4.9: Thermally resolved integrated SAXS profiles of Somasif MAE organoclay.

and light, and dark and dark surfaces, respectively, are facing each other. Figure 4.10 illustrates three possible arrangements for the stack. The stack with a single organic layer thickness possesses an equidistant period of either all long (AA-type) or all short (BB-type) long spacings, as illustrated in Figure 4.10a and c, respectively. If the stack possesses an alternating sequence of long and short organic layer thicknesses, we refer it as the Peierls-distorted stack with AB-type periodicity Figure 4.10b. This alternating stack structure is intercalated by organic layers that, for reasons yet to be determined, preferably assume one of two possible discrete thicknesses. At 30 °C, the first-order maximum in SMAE Figure 4.10b clearly consists of two peaks centered at 0.28 and 0.33 nm^{-1}, respectively. Similar splitting of a second-order maximum (at 0.32 and 0.64 nm^{-1}) suggests the presence of at least two independent lamellar systems: α (s1α = 0.28 nm^{-1}) and β (s1β = 0.32 nm^{-1}).

The presence of a weak peak at 0.16 nm^{-1} indicates the Peierls distortion in the β lamellar system. At 50°C, the Peierls peak disappears and the two split first-order

a)

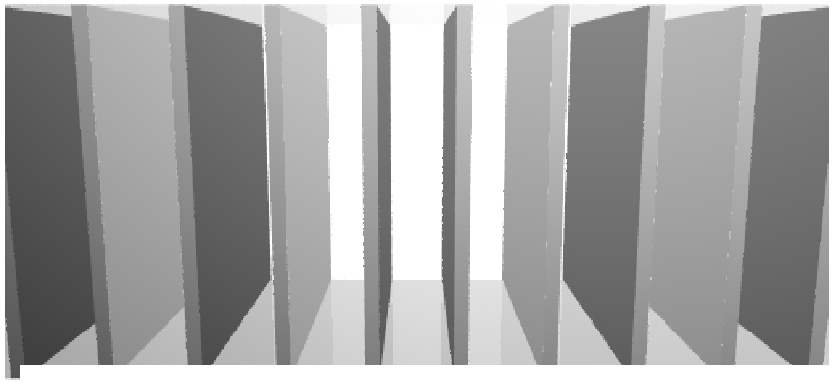

b)

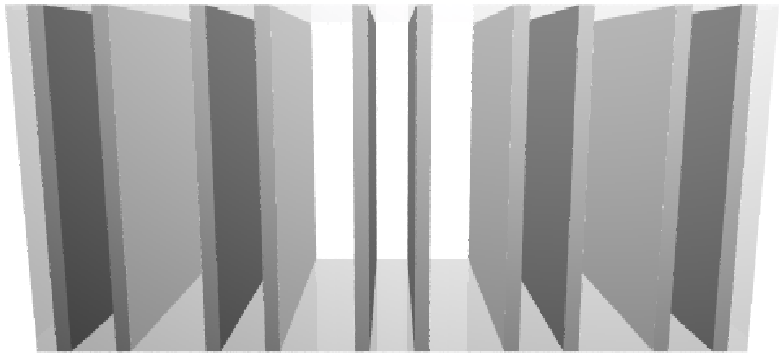

c)

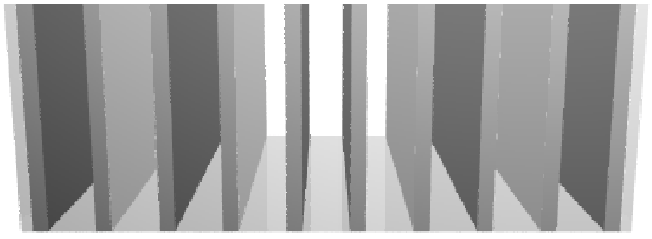

Figure 4.10: Somasif MAE “Peierls distorted stack“ [183].

peaks merge into a sharp symmetric peak having Lorentzian characteristics (the peak is centered at s = 0.3 nm^{-1}). With the further temperature increase, the first-order SAXS peak is shifted towards a lower s value (e.g. at 260°C, the peak is centered at s = 0.26 nm^{-1}). Components of the asymmetric second-order SAXS peak, initially centered at 0.6 nm^{-1}, also gradually merge as temperature increases. At 180°C, the second-order peak becomes symmetric and positioned at the s value exactly twice the position of first-order peak, which is indicative of a unimodal layer thickness distribution. As temperature increases to 280°C, the SAXS peaks become weaker and non-equidistant with s2 > 2*s1, indicating some organic layers are collapsed as a result of the thermal degradation of DMDHTA. Similar structure changes (i.e., the weakening of scattering signals and the re-occurrence of non-equidistant peak positions) have also been observed in the C20A. As temperature decreases from 280 to 30°C during cooling, the SAXS maxima become broader and shifted towards higher s values, indicating the decrease in the long spacing that is consistent with the surfactant loss. The Peierls peaks cannot be observed in the scattering profiles from the cooled SMAE samples. It appears that the surfactant degradation results in the loss of AB-type periodicity (i.e., the Peierls alternating stack).

4.1.5 Optical activity of Organoclays suspension

Dispersion of organoclay is observed when a lower weight percentage of organoclay is dispersed in solvent and as the weight percentage of the organoclay is increased the gelation of clays occurs as shown in Figure 4.11. Also at the higher concentration of organoclay in solvent color of suspension changes which might be possibly due to reaction between solvent and surfactants. Increased gelation or better dispersion is not measure of exfoliation. In short, we observe that the homogeneous dispersion of organoclays can be assisted by higher polarity of the solvent. However, the very high polarity can also hurt the dispersion behavior. Suspensions of lamellar stacked clay particles can be dispersed, flocculated, or exist as a mixture of both states. Three basic

modes of particle association may occur: face-to-face (FF), edge-to-face (EF), and edge-to edge (EE). The FF association will lead to thicker flakes (tactoids). The EF association may involve the reaction of the edge -OH group of the nanolayer with the ammonium ion on the organoclay surface. The EE association involves the hydrogen-bonding interactions between the edge -OH groups. The EF and EE association will produce three-dimensional, voluminous card-house structures, which can result in a gelatin like viscous suspension. Also, at higher concentrations of organoclay in solvent, the color of the suspension changed which might be possibly due to the interaction or reaction between solvent and surfactants.

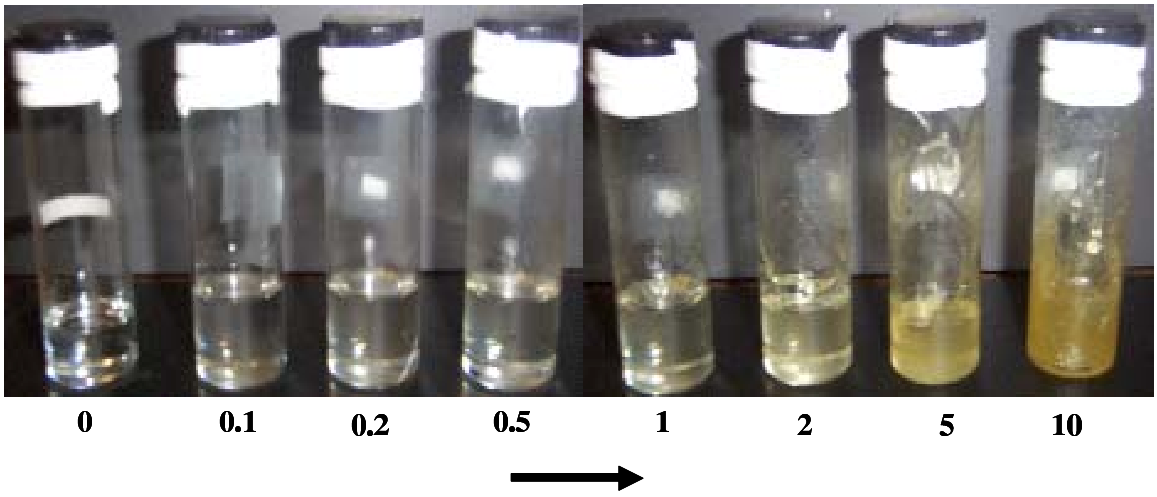

Figure 4.11: Photographic evidence of dispersion of C20A in Toluene.

4.1.6 Structure analysis of dispersion using SAXS

SAXS profiles of different concentrations of organoclay C20A dispersed in Toluene and Methyl Ethyl Ketone (MEK) is illustrated in Figure 4.12, Figure **??**, and Figure **??**, respectively. Photographic results of C20A dispersed in toluene Figure 4.11 suggest that the clay dispersion is concentration dependent. Transparent or cloudy dispersion of organoclay was observed at lower concentrations of organoclay in Toluene, but gelation occurred as the wt % of the organoclay is increased. Increased viscosity is

not a measure of clay exfoliation in the solvent; hence we rely on the SAXS analysis to probe the structure of organoclay dispersed in various solvents. The concentration dependence of the organoclay structure in varying solvents was carefully studied by SAXS. Figure 4.12 shows the integrated results of SAXS data for the dispersion of C20A dispersed in Toluene, MEK and suspension of SMAE in MEK.

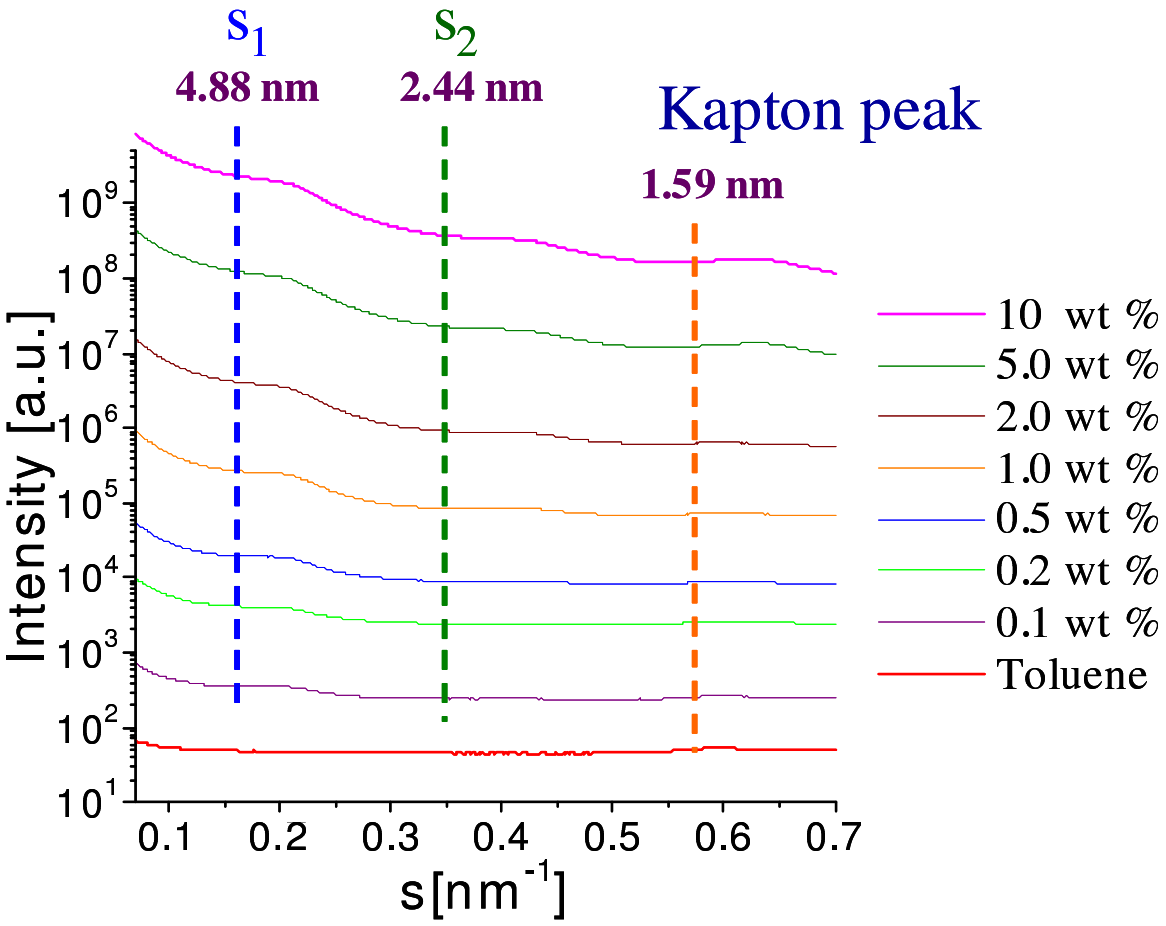

Figure 4.12: Integrated SAXS profiles of C20A dispersed in Toluene.

Based on the integrated scattered intensity data in Figure 4.11 and Figure 4.14, we observe lamellar peaks arising from clay stacks at all weight percents of C20A dispersed in toluene. First and second order peaks were observed even at higher weight percent (10%) dispersed in Toluene. The *d*-spacing of C20A in dry powder state is 2.44 nm and it was observed to increase to 4.88 nm upon dispersing in Toluene. This suggests that, in Toluene, intercalation takes place and the solvent penetrates the

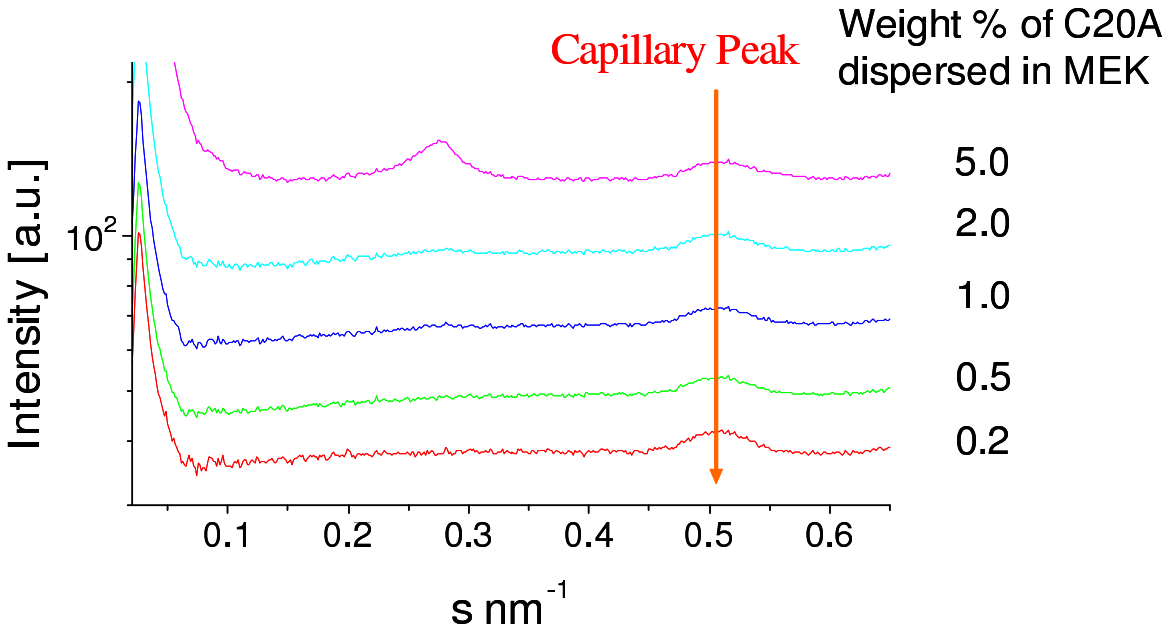

Figure 4.13: Integrated SAXS profiles of C20A dispersed in Methyl Ethyl Ketone.

layers without breaking the clay tactoids as is evidenced by the appearance of the lamellar scattering peaks. Hence we can visualize that lamellar stack of C20A remains intact with expanded *d*-spacing which is possible due to salvation of surfactants in presence of Toluene. In the case of MEK, there were no lamellar peaks observed at lower weight percents of C20A, but the peak due to lamellar stacks re-appears with increasing weight percent or concentration of C20A dispersed in MEK. This suggests that, in MEK, organoclays may possibly be exfoliated at lower concentrations, or at least that the periodicity of clay stack is completely lost, while the extent of exfoliation may decrease with increasing the clay concentration. In case of Somasif MAE dispersed in MEK we don't observe any peak even at concentrations as high as 5 wt%. This can be attributed to an excess of surfactants in SMAE (45 wt %) while in C20A its only 35 wt%. The surfactants from SMAE possibly solvates and forces the clay stacks apart resulting in exfoliation of clay stack or at least loss in complete periodicity of the clay stacks.

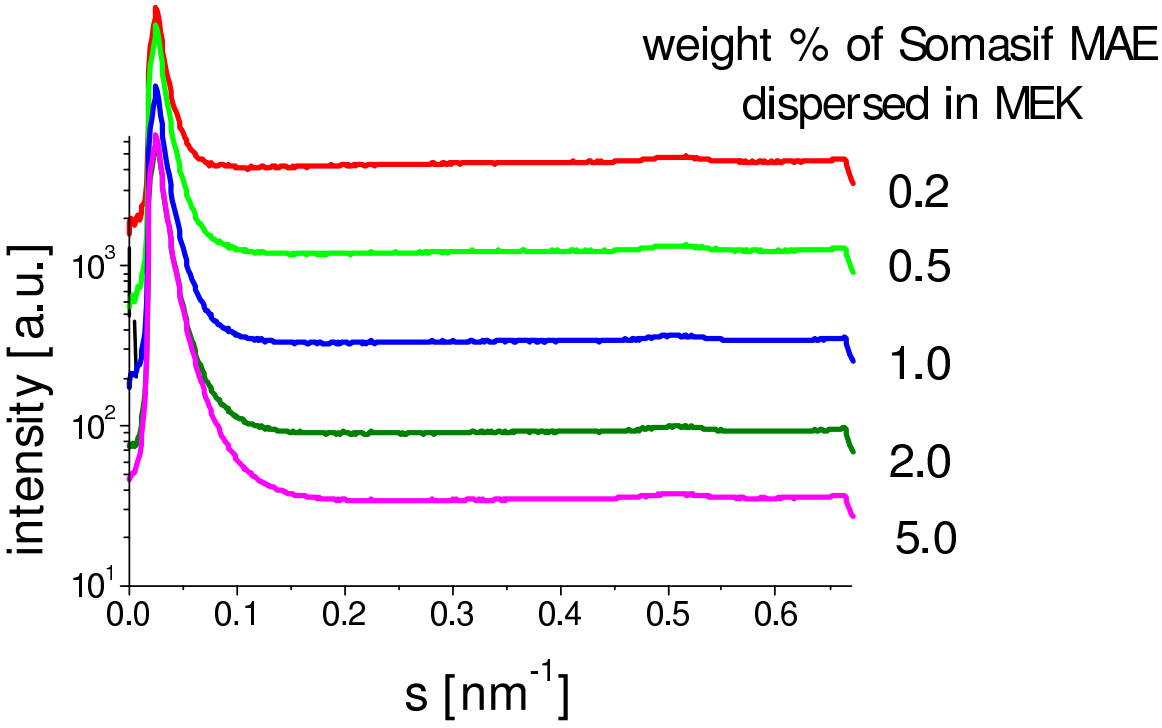

Figure 4.14: Integrated SAXS profiles of Somasif MAE dispersed in Methyl Ethyl Ketone.

4.1.7 X- ray analysis of microwave irradiated clays

Dried powder of smectites (MMT and C20A) and flourohectorites (SME100 and SMAE) were subjected to microwave irradiation for different length of time. Integrated SAXS profiles of all clays irradiated with Microwaves are illustrated in Figure 4.15etc.. From SAXS data we don't observe any structural changes in any of these clays except for SMAE, as shown in Figure 4.18. With irradiation of SMAE by Microwaves, initial increase of *d*-spacing is observed and as the irradiation time is increased (from 30s to 70s) clay lamellar peaks broadens suggesting that the clays stacks are broken into small tactoids. When irradiated for an even longer time (78s) periodicity of stack is completely lost or clay is completely exfoliated. This can be attributed to the change in conformation of surfactants that might occur in the presence of Microwaves. We hypothesize that the surfactants in SMAE are in a particular

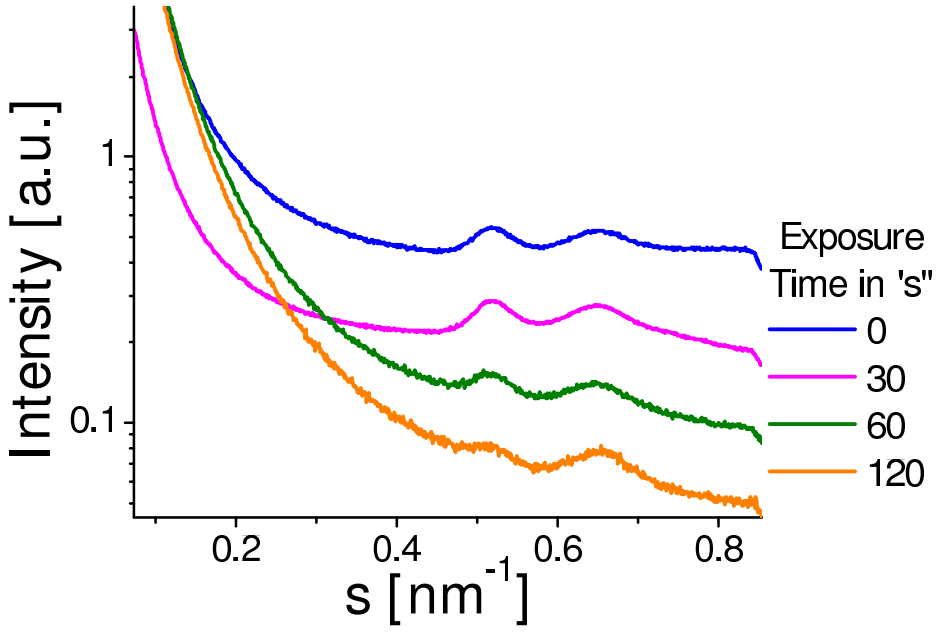

[htbp]

Figure 4.15: Integrated SAXS profiles of mineral clay Montmorillonite irradiated with Microwaves.

(random coil) conformation and they can act as a dipole. In the presence of microwaves these surfactants change their conformation to a stretched chain and the stretching of surfactants causes increase in the *d*-spacing initially and finally when the electrostatic energy holding the clay is overcome due to separation of the layers, the clay stack is broken into individual clay platelets. Another possibility is that super heating might take place within the clay layers, which might result in exfoliation of stacks as the energy generated will be enough to overcome the electrostatic barrier that holds the clay.

Microwave-irradiated SMAE clays were dispersed in Toluene, as we observed in the case of C20A dispersed in Toluene no exfoliation takes place shown in Figure 4.19 attributed to higher surface energy of Toluene. Lamellar peaks were observed for all microwave irradiated SMAE except for the one irradiated for 70s. The suspension of this sample doesn't show any clay peak suggesting that due to microwave irradiation the surfactants were already stretched and upon introduction of solvent these

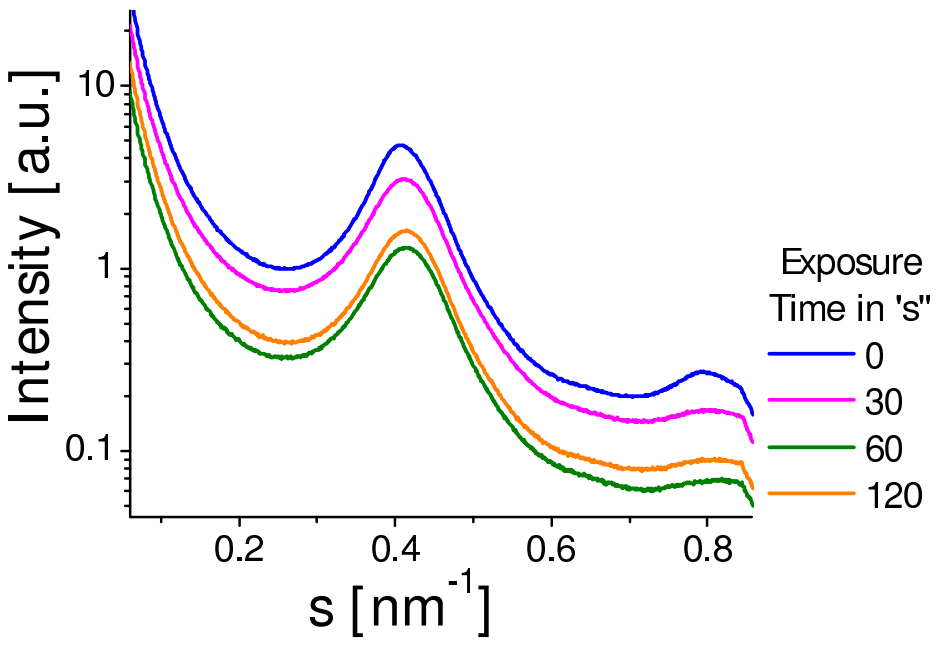

Figure 4.16: Integrated SAXS profiles of organoclays C20A irradiated with Microwaves.

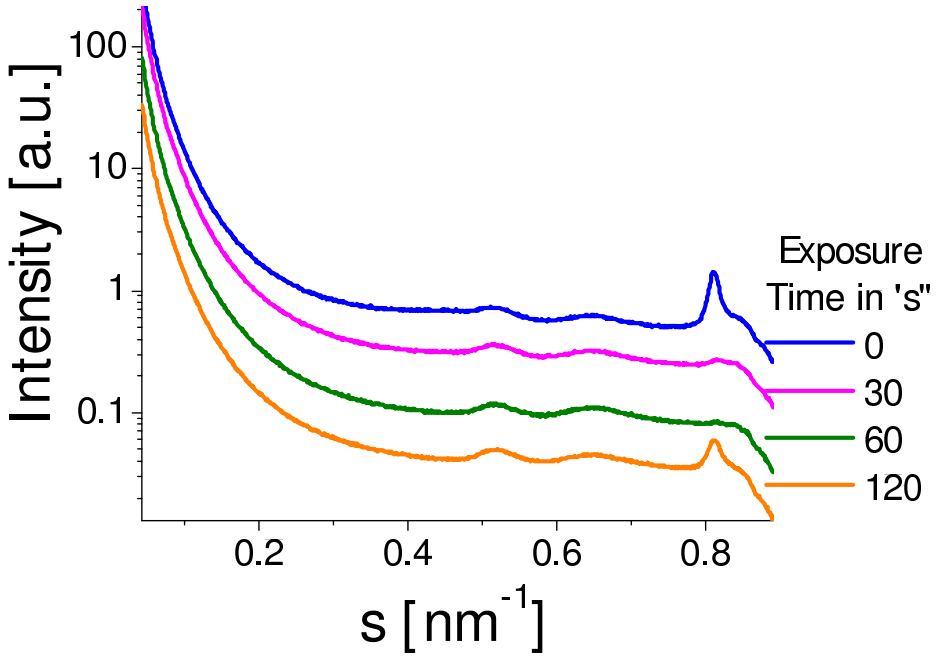

Figure 4.17: Integrated SAXS profiles of mineral clay Somasif MEEE irradiated with Microwaves.

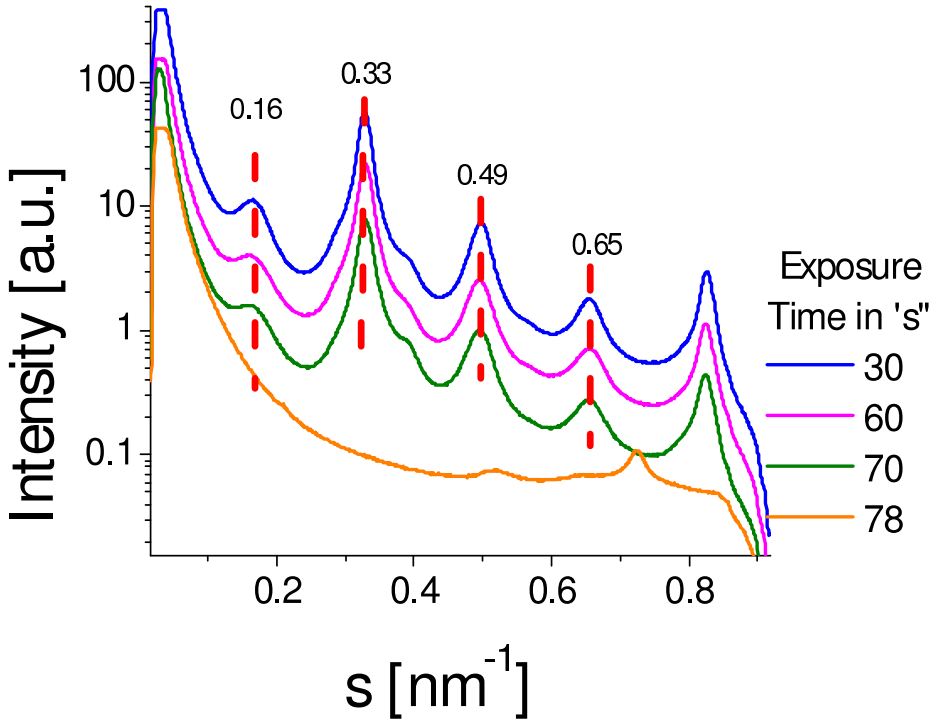

Figure 4.18: Integrated SAXS profiles of organoclays Somasif MAE irradiated with Microwaves.

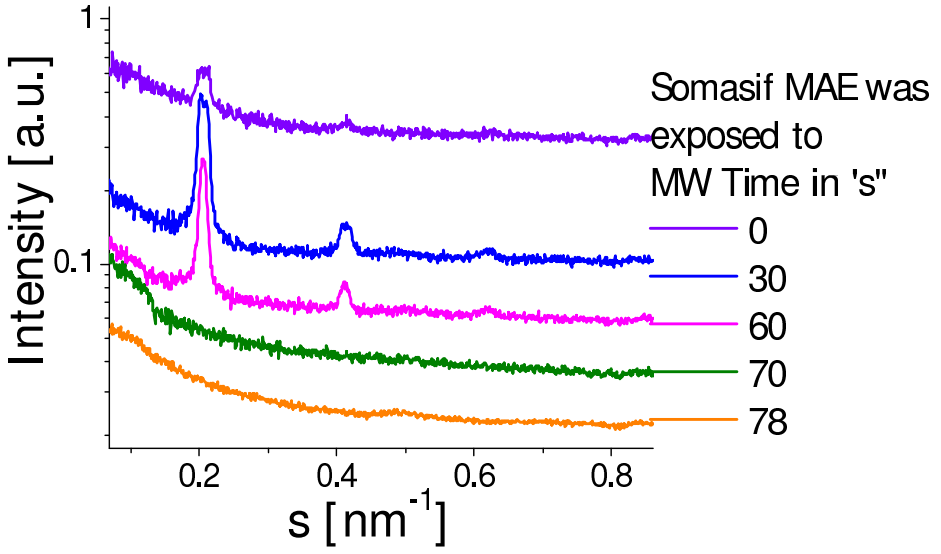

Figure 4.19: Integrated SAXS profiles of organoclays Somasif MAE irradiated with Microwaves and dispersed in Toluene.

surfactants solvate and induced exfoliation of lamellar stacks. For clay exfoliated by Microwave irradiation there is no change in the SAXS profile as appearance of peak due to lamellar was observed. In another step the solvent was allowed to evaporate by air drying and the integrated SAXS profiles of these of dried samples is illustrated in Figure 4.20. We observe that lamellar peaks reappear for all the samples irradiated from (0 to 60s) and peak features are refined suggesting that solvation of surfactants brings structural change in the periodicity of clays. For clays irradiated for 70s which in its dry powder state didn't appear to be exfoliated but once dispersed in Toluene exfoliation occurs and they didn't form the layered structure upon drying. Hence we can say this clay was fully exfoliated in Toluene due to solvation of organic surfactants and the structure of the clay was not regained.

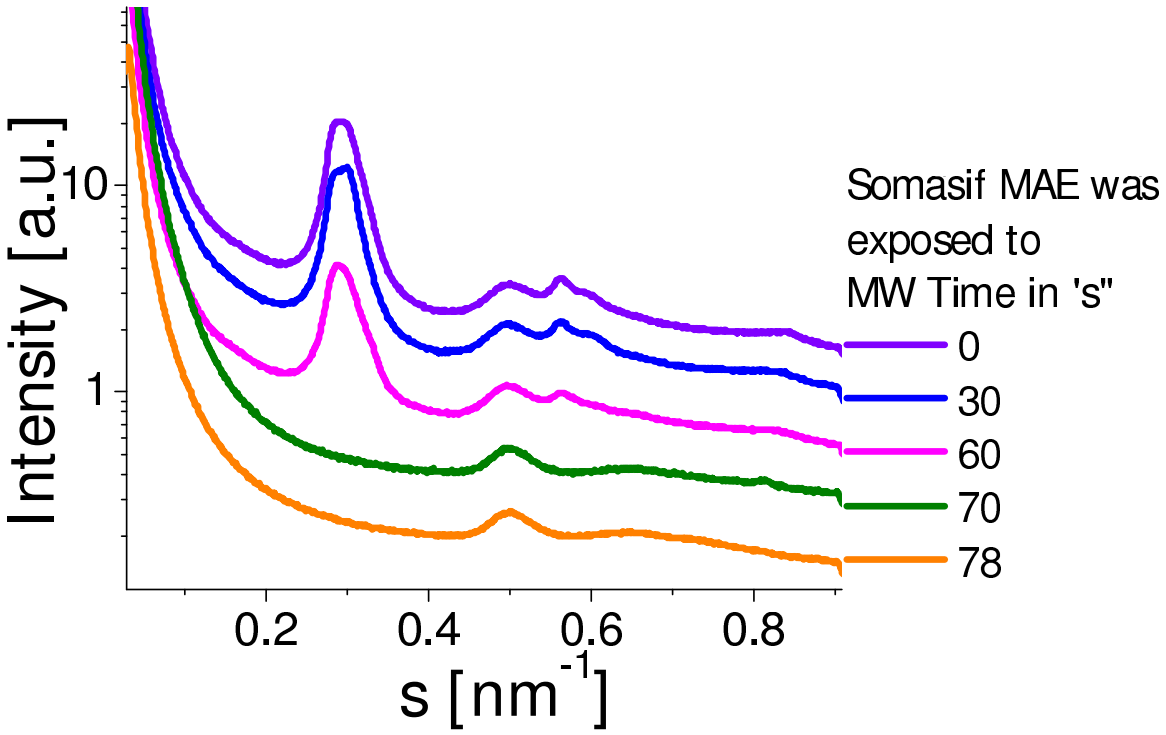

Figure 4.20: Integrated SAXS profiles of organoclays Somasif MAE irradiated with Microwaves and dispersed in Toluene.

4.1.8 TEM and X-ray analysis of Nanocomposites

SAXS analysis of organoclay alone is not enough evidence for concluding exfoliation of SMAE. We further provide SAXS and TEM analysis of nanocomposites formed using these microwave irradiated clays. Figure 4.21 illustrate 2D SAXS images of SMAE melt compounded in the EVA co-polymer. We observe that there are no reflections arising due to lamellar structure of clays for samples that were irradiated for 78s, and very weak meridonial reflections are seen for the clay irradiated for 70s. Other 2D images obtained for nanocomposites from SMAE as labeled show strong reflections suggesting presence of stacks in nanocomposites. TEM images illustrated in Figure 4.22 reveal that the partial exfoliation takes place in all cases, while in the case in which microwave irradiated clay (70s and 78s) is used, we observe greater numbers of single platelets. This further suggests that Microwave irradiation is helpful to exfoliate the clay stack. At this point we don't have further results, such as property enhancement of nanocomposites, which could help to conclude exfoliation. To completely elucidate the effect of Microwave irradiation on the structure of clay, the control of various parameters and usage of Microwave reactor will be beneficial.

4.1.9 Discussion

Morphological changes and structure analysis of layered sillicates were investigated at different temperatures using TGA and *in-situ* thermally resolved X-ray techniques. From TGA we can conclude that due to absence of hydroxide bonds in the apical position, residual water retained is negligible. On the basis of SAXS experimental results, the structures of cloisite organoclays can be divided into three types, depending on the temperature regions. (1) In the zone 1 temperature range (room temperature to about 40°C) a bimodal organic layer thickness distribution exists in organoclays. (2) In the zone 2 temperature range (40-180°C), the content of thicker layers drastically decreases. Organoclays undergo a melting-like order-disorder transition, resulting in

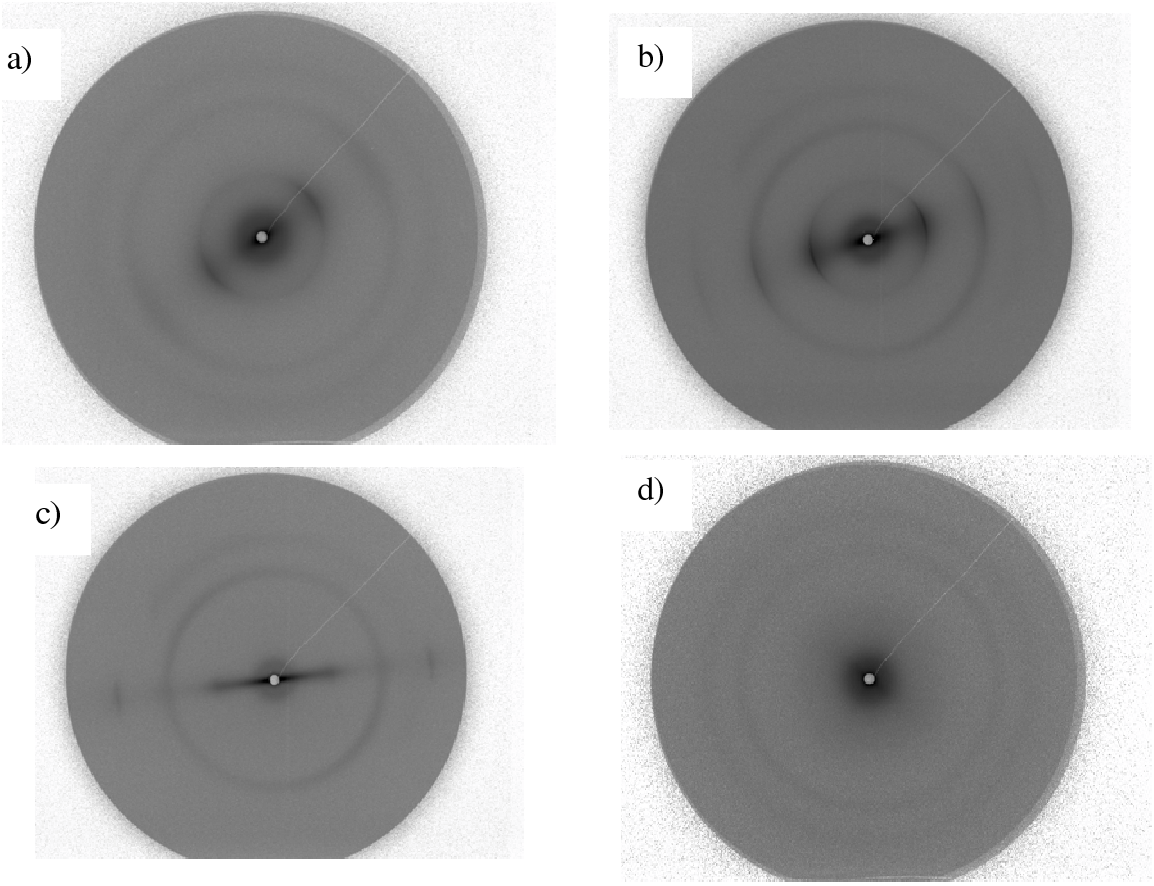

Figure 4.21: 2D-SAXS profiles of organoclays Somasif MAE irradiated with Microwaves and dispersed in EVA.

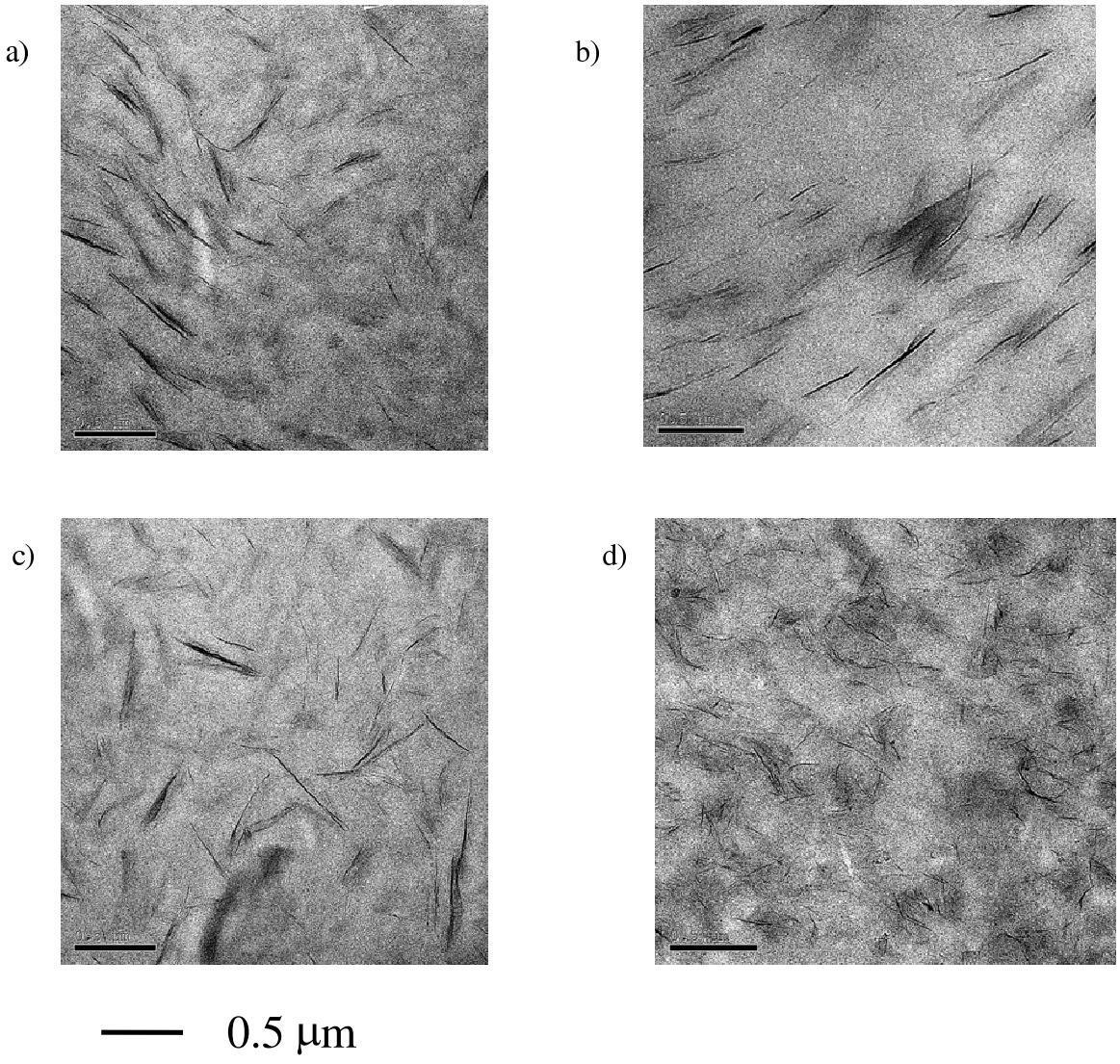

Figure 4.22: 2D-TEM micrographs of EVA co-polymer nanocomposites containing organoclays Somasif MAE irradiated with Microwaves.

the randomization of surfactant conformation. (3) In the zone 3 temperature range (180-260°C), the layer thickness distribution becomes bimodal again, organoclays containing disordered monolayers of bound surfactant and fused silicate layers. The drastic increase in the content of fused silicate layers above 200°C can be attributed to thermal degradation and/or escape of bound surfactant molecules. Thermal stability and corresponding structure changes of organoclays based on synthetic Somasif minerals investigated by SAXS data prove that the surface properties of alternating sides of the Somasif mineral sheets are different, resulting in "Peierls-distorted stacks" with AB-type periodicity in the corresponding organoclays. It is clear that Somasif-based organoclays consist of two populations of organic layer thicknesses, which can undergo thermal transitions and desorption leading to different lamellar structures. When clay is dispersed in various solvents the resulting change in the structure of clay will depend on the surface energy and polarity of the solvent used. We have observed that the solvents molecules solvates the surfactants resulting in increase of *d*-spacing. The solvation of surfactants can go to an extent that the electrostatic barrier holding the clay stack is overcome resulting in complete loss of periodicity or exfoliation, of the clay stacks. It was found that the clay dispersion exhibited concentration dependence and exfoliation was also dependent on the concentration of organoclays in solvent, as observed by scattering. When C20A is dispersed in Toluene, intercalation of solvent takes place and Toluene penetrates the layers without breaking the clay stacks, as evident from the appearance of peaks in integrated SAXS profile, this can be attributed to higher surface energy of Toluene, and it was observed that the structure of clays remain intact and the stacks results with expanded *d*-spacing. While in the case of MEK there are no peaks observed in integrated SAXS profiles for a low weight percentage, as we go higher in percentages of clay dispersed peak due to lamellar structure appears. In another section we have discussed results of Microwave irradiation on the structure of clay which is attributed to the electronic properties of the clay. Clay is

dielectric in nature due to the charged ion in the basal spacing, and in organoclays these are replaced by organic surfactants which act as dipoles. We have observed that there is a drastic effect of thermal energy on the *d*-spacing of organoclays which possibly arises due to change in conformation of surfactants present within the layer spacing of clays. The increase in the *d*-spacing can arise only from the reorientation of surfactant chain as silicate will remain stable to heat at temperatures as low as 100°C, thus any increase in d- spacing is due to surfactants. When organoclays are exposed to microwaves the surfactants present in the gallery will polarize and reorient them from a random coil conformation to a stretched chain conformation. Flourohectorites have fluoride bonds at the apical position as compared to hydroxide groups of smectites. We hypothesize that there is residual water retained in the structure of C20A due to extensive hydrogen bonding and any effect of Microwave is absorbed by these water molecules. While in flourohectorites Microwaves have direct influence on the conformation of surfactants and due to the polymer chain extension the clay stack breaks apart. Other possibility is that superheating occurs within the layers of flourohectorites and the energy released is enough to overcome the electrostatic barrier holding these clays together. In both the tested mineral clays MMT and SME100 exfoliation doesn't occur, as due to the absence of surfactants molecules no conformation change resulting in increased *d*-spacing will take place. Upon dispersion of Microwave irradiated clays in EVA co-polymer we observe mostly exfoliated morphology while in case when regular SMAE was dispersed we observed mixed, "exfoliated and intercalated", morphology. At this point we cannot say whether other clays can be exfoliated using Microwave radiations or not. An in depth study using Microwave reactor for various length of time and changing various parameters will give us better understanding of effect of Microwaves on the structure of clays.

4.2 Orientation of clay in Polymer Nanocomposites

The orientation distribution of inorganic filler particles dispersed in a polymeric film is one important aspect to understand the enhancement of polymer nanocomposite properties. Using transmission electron microscopy (TEM) and X-ray scattering, the status of the filler particles dispersed and the morphology of polymer nanocomposites can be determined. X-ray scattering can be used to determine the complete orientation distribution of inorganic filler particles with preferred orientation and correlated with permeability. Polymer nanocomposites containing different weight fractions of organoclays (Cloisite C20A®) dispersed in ethylene-vinyl acetate (EVA) copolymers were prepared. The dispersion of organoclays in the polymer matrix, their morphology, and the orientation distribution were studied using a combination of transmission electron microscopy (TEM) and multi directional small angle X-ray scattering (SAXS) as sketched in Figure 4.23. The preferred orientation was quantified based on the SAXS data. In Figure 1.3, the intercalated clay tactoids with preferred orientation parallel to the plane of the pressed film and the corresponding directional SAXS pattern are illustrated. Preferred orientation of clay particles has been quantified using Hermans' orientation factor. The permeation of molecules through these membranes was studied, and a correlation of permeability with the preferred orientation, average aspect ratio, and morphology of polymer nanocomposites was established.

4.2.1 Theory

We assume the stack axes to be preferentially oriented about the film normal, under cylindrical rotational symmetry for both the individual stack in its coordinate system and for the film as a whole ("simple fiber symmetry"). The orientation distribution g (β) describing the preferred orientation of the clay stacks depends on a single angle β which is the angle between the stack axes/ layer normal of a given stack or layer and the film normal. For the edge on scattering geometry we will refer to the vertical

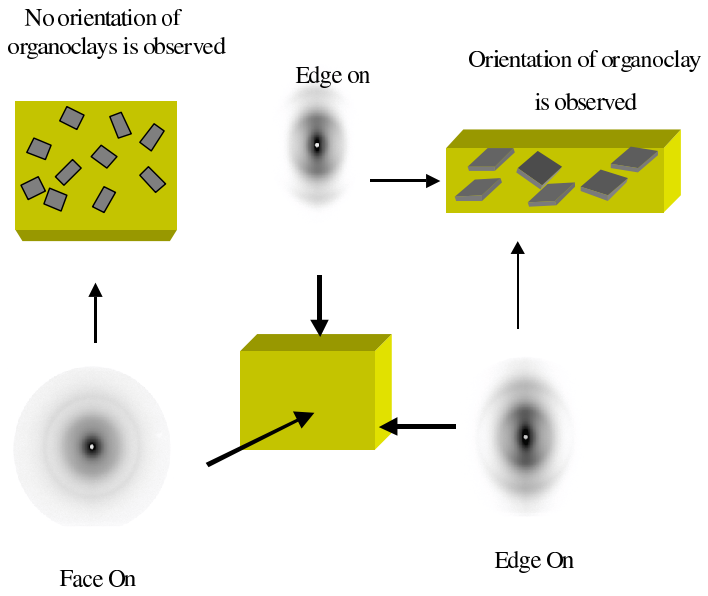

Figure 4.23: Sketch of possible X-ray pattern than can be obtained by changing sample to beam orientation edge-on and face on.

directions as the "meridian" and to the horizontal directions as the "equator". For a system with moderate preferred orientation in edge-on geometry meridionial arcs as observed in 2D SAXS shown in Figure 4.24 can be factorized into a radial and an angular component. The latter can be used to determine the orientation distribution of the clay particles dispersed in polymer. The relationship between the intensity distribution of the structural unit, of the sample and the orientation distribution g(β) is given by the following integral transformation Ruland 1968, (Equation 4.1:

$$J(s,\phi) = \int_0^{\pi/2} I(s,\phi)F(\phi,\phi)\sin\phi d\phi \tag{4.1}$$

depends on g(β) by another integral transformation shown in equation 4.2.

$$F(\phi,\phi') = \frac{1}{\pi}\int_0^{\pi} g(\beta)d\eta \tag{4.2}$$

and the dependence of β and n is given by following equation4.3

$$\cos(\beta) = \cos\phi\cos\phi' + \sin\phi\sin\phi'\cos\eta \tag{4.3}$$

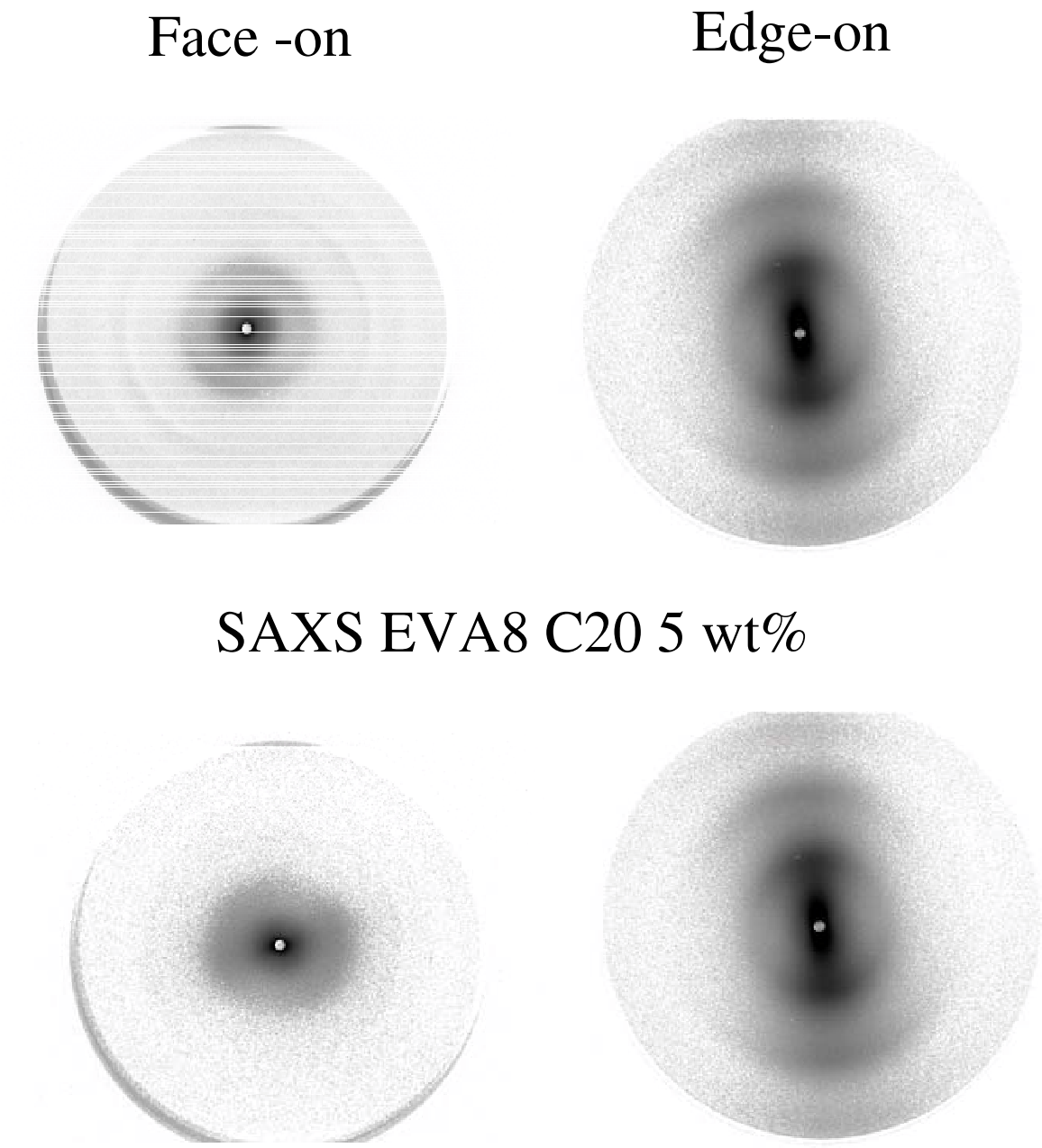

Figure 4.24: 2D-SAXS profiles of organoclays C20A (5 wt% and 10wt%) dispersed in EVA, edge-on and face on patterns.

Here *phi* is the polar angle of the coordinate system if it consists of a single stack or layer and is the polar angle of the scattering from the ensemble. Angular sections through the 2D SAXS image at the highest intensity arc were used to determine the orientation distribution contribution of the clay particles by fitting to a modified Onsager distribution shown in equation 4.3.10.

$$g(\beta) = p_0 + (1 - p_0) * (\frac{p}{\sinh p}) * (\cosh(p \cos \beta)) \tag{4.4}$$

where p is related to the width of distribution of oriented particles in system. The value of p can range between zero to infinity, with p = 0 for an isotropic system and p = 1 for perfectly oriented system. p0 is the isotropic contribution and its value lies between 0 to 1. For "p = 0" p0 doesn't make any contribution. For unoriented system p = 0 or p0 = 1

The width of the orientation distribution and thus the extent of the preferred orientation of these organoclay stacks can be quantified using Hermans orientation parameter give in equation 4.3.10:

$$P_2 = 0.5 * \left[3 * \frac{\int_0^{\pi/2} g(\beta) \cos^2(\beta) \sin(\beta) d\beta}{\int_0^{\pi/2} g(\beta) \sin(\beta) d\beta} \right] \tag{4.5}$$

Using data fitted using Onsager's equation, Hermans Orientation parameter in equation 5 is calculated to estimate the degree of the orientation of organoclays in polymer matrix. To further understand the complete angular orientation distribution, the 2D image can be calculated and the orientation distribution can be obtained from it.

4.2.2 Small Angle X-ray Scattering (SAXS)

In the SAXS profile of C20A as received, shown in Figure 4.25, scattering peak positions are non-equidistant, suggesting multimodal thickness distributions of thickness of organomineral layers, where layers overloaded by surfactant above average cation exchange capacity (CEC) co-exist with layers having low surfactant content within the same stacks. According to the SAXS profile of the polymer nanocomposites

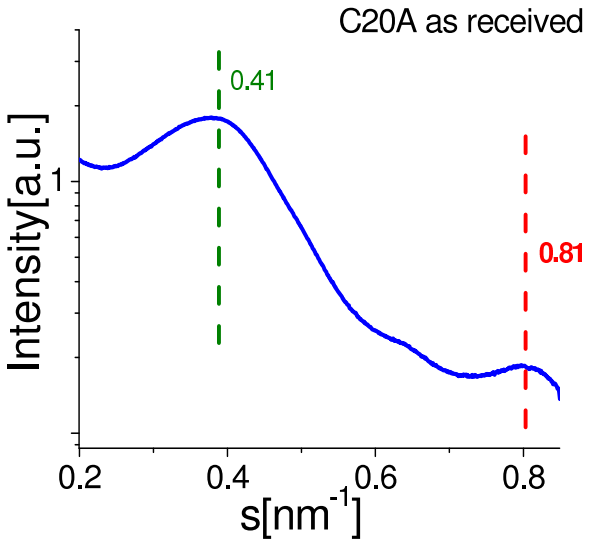

Figure 4.25: Integrated SAXS profile of Cloisite C20A organoclay.

Figure 4.26, the organoclay peak due to the layer-stacking period almost disappears in EVA350-C20A nanocomposites. The broadening of the peaks indicates a change in periodicity of clay stack, most likely in the form of an increase in stacking disorder. This could also lead to the conclusion that the organoclay stacks may be completely exfoliated in the polymer matrix. While the presence of a gallery spacing peak in the SAXS pattern of a polymer nanocomposite is proof for at least partial intercalation, the absence of such a peak is not sufficient to prove that exfoliation occurred. In the experimental SAXS patterns in edge on geometry the meridional peaks are observed at low scattering angles, indicating the presence of clay stacks with the preferred orientation as discussed above. The absence of any peaks in the integrated SAXS patterns shown in Figure 4.26 indicate that there are no clay particles that orient in the direction perpendicular to the plane of polymer film. The purpose of this study is to demonstrate that clay dispersed in a polymer film preferentially orients in the direction parallel to the film and to quantify the degree of preferred orientation the polymer chains themselves may orient during extrusion but due to subsequent relax-

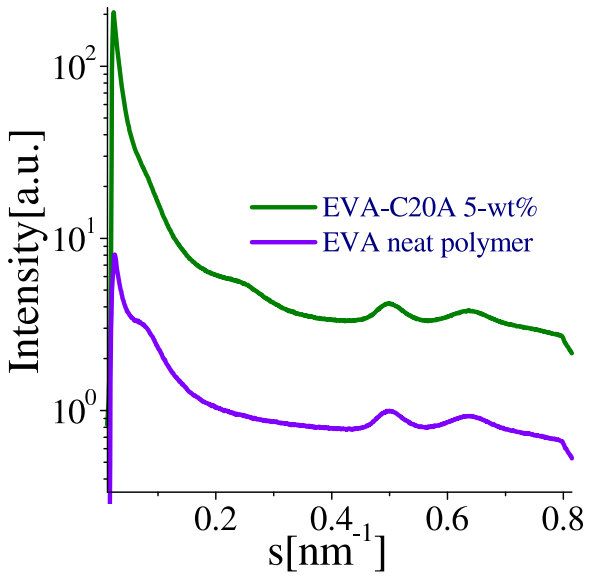

Figure 4.26: Integrated SAXS profile of EVA C20A nanocomposite.

ation they lose their orientation. Hence, all orientation observed should be due to inclusion of clay into the polymer film.

This orientation must be completely driven by the compression of the films, as such streaks were not observed always in extruded samples. Hence in extruded samples clay was randomly oriented. The observed 2D SAXS data was also used to estimate the degree of preferred orientation of using Herman's Orientation factor. The intensity of meridional streaks varies with the percentage of filler particles, as does the calculated orientation. The values of preferred orientation were calculated using Herman's Orientation factor and are tabulated in Figure 4.27(Table).

Here we present SAXS data that was collected for two different samples to X-ray beam orientations as shown in Figure 4.23, and it was observed that organoclays stacks are oriented in the polymer film in a direction parallel to the plane of polymer film. In integrated SAXS data of EVA 350-C20A and EVA 770-C20A polymer nanocomposites shown in in Figure 4.28, Figure 4.29,in Figure 4.30and Figure 4.31, we observe different behavior of lamellar peaks. Hence we can say that these stacks were oriented in the

EVA 350 and C20 A Nanocomposite	Permeability ($mm.cc/m^2.day$)	Orientation factor[P_2]
0 wt % of C20 A	53.42	0.00
5 wt % of C20 A	42.59	0.1387
10 wt % of C20 A	36.05	0.3108
10 wt % of C20 A (from calculated image)	36.05	0.3267

Figure 4.27: Relationship between clay orientation and gas permeability for EVA C20A nanocomposite containing various filler percent.

direction perpendicular to the direction of compression of polymer nanocomposites in films as shown in Figure 1.3. Every particle has an excluded volume hence due to which volume available for other particles decreases. Hence due to hindrance in rotation or decrease in free volume available for rotation of the clay stack, they align themselves in a direction parallel to the plane of film during compression. Extruded samples, which were not pressed, did not always show the orientation pattern in SAXS either, hence it could be said that compression of polymer nanocomposites into film allows the clay stacks to orient themselves due to thermal fluctuation. Before compression these are randomly oriented in the polymer matrix. Angular intensity, obtained from X- ray data, can be used to estimate the molecular orientation using Herman's orientation function by considering half width at half maxima for calculating orientation. In our study the Herman orientation factor (P_2) as given in the equation 4.3.10 was used to estimate the degree of preferred orientation of clay in the polymer matrix from the edge-on patterns.

For a completely aligned system the value of will be equal to 1 while for a complete random system this value will be 0. Azimuthally averaged data for EVA 350-C20A and

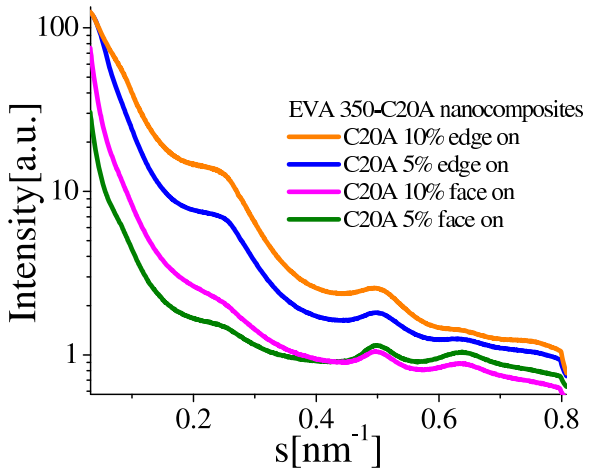

Figure 4.28: Integrated SAXS pattern of polymer nanocomposites with various weight fraction of C20A dispersed in EVA 350 co polymer, at face-on sample orientation.

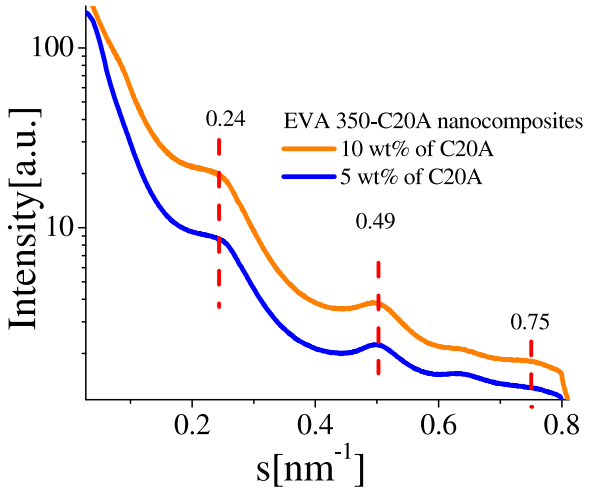

Figure 4.29: Integrated SAXS pattern of polymer nanocomposites with various weight fraction of C20A dispersed in EVA 350 co polymer, at edge-on sample orientation.

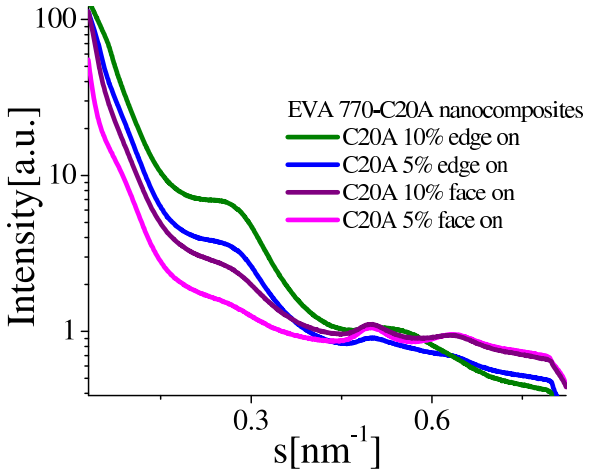

Figure 4.30: Integrated SAXS pattern of polymer nanocomposites with various weight fraction of C20A dispersed in EVA 770 co polymer, at edge-on sample orientation.

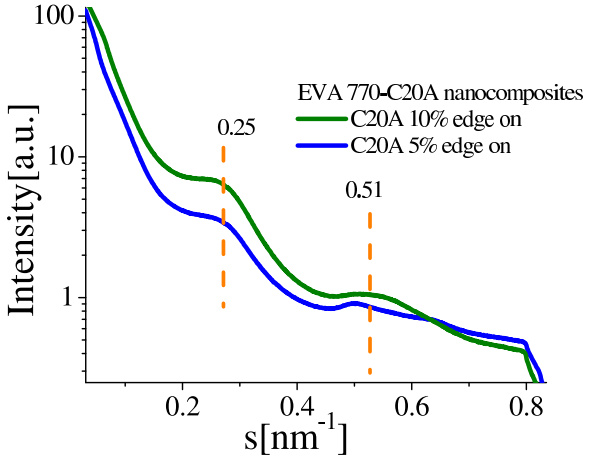

Figure 4.31: Integrated SAXS pattern of polymer nanocomposites with various weight fraction of C20A dispersed in EVA 770 co polymer, at edge-on sample orientation.

EVA 770-C20A polymer nanocomposites is shown in Figure 4.32 and Figure 4.33.It was observed that with the increase in the weight fraction of clay in the polymer matrix higher orientation of clay is obtained. This complies with our hypothesis that the free volume available for the clay stack to rotate decreases with the increase of the clay fraction in polymer nanocomposites and hence the thermal fluctuations of these particles also decrease which leads them to orient in a direction imposed by the compression of these polymer nanocomposite films. Orientation distribution of 2D was obtained from the calculated SAXS pattern shown in Figure 4.34 and the values obtained are in good proximity with orientation values obtained in angular fit.

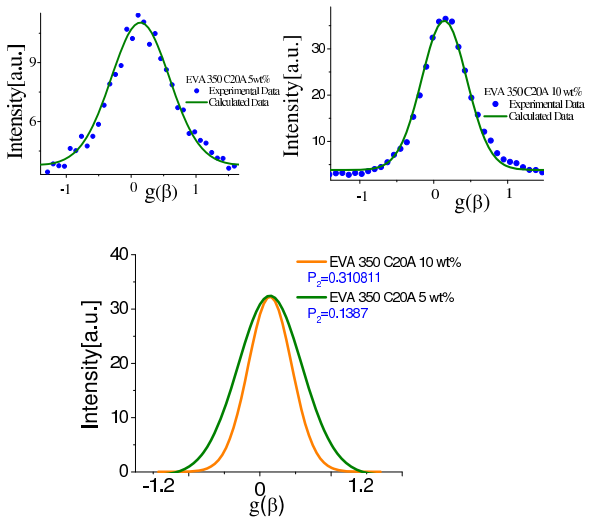

Figure 4.32: Angular intensity plotted against orientation distribution for various weight fractions of C20A dispersed in EVA 350 and orientation factor is calculated.

4.2.3 Transmission Electron Microscopy (TEM)

SAXS of polymer nanocomposites shows a peak indicating the presence of polymer chains intercalated in to the organoclay galleries. Disappearance of peak could mislead to the conclusion that the clay stack is completely exfoliated. Photographic evidence of the morphology of the polymer clay nanocomposite is imperative to draw a definite conclusion related to the morphology of the polymer nanocomposite of such complex nature. TEM images of various weight fractions of clay dispersed in two different

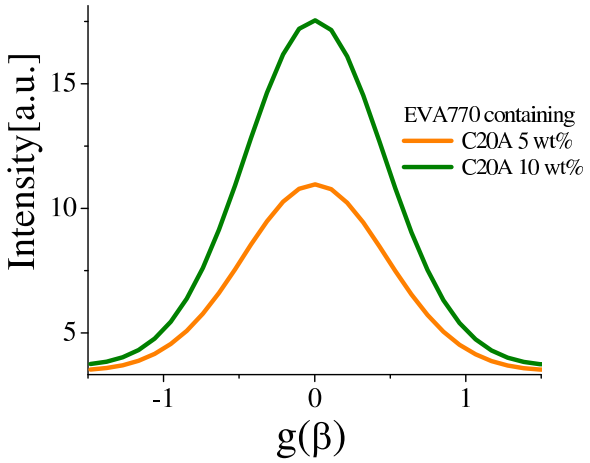

Figure 4.33: Angular intensity plotted against orientation distribution for various weight fractions of C20A dispersed in EVA 770 and orientation factor is calculated..

polymer matrices (EVA 350 and EVA 770) are shown in Figure 4.35 and Figure 4.36. These images reveal that there is no large aggregation of organoclay stacks in either of the polymer matrix, hence indicating the homogeneous dispersion of organoclays in the polymer matrix. This also holds good for weight fraction as high as 30-wt% of organoclays dispersed in polymer matrix. At lower magnification of the TEM image the organoclays appear to be well dispersed in the polymer matrix. On increasing the magnification of these images we see the presence of individual silicate layers all across the polymer matrix. These individual layers are formed during the melt intercalation of polymer chains in between the layers of organoclays. During the process of melt mixing the polymer chains penetrate the layers of organoclays and break them into tactoids. In doing so a single silicate layer can possibly tear apart from the stack due to mechanical force, which might be loosely held depending on the interaction of surfactants with the silicate layer. As we know that surfactants are dispersed in organoclay and they replace the inter-layer ion of silicates, there is a possibility that all silicates are not held by similar electrostatic force. Hence layers with weaker electrostatic interactions can fall apart during intercalation of

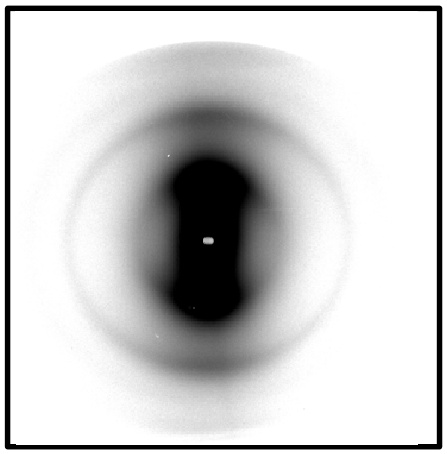

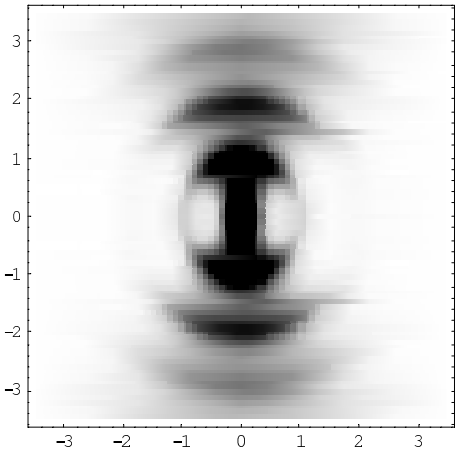

Experimental

Calculated

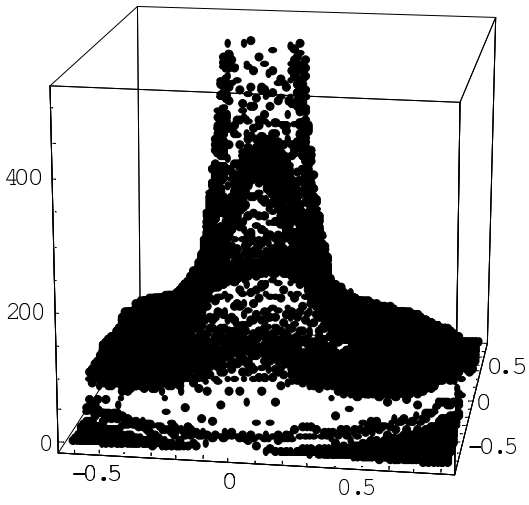

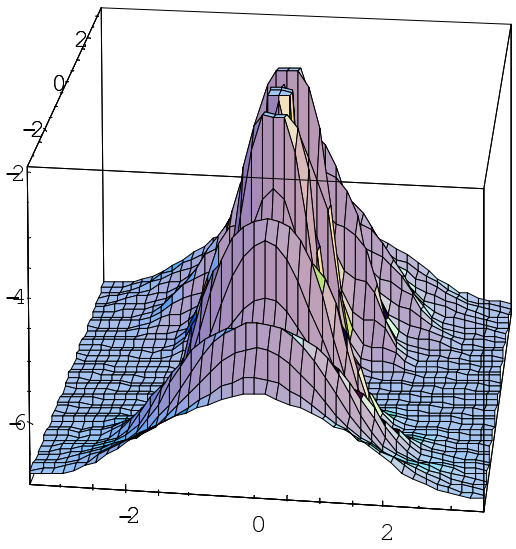

Figure 4.34: Calculated 2D SAXS image for EVA-C20A (10 wtorientation distribution.

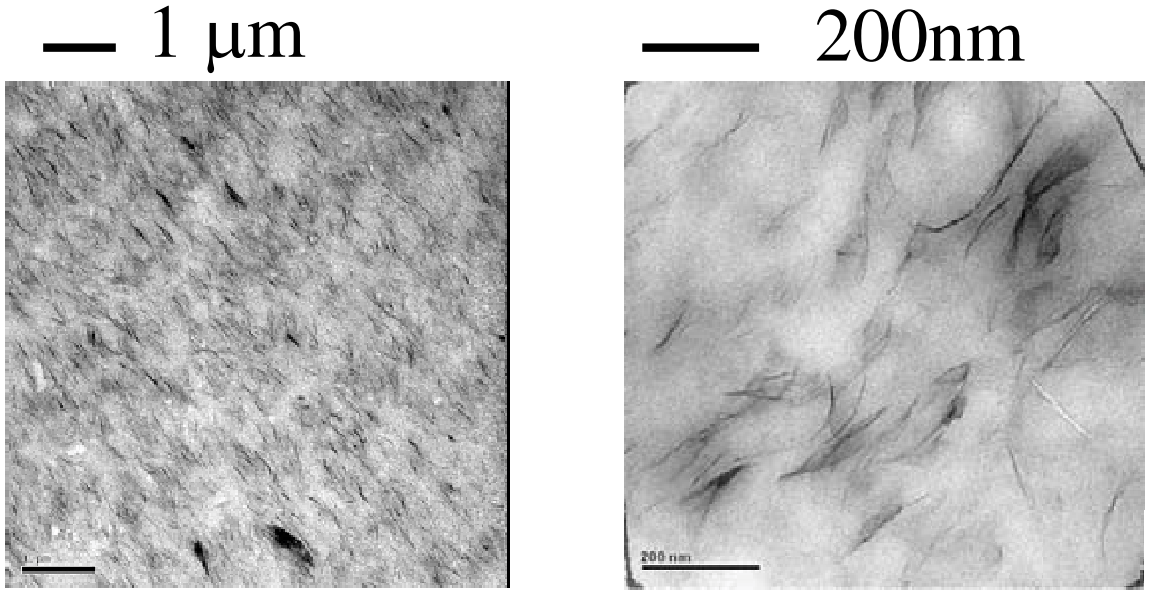

Figure 4.35: 2D TEM images of various weight fraction of C20A dispersed in EVA 350 at different magnifications.

polymer chains. It is quite clear for the 2D TEM images that the possibility of partial exfoliation is higher where weight fraction of polymer is higher as more chains are available for penetration through the inter-layer spacing of the organoclays, hence a higher probability of exfoliation. This could be a possible explanation for the change in peak features of organoclays when dispersed in polymer nanocomposites, even though there is not much difference in dispersion at higher weight fraction of organoclays and there appears no aggregation of mineral. To confirm the dispersion and partial exfoliation of organoclays in the polymer matrix 3D TEM image shown in Figure 4.37 was collected. This images shows that there are no overlapping effects, and the spatial distribution provides an estimate of dispersion state.

4.2.4 Permeability & Equivalent Projected Aspect Ratio

In this section we have utilized equation 4.2.4, or the Gusev and Lusti equation, for perfectly aligned platelets to describe our data and to determine the equivalent projected aspect ratios of smectites in polymers. This equation, despite its empirical nature, excellently models both our polymer-organosilicate nanocomposite data and data from the literature for nylon-layered silicate nanocomposites.

$$P/Po = exp[-(af/3.47)0.71] \tag{4.6}$$

Using the simple Equation , instead, a single permeability value can be applied to calculate the equivalent projected aspect ratio of any organosilicate in a polymer nanocomposite. Hence, in this study, the equivalent projected aspect ratios for several polymer-organosilicate systems are obtained and applied to quantify their corresponding dispersion and orientation states. The equivalent projected aspect ratios as calculated from Equation 4.2.4 6, for organoclays of various weight fractions of C20A dispersed in EVA350 and EVA770 are tabulated in Figure 4.38(Table). A progressive increase in aspect ratio with increasing loading reflects the observed increase in planar orientation of Cloisite in EVA from TEM micrographs. The orientation effect with

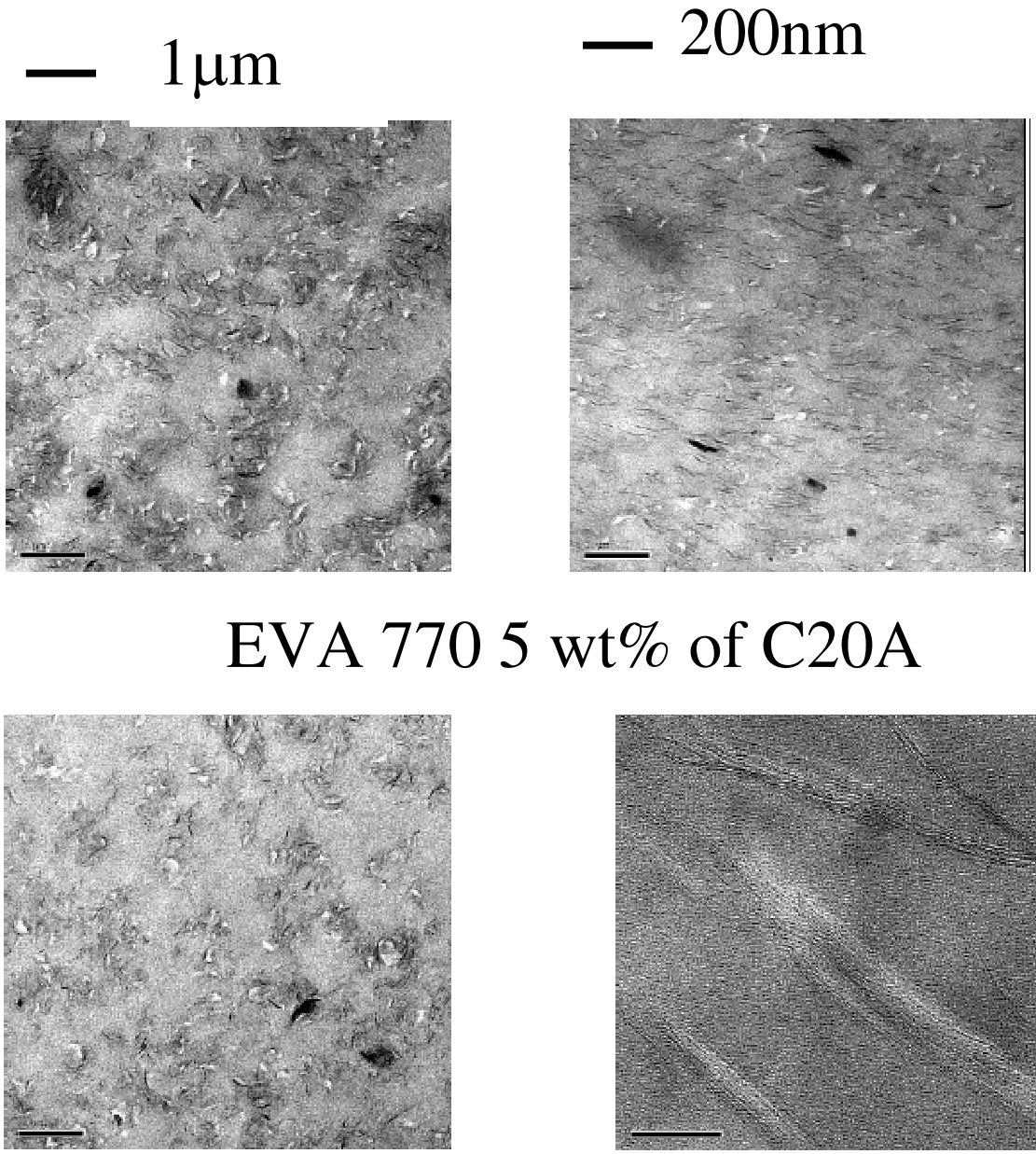

Figure 4.36: 2D TEM images of various weight fraction of C20A dispersed in EVA 770 at different magnifications.

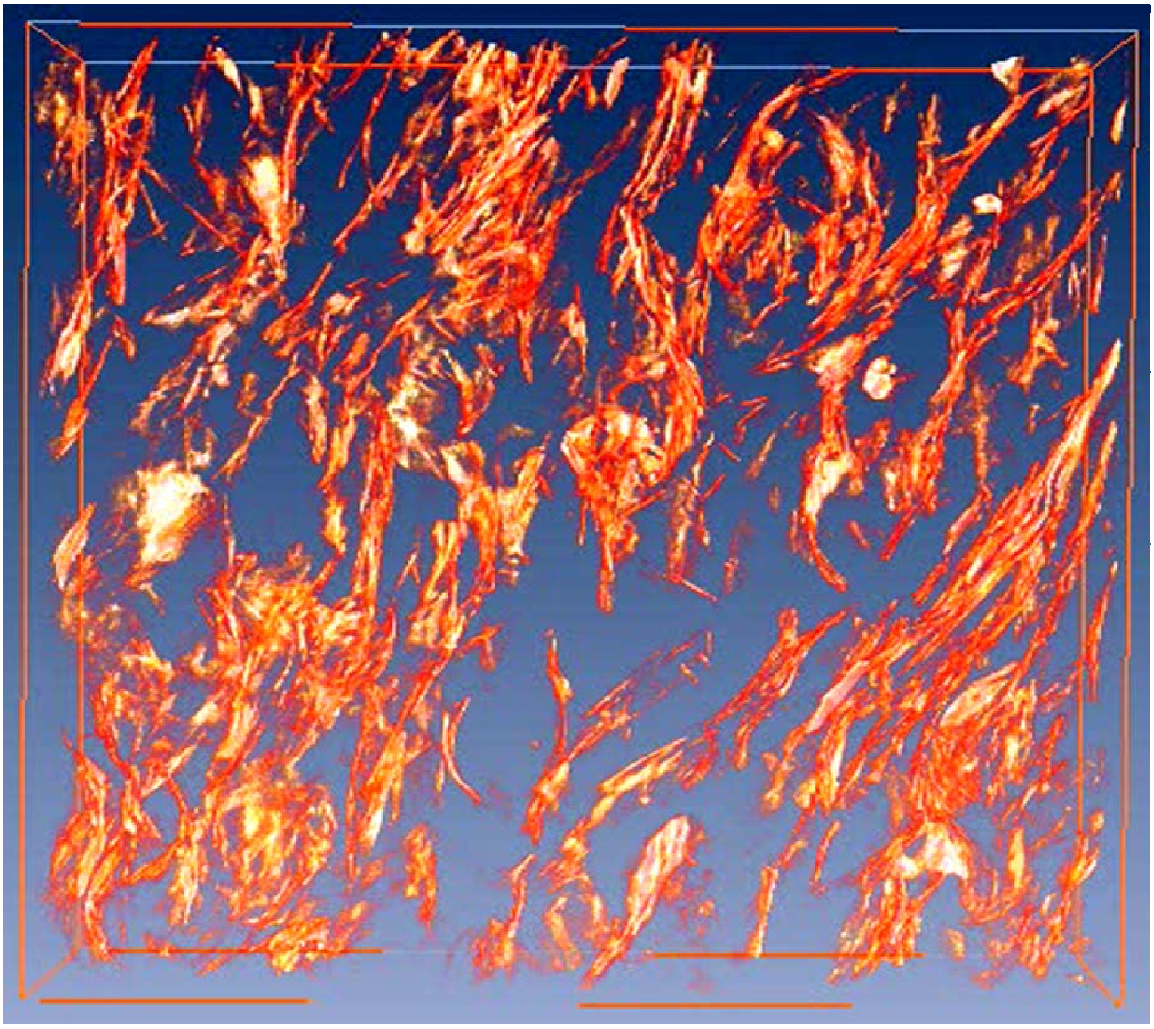

Figure 4.37: 3D TEM of image of 10 weight percent of C20A dispersed in EVA 350.

EVA	Weight % of C20 A	Permeability Ratio	Equivalent Aspect Ratio	Avergae Aspect Ratio
EVA 350	5	0.79	13	22
EVA 350	10	0.49	32	22
EVA 770	5	0.81	11	15
EVA 770	10	0.60	19	15

Figure 4.38: Equivalent projected aspect ratios of Cloisite 20A in EVA and permeability of various nanocomposites.

increasing load seems to be stronger in EVA 350 than that in EVA 770. This observation, again, seems to be in agreement with TEM micrographic findings. Taking the average aspect ratio, averaging over the values obtained for different Cloisite concentrations, EVA 350 appears to disperse Cloisite better than that of EVA 770. EVA 350 contains 8 mol% of vinyl acetate whereas EVA770 contains only 3wt%. As EVA 350 is more polar hence shows better dispersion of organoclays.

The permeability of EVA-Cloisite compounds increase with decreasing Cloisite load since with increasing clay fraction in the polymer the preferred orientation increases, given in Figure 4.38(Table) and for high degrees of preferred orientation the tortuosity will be very high. Morphology and particle orientation play a very important role in decreasing the permeability as they create a tortuous path for the permeating molecule and this tortuosity will increase with an increase of orientation. A sketch in Figure 4.39 shows the random walk path traveled by the permeating

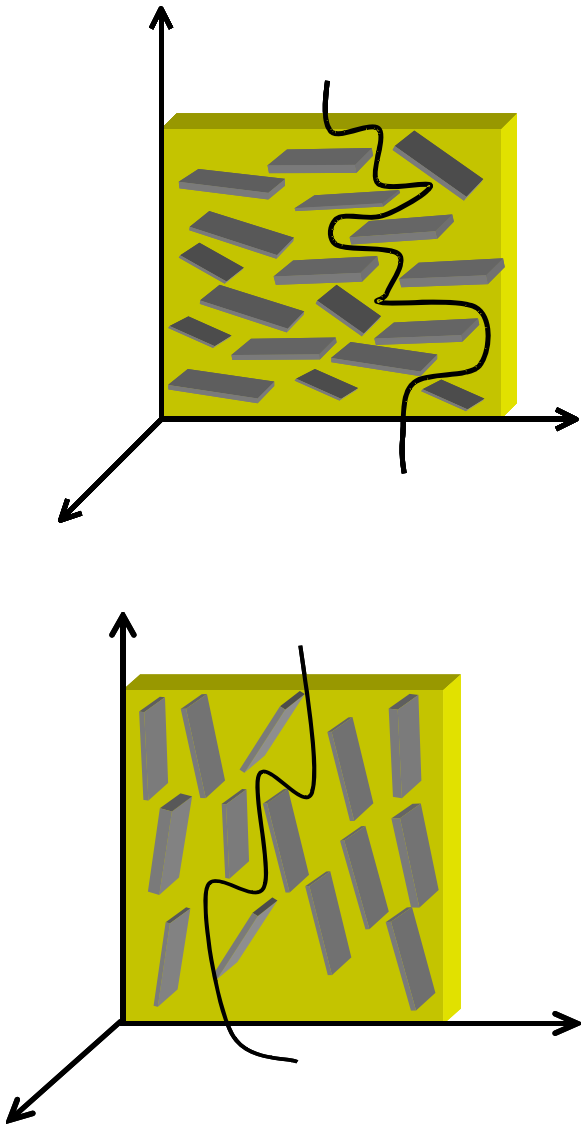

Figure 4.39: Schematic sketch of tortousity when organoclays are oriented in different directions and the random walk path generated for permeating molecules.

molecule in a system with orientation perpendicular and parallel to the polymer film, respectively.

4.2.5 Discussion

Photographic evidence of the morphology of polymer nanocomposites shows that the dispersion of clay is uniform throughout the matrix and there are no aggregates

formed. Morphology as expected is a mix of both the exfoliated and intercalated structures. There is a stack height distribution of tactoids, a finite fraction of tactoids, and a finite fraction of tactoids with a stack height of one i.e. single lamella. The individual platelets that fall apart appear like fine fibers or hairs. This could be from various factors right from processing of MMT to compounding of polymer melt with organoclays. Due to the presence of the individual silicate layer in polymer nanocomposite the average aspect ratio of fillers in the polymer nanocomposite increases, thereby decreasing its permeability. SAXS analysis is used to quantify the orientation distribution of dispersed organoclay particles in polymer matrix. Results from SAXS where 2D images obtained show orientations along meridional axis which were used to calculate orientation distribution using angular scans and from the calculated SAXS pattern. It has been observed that organoclays orient themselves in the direction parallel to the plane of polymer matrix and with the increase of the fraction of organoclay in polymer matrix the orientation increases. Due to thermal fluctuations, under compression the layered silicates orient themselves along the plane of polymer film, which may be possibly due to a decrease in available free volume for thermal fluctuation of organoclay particles. The oxygen permeability of polymer nanocomposites film decreases with increase of orientation of organoclays. Hence, it can be said that exfoliation and orientation of organoclays together are responsible for the improvements in permeability properties of polymer matrix.

4.3 Effect of carbon black on the orientation of clay and permeability of polymer.

In this chapter we have elucidated the effect of carbon black on the morphology of nanocomposites and the orientation factor of organoclays is also calculated. Due to the alignment of clay tactoids and single platelets formed during processing along the in-plane direction of the polymer film, TEM and multi directional X-ray scattering

techniques have been used to provide quantitative and complimentary structural information with and without carbon black as additional filler. Hermans' orientation factor for organoclay is calculated for a series of nanocomposites with or without carbon black as additional filler. The effect of carbon black on the orientation of organoclay was calculated and it varied depending on the interaction of carbon black with organoclays and polymer matrix. Permeability values of various nanocomposites were determined, and a relationship was established between orientation and permeation of nanocomposites. It was established that the permeation of polymer nanocomposites not only depends on dispersion or morphology of fillers but also on the orientation of filler particles.

4.3.1 2-D TEM Characterization

TEM micrographs are used as a photographic evidence to determine the morphology of inorganic fillers dispersed in the polymer matrix. Inorganic fillers, organoclay, and carbon black are dispersed in BIMS (Brominated isobutylene p-methyl styrene) and functionalized BIMS using surfactants tri ethyl amine (TEA) and dia benzoic acid (DBA) to form a series of nanocomposites. TEM micrographs of these polymer nanocomposites are portrayed in Figure 4.40, Figure 4.41 and Figure 4.42. In these micrographs we see that the fillers are dispersed evenly and no large aggregates are observed. In this section we will further discuss the morphology of various nanocomposites and see how the synergy between organoclay and carbon black affects the morphology.

4.3.2 Composites containing clay only (BIMS and Functional BIMS):

In polymer nanocomposite samples where there is no carbon black as additional filler in the system, the clay seems to be dispersed evenly in the polymer matrix. TEM images of nanocomposite in Figure 4.40(a, b and c) reveal that there are no large aggregates of organoclay stacks, hence indicating the homogeneous dispersion of

organoclays in the polymer matrix. At lower magnification it appears as if they form well-dispersed intercalated structures with polymer but as we increase the magnification we observed that clay breaks into small tactoids and some platelets are detached from the stacks which appear as hairline dark streaks resulting in mixed exfoliated intercalated morphology. This is possibly due to extensive shearing applied on clays while forming polymer clay nanocomposite by melt compounding.

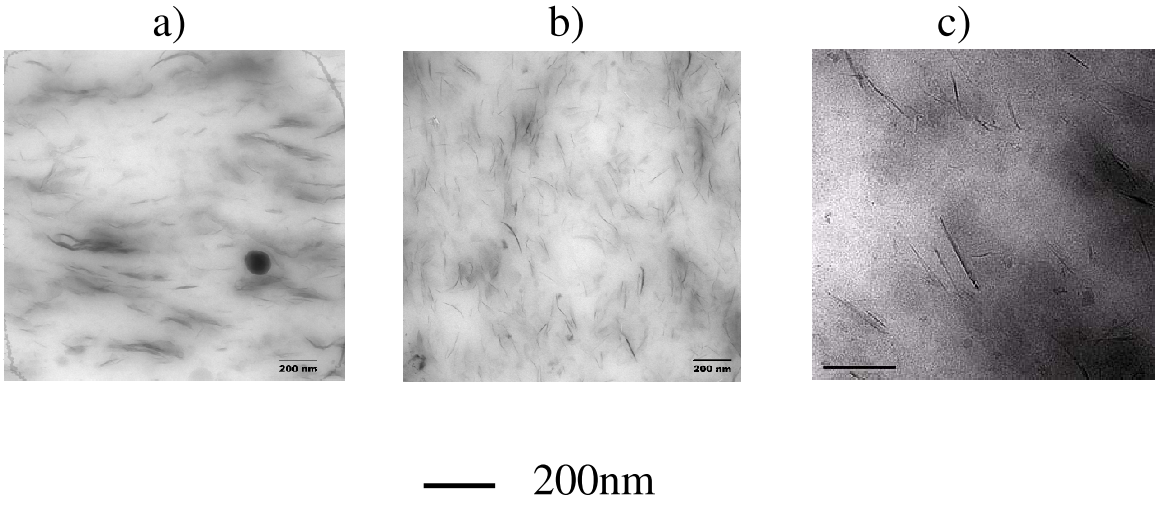

Figure 4.40: TEM micrographs of composites containing clay only a)Dimethyl benzoic acid treated Exxpro:, b)Triethylamine treated Exxpro and c)Exxpro.

Another visible effect of extensive shearing on the clay particles, as evident from TEM micrographs in Figure 4.40, is that these organoclay stacks or single platelets don't appear geometrically straight rather they appeared bent or are curved like a "sickle cell", suggesting that the extensive shearing also has an effect on the lateral dimension of organoclays. Figure 4.40 c shows samples with BIMS composite and Figure 4.40 a and b shows functional BIMS composite, with organoclays. We observed TEA functionalized BIMS shows best association with organoclay and we see that filler particles are is very well dispersed and degree of exfoliation is higher. This probably is due to the fact that clay interaction with tri ethyl amine is stronger and it helps clay platelets to overcome the energy associated in holding two platelets together.

4.3.3 Composites containing carbon black only (BIMS and Functional BIMS):

Dispersion of carbon black is very well defined by the percolation phenomenon where polymer chain and carbon black form a network resulting in improved mechanical strength of such polymer composites. Uniform dispersion obtained is due to low viscosity polymer which can more fully wet the filler particles.

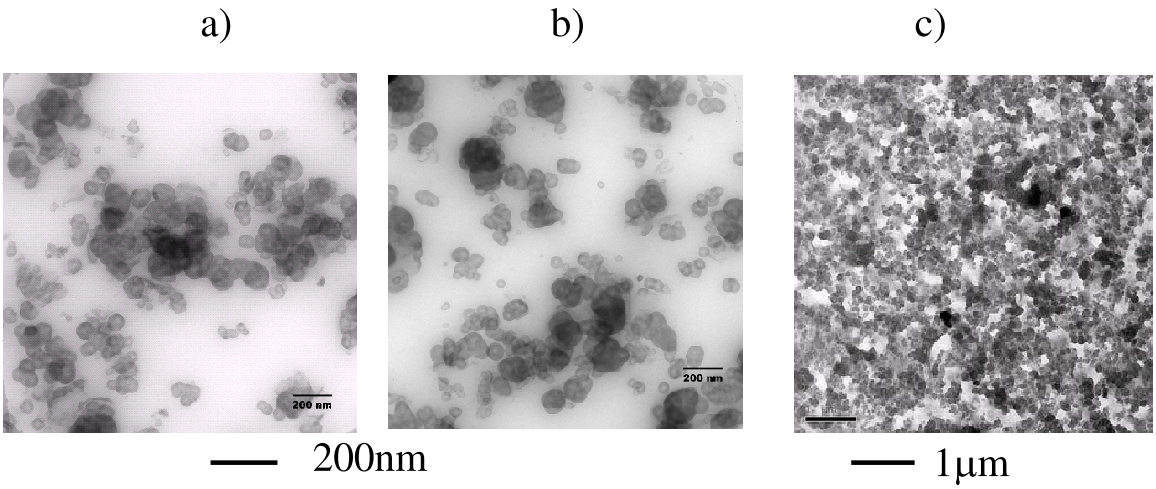

Figure 4.41: TEM micrographs of composites containing Carbon Black only a) Dimethyl benzoic acid treated Exxpro:, b)Triethylamine treated Exxpro and c)Exxpro.

TEM micrographs in Figure 4.41 show that carbon black is very well dispersed in polymer matrix and clusters of carbon blacks can be seen in these composites. On the other hand, due to small lateral dimension of carbon black they don't appear to curve or bend like organoclay due to extensive shearing. Figure 4.41 c shows samples with BIMS composite and Figure 4.41 a and b shows functional BIMS composite. We observed that TEA functionalized BIMS shows best association with carbon black and excellent dispersion is obtained, while in DBA clusters are formed. Previously we observed the strong association of organoclay with TEA and here we observe TEA strongly interacts with carbon black as well. Carbon black is aligned in the direction parallel to the surface of polymer matrix.

4.3.4 Functional BIMS composites containing carbon black and clay:

In functionalized BIMS containing both carbon black and clay, various set of morphology can coexist. The presence of irregular shaped CB clusters network can induce directional change of organoclays platelets but they preserve stacks. TEM micrographs containing organoclays and carbon black are shown and excellent spatial resolution with clear definition of individual platelets of organoclay could be seen in these micrographs. Polymer nanocomposites with both clay and carbon black exhibit various morphological characteristics. TEM micrographs of polymer nanocomposites as shown in Figure 4.42, the dark hexagonal or circle shaped parts represent carbon black, grey or whiter area represents that polymer matrix and organoclay platelets are seen as dark curved or straight lines. Clay appearing as dark lines can be observed as a bundle of lines (intercalated) or single individual lines (exfoliated). Due to interaction between carbon black organoclay and polymer matrix there exist different morphologies. As evident from TEM micrographs shown in Figure 4.42 carbon black and clay have strong interaction and act as one unit, this is possibly due to presence of surfactants used to functionalize BIMS, that hold both the filler particles together. TEM micrographs reveal that the organoclay platelets attempt to envelop the carbon black particles, suggesting that due to extensive shearing applied during melt compounding, the clay platelets bent around the stiff carbon black particles or are closely associated with carbon black particles as shown in Figure 4.42. It was observed in functional BIMS composites that carbon black and clay exhibit morphology with strong associations both with each other and the polymer. They don't overlap with each other but are closely wrapped around or associated with each other, which results in fluctuation of their preferential orientation. For such cases we expect a decrease in orientation value along the plane of polymer matrix, as carbon black will restrict the motion of the clay stack in the melt to achieve a higher degree of orientation.

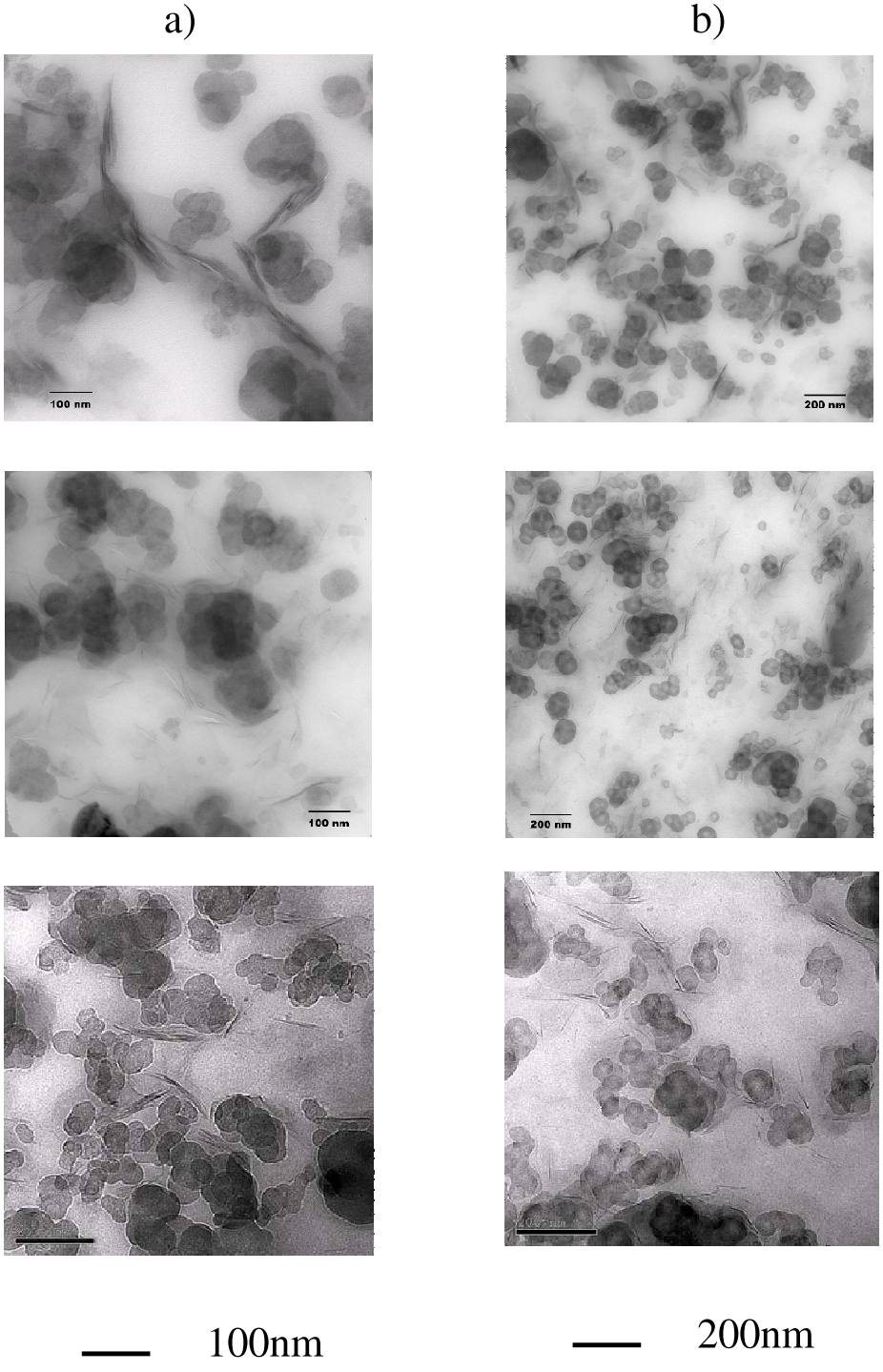

Figure 4.42: TEM micrographs of composites containing Clay and Carbon Black a)Dimethyl benzoic acid treated Exxpro:, b)Triethylamine treated Exxpro and c)Exxpro.

4.3.5 BIMS composites containing carbon black and clay:

In polymer nanocomposites where neat BIMS (Exxpro without any surfactant or functional group) is used we observe that the clay platelets can either overlap or envelope, the carbon black clusters as shown in Figure 4.42 c. In another morphological state we observe that the clay platelets lie independently in between the carbon black clusters as evident in Figure 4.42c. These exfoliated clay layers might be curved or bent but they do interact with carbon black particles and do not form contours, as observed in the case of functionalized BIMS nanocomposites. The mixing sequence has no impacts on the dispersion quality of polymer nanocomposites compounds containing organoclay and carbon black, but at this point we can say that without surfactant association with carbon black is less. All TEM micrographs reveal that partial exfoliation of organoclay stacks takes place in all above cases irrespective of either carbon black being added as additional filler or regardless of the BIMS matrix used.

4.3.6 SAXS Characterization

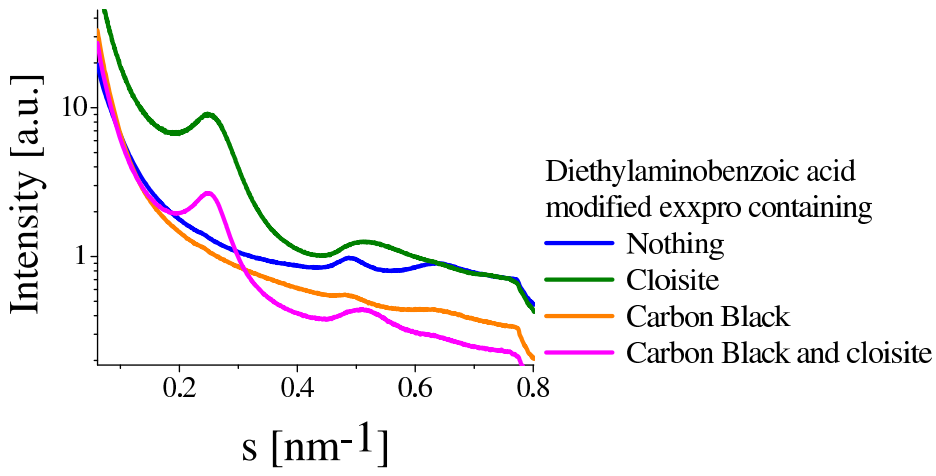

Figure 4.43: Integrated small angle X-ray profiles of nanocomposite of Dimethyl benzoic acid functionalized Exxpro, Face-on.

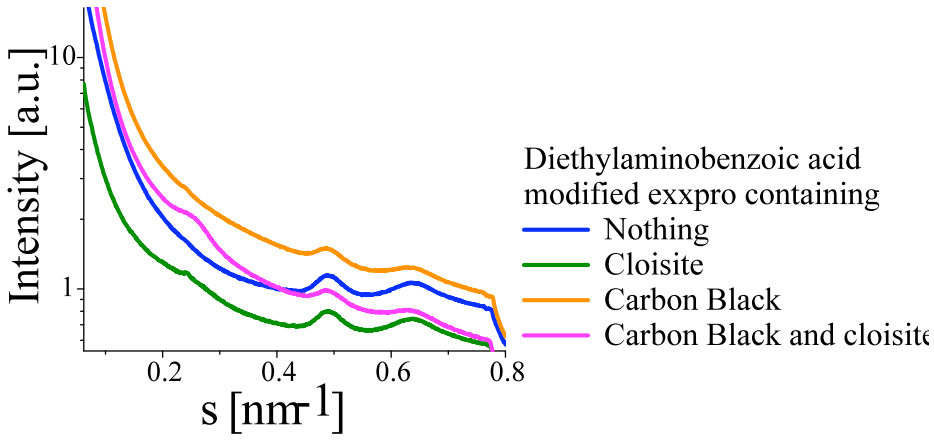

Figure 4.44: Integrated small angle X-ray profiles of nanocomposite of Dimethyl benzoic acid functionalized Exxpro, Edge-on.

In the SAXS profile of as-received clay C20A as shown in Chapter 4.1, Figure 4.25, scattering peak positions due to clay stacks were non-equidistant, indicating multimodal distributions of thickness of organomineral layers, where layers overloaded by surfactant above average CEC co-existed with layers having low surfactant content within the same stacks. If in the SAXS profile of polymer nanocomposites the organoclay peak due to the layer-stacking period almost disappears, which could lead to the conclusion that organoclay stacks are completely exfoliated in the polymer matrix, which is contradictory to the results obtained from TEM micrographs where we observe tactoids and clay stacks. To completely understand the morphology of fillers dispersed in polymer matrix especially the orientation of clay, it is imperative that X-ray analysis is done of various sample-to-beam orientations. For samples with functionalized BIMS we present multi-dimensional X-ray analysis where we have collected the SAXS data from three different sample orientations face and edge, shown in Figure 4.43, Figure 4.44 and Figure 4.45 and Figure 4.46 for sheet like (compressed) samples. A detailed study of samples with BIMS composite have been carried out where not only the sample orientation was changed during X ray measurement , but

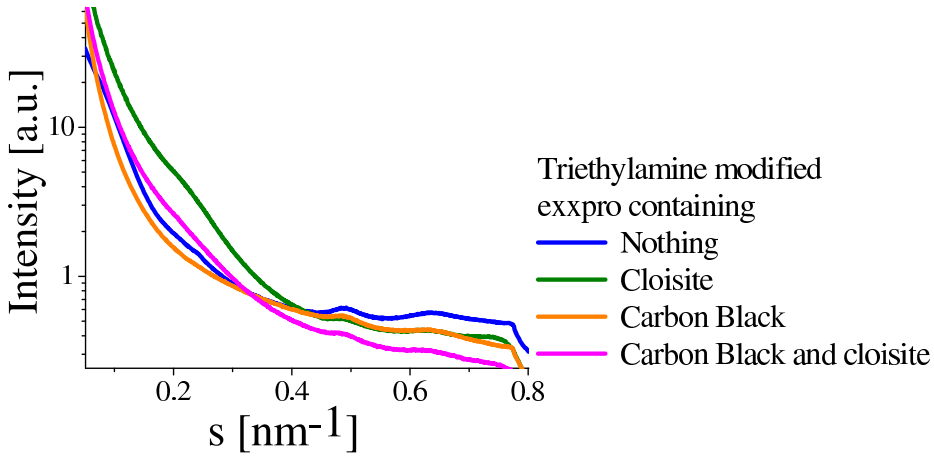

Figure 4.45: Integrated small angle X-ray profiles of nanocomposite of Triethylamine benzoic Exxpro, Face-on.

also these samples were collected at three different stages and X-ray characterization was carried out for all samples. Here we present a multi-dimensional X-ray analysis of series of polymer nanocomposites, where we have collected the SAXS data for raw samples from melt mixer Figure 4.47and Figure 4.48, for two different sample orientations face and edge for rod like (extruded) samples shown in Figure 4.49 and from three different sample orientations: face, edge-1 and edge-2, shown in Figure 4.50 for sheet-like (compressed) samples.

4.3.7 Samples of functional BIMS nanocomposite:

X-ray profiles of functional BIMS and its nanocomposites containing clay only, carbon black only, and with clay and carbon black were obtained as 2D images and were integrated for various sample orientation. In nanocomposite containing clay only, X-ray images obtained showed strong orientation for clay from edge directions observed as meridonial streaks, while in the face direction none or very weak orientation can be seen. In the case where we have used functionalized BIMS, with addition of carbon black orientation is observed unexpectedly to the decrease in the edge direction and

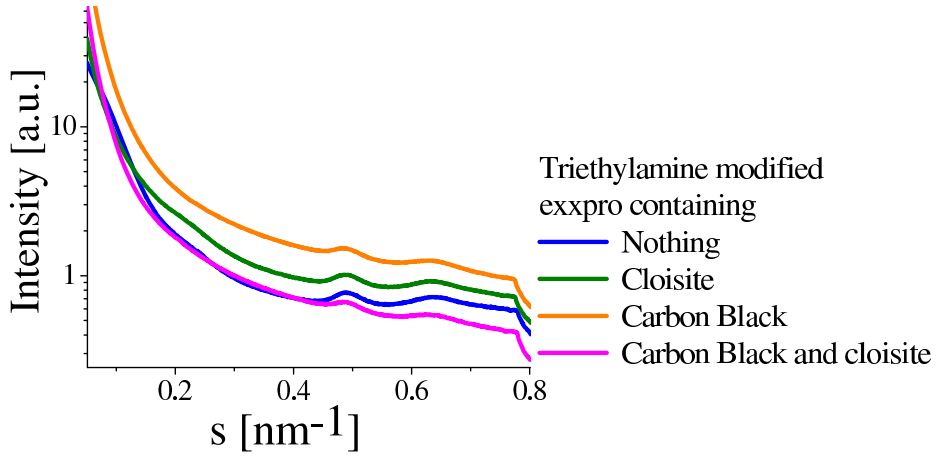

Figure 4.46: Integrated small angle X-ray profiles of nanocomposite of Triethylamine benzoic Exxpro, Edge-on.

this possibly is due to strong association of functionalized polymer with clay and carbon black as evident from TEM micrographs in Figure 4.42. Also clay is strongly associated with carbon black Figure 4.42 where it tends to envelop the carbon black. In polymer nanocomposite of functional BIMS containing clay and carbon black, possibly they act as one unit and this results in decrease of orientation of clay. Strong association of clay with carbon black in the presence of functional group will hinder its movement in the melt state and hence restrict it from achieving a higher degree of orientation. Hence the interaction of carbon black with clay and polymer plays a very crucial role in orientation of clay dispersed in polymer matrix. Figure 4.43, Figure 4.44, Figure 4.45, and Figure 4.46 shows integrated X-ray data for functionalized BIMS and its nanocomposites. We observe strong meridonial streaks in 2D images and integrated data also show strong peak in edge direction for oriented clay, but with the addition of carbon black we see these peaks diffuse or become weaker.

Samples of BIMS and its nanocomposite were obtained directly from the melt mixer and X-ray data was obtained. No strong orientation was observed in this case, possibly due to the presence of many clay stacks randomly oriented in all directions.

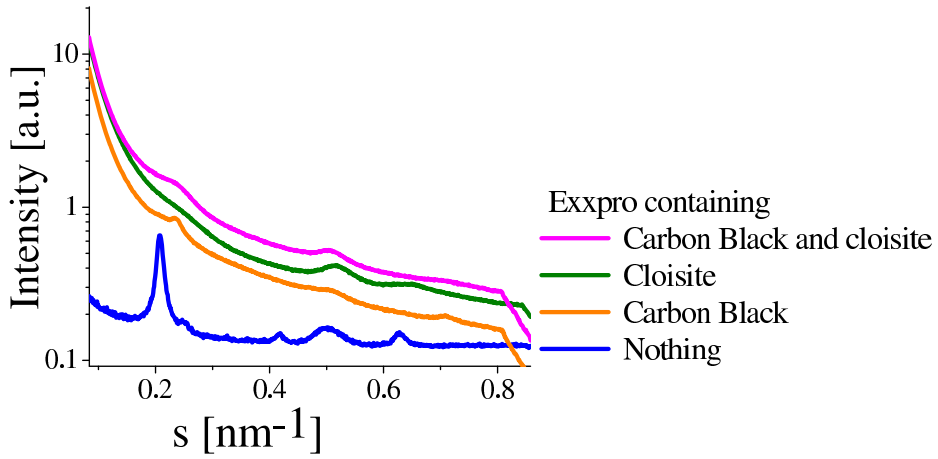

Figure 4.47: Integrated small angle X-ray profiles for nanocomposite of Exxpro, from one part of sample obtained from melt mixer.

The randomization of clay in the polymer matrix can be attributed to extensive shear force and multidirectional flow of the melt. As most times clay particles will tend to align themselves in the direction of flow (squeeze or extrusion), hence in un-extruded samples from melt mixer orientation of clay may or may not be observed. Integrated data for BIMS composites as shown in Figure 4.47 and Figure 4.48, indicates that very weak peaks appear as compared to strong peaks observed in neat BIMS. Once carbon black is added the strong peaks disappear and peak features are no longer visible. Upon addition of clay in BIMS very weak peak appear and this remains true for BIMS composites containing carbon black and organoclays. This suggests that any peak that appears in BIMS nanocomposites are from clay stack only and not from polymer itself or carbon black. Also orientation is randomized as we see weak orientation from two different sections of samples from melt mixer in Figure 4.47 and Figure 4.48.

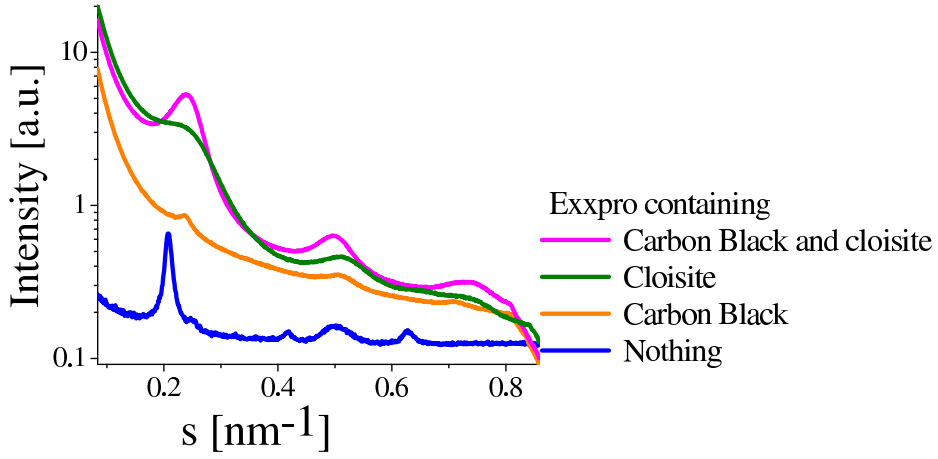

Figure 4.48: Integrated small angle X-ray profiles for nanocomposite of Exxpro, from another part of sample obtained from melt mixer.

4.3.8 Samples of BIMS nanocomposite which are extruded in rod like shape:

After melt compounding when samples are extruded from the mixer they come out in cylindrical rod like shape. Integrated X-ray profiles of 2D data collected obtained from two different sample to beam directions are shown in Figure . Due to extrusion flow force the clay stacks or clay platelets will tend to orient themselves along the extrusion direction, hence we observe strong orientation in edge direction. We also observe orientation in the face-on direction, possibly because the flow force itself is not enough to control orientation of all clay particles. Once extruded it is still in semi-melt stage and some clay stacks can reorient themselves, resulting in orientation in face-on direction as well. Integrated X-ray data is shown in Figure 4.49 for the extruded samples showing orientation in both face-on and edge-on directions. In Figure 4.49, in the presence of carbon black slight increase of orientation occurs and this is possibly due to unavailable free volume for clays when carbon black is added. Upon extrusion the reorientation of clay may not be feasible in presence of carbon black. In Figure 4.49, X-ray profiles of extruded BIMS composite are shown and in the case where

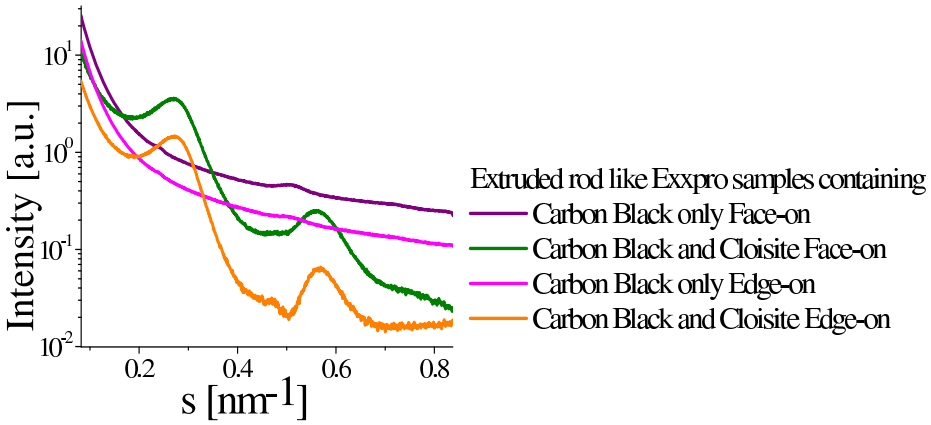

Figure 4.49: Integrated small angle X-ray profiles for Exxpro nanocomposite extruded in cylindrical rod shapes.

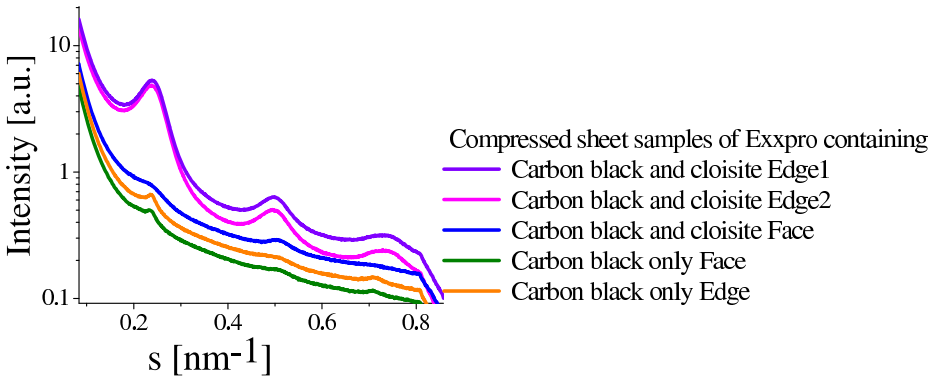

Figure 4.50: Integrated small angle X-ray profiles for Exxpro nanocomposite compressed into sheets.

only carbon black is used as filler it did not show any orientation in edge-on or face-on direction. Thus we can say that any orientation observed in this nanocomposite comes only from clay.

4.3.9 Samples of BIMS nanocomposite which are compressed to thin sheets:

Once extruded, samples are compressed into sheets by the melt pressing machine at 180°C temperature, and we expect the orientation of clays to change in melt due to squeeze flow force. X-ray profiles and integrated X-ray graphs for BIMS and BIMS nanocomposites are shown for various sample orientation. In Figure 4.50, SAXS profile of BIMS nanocomposite sample without carbon black is shown and strong orientation is observed along edges (both E1 and E2). Observation of clay peaks only in the edge-on directions suggests that clay tactoids were aligned in the direction parallel to the film due to applied squeeze flow force on the melt. In the SAXS profile for this sample obtained from the face direction, a slight peak appears but that cannot be taken as evidence of any orientation in this direction. In addition, broadening of the clay peak suggests that the initial clay stacks might have been broken into smaller tactoids. This is also observed in our photographic evidence of clay morphology from TEM micrographs, shown in Figure 4.40, Figure 4.41 and Figure 4.42. During shearing clay stack break into small tactoids and some clay layers fall apart as exfoliated layer X-ray profiles of BIMS clay carbon black nanocomposites were obtained and integrated for various sample orientation. Strong orientation of the clay was observed along both the edges and in the presence of carbon black orientation of these clay tactoids increases. This is possibly due to less volume fraction available for clay tactoids in presence of carbon black and squeeze flow together that most of clay tactoids are oriented in direction parallel to the film. The X-ray profile of composite containing carbon black only did not show any orientation in edge or face direction. Thus we can say that any orientation observed in BIMS and its nanocomposites is only from clay stacks.

4.3.10 Calculation of orientation factor from SAXS

Organoclay stacks are assumed to have a 2D symmetry with poor preferred orientations in polymer nanocomposite films. The orientation of organoclays can be fully described by an orientation distribution function g(β), depending on a single angle β, which is defined as the angle between the normal of organoclay stack and the normal of the film plane film. Azimuthal sections for the SAXS analysis for lamellar stacks thus can be described using a modified Onsager orientation distribution function:

The extent of the preferred orientation of these organoclay stacks can also be expressed using the Hermans' orientation parameter:

Hermans' orientation factor P_2 of clay particles were calculated using the scheme in Chapter 4.2 for all the samples by performing azimuthal scans of the first intense maxima of SAXS image in cases where orientation was observed and these values are tabulated in Figure 4.51(Table). Azimuthal scans of all samples were done at first maxima and using equation , and equation , Hermans' orientation factor was calculated. For the functionalized BIMS nanocomposites the calculated value of Hermans' orientation factor for clay dispersed in polymer matrix decreases with the addition of carbon black. No orientation is observed in the face direction but is only observed along the edges of polymer nanocomposites for all sheet shaped samples. In samples where there is no clay no orientation is observed.

For BIMS nanocomposites Hermans' orientation factor was calculated for various polymer nanocomposites with different geometrical shapes (cylindrical and sheets) and are tabulated in Figure 4.52(Table). The values of Hermans' orientation factor obtained from SAXS analysis of BIMS nanocomposites of different shapes and sizes suggests that the orientation of clay was always observed in the in-plane direction as illustrated in Figure 4.50 and for rod like samples orientation was observed in both sample orientation shown in Figure 4.49 and was calculated for both direction. Also it can be said with compression clay tactoid orient them completely in direction

Nanocomposites	Carbon Black	Orientation factor (P2)
Dimethyl benzoic acid functionalized BIMS.	No	0.5750
Dimethyl benzoic acid functionalized BIMS.	YES	0.2740
Triethylamine functionalized BIMS	No	0.4069
Triethylamine functionalized BIMS	YES	0.2422
BIMS compressed sheet like	No	0.5537
BIMS compressed sheet like	Yes	0.6079
BIMS extruded rod like (edge)	Yes	0.4622
BIMS extruded rod like (face)	Yes	0.2369

Figure 4.51: Hermans' orientation factor as calculated from SAXS profiles for various polymer nanocomposites.

parallel to the polymer matrix and no orientation is observed in face direction of polymer nanocomposites. In extruded samples and in the samples where there is no clay, orientation is not observed.

4.3.11 Permeability

In a pure polymeric membrane permeation of molecules depends on the free volume, diffusivity and solubility of permeant molecules. Morphology of polymer nanocomposite plays an important role in affecting any property of neat polymer, hence in the case of membranes made from polymer nanocomposite, permeation will in addition also depend on the filler particles and their properties. In a neat polymer, permeating molecules will only be restricted by polymer chains and their interaction with permeant, but in polymer nanocomposites the path followed by permeating molecules will depend on the proper dispersion of fillers and the orientation of filler particles. Inclusion of sheet-like inorganic particles renders reduced permeability of the surfaces, and these sheet-like fillers, if they are oriented in the direction perpendicular to the permeating path, can create a longer tortuos path for the permeating molecules. The random walk path followed by the permeating molecule is further restricted due to the inclusion of clay and carbon black in system. In our study we have established a relationship between the permeability of such polymer nanocomposite membranes with the orientation of filler particles. Permeability of membranes made from nanocomposites containing carbon black and clay as filler particles was determined and is tabulated in Figure 4.52(Table). With the increase in the orientation of filler particles along the direction of flow or direction parallel to the plane of the membrane of filler particles within the membrane the permeability (perpendicular to direction of flow) decreases. We also observe that the inclusion of filler particles decreases the permeability of membrane, but due to various coexisting morphologies and association of carbon black with clay reduces the net effect of clay on the membranes. We determined the reduction of permeability due to clay platelets in the membranes in

Nanocomposites	Carbon Black	Clay	Permeation Rate (mm-cc/m^2-day)
Diethyl amino benzoic acid BIMS.	NO	NO	145.0
Diethyl amino benzoic acid BIMS.	NO	YES	
Diethyl amino benzoic acid BIMS.	YES	No	129.4
Diethyl amino benzoic acid BIMS.	YES	YES	95..0
Tri ethyl amine BIMS	NO	NO	146.0
Tri ethyl amine BIMS	NO	YES	108.0
Tri ethyl amine BIMS	YES	No	102.0
Tri ethyl amine BIMS	YES	YES	86.0
BIMS compressed sheet like	NO	NO	155.0
BIMS compressed sheet like	NO	YES	122.0
BIMS compressed sheet like	YES	No	120.0
BIMS compressed sheet like	YES	YES	105.0

Figure 4.52: Permeability values obtained for various polymer nanocomposites samples.

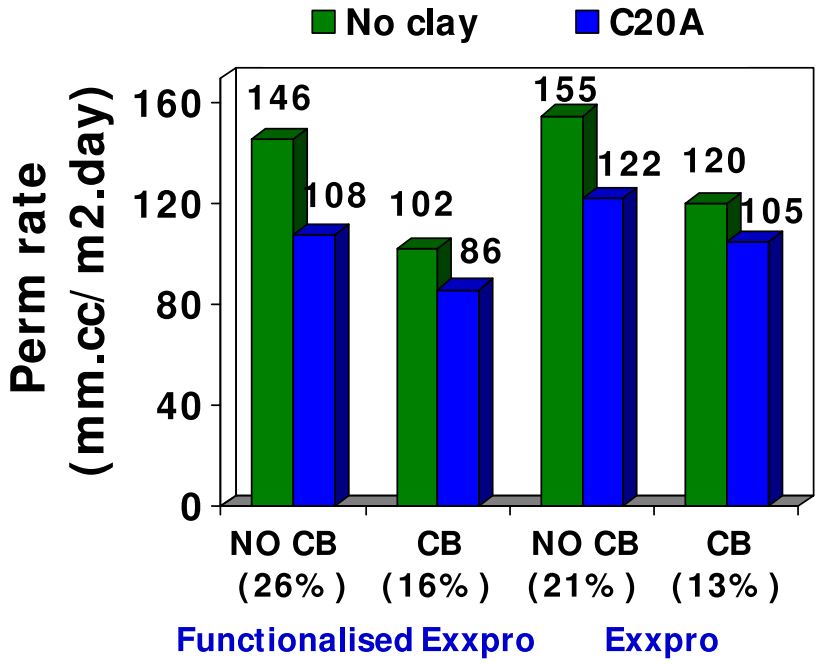

Figure 4.53: Chart showing the effectiveness of clay reduces in the presence of carbon black.

the presence or absence of carbon black. It can be concluded that the effectiveness of clay reduces in the presence of carbon black and this was true for orientation factor for clays as well, shown Figure 4.53

4.3.12 Discussion

During the process of melt compounding the clay is added to polymer melt and polymer chains penetrate between the galleries of clay. This decreases the interaction between the clay. Upon extensive shearing a clay stack can break into a smaller stack often termed as tactoid or a single layer of clay can fall apart and this will depend on number of polymer chain penetrating the silicate gallery. Partially intercalated and exfoliated morphology can be observed for melt compounded polymer nanocomposites. Further addition of carbon black and curing agent doesn't affect the morphology of polymer nanocomposites but as the orientation of clay platelets takes

place in the melt this can vary in presence of these additives. Orientation depends on the free volume available for clays to move during compression. The orientation in sheet-like particles takes place during compression and is dependent on squeeze flow force. For cylindrically extruded samples from the melt mixer, the orientation of particles is dependent on the extrusion flow force and once they are extruded the polymer is still in semi-melt state and it takes time to completely cool down. During this relaxation time some clay stacks can reorient themselves hence orientation can be observed in both face-on and edge-on direction. Samples from melt mixer may or may not show orientation as the flow force is multi-directional. In addition, orientation of clay particles in the compressed sheet-like sample was higher than the orientation of clay particles in extruded rod-like samples, which could be explained by the difference in effects of flow fields (i.e., squeeze flow versus extrusion flow). In squeeze flow, the force is acting on the melt in a direction perpendicular to the film. This force can be controlled and it remains constant till samples are cooled down. In contrast, in the extruded samples the moment they are extruded the force is no longer in act while sample is still in melt state clay stacks reorient. In this work we observed that in BIMS when carbon black and clay are dispersed together these particles may have multiple morphologies depending on various factors. For BIMS nanocomposites clay and carbon black particles remained independent of each other and TEM images showed they either lie independent or may overlap each other. In the case of functionalized BIMS, the association of clay and carbon black changes and they appear as single bundle. This bundling together leads to change in the orientation of clay stack and will finally affect the permeability of membrane. The permeability of the membrane was evaluated and was observed with inclusion of fillers permeability decreases and this is possibly due to two reasons. Firstly, these membranes contain impermeable silicate layers and carbon black particles which will not allow permeation through their surface. As these particles within layer are oriented parallel to the

plane of polymer and perpendicular to permeating molecule their path is hindered. Secondly, the inclusion of these oriented particles creates a tortuous path for permeating molecule and thus decreasing the permeability of such membranes. From the TEM micrographs, we observed association of carbon black with clay in functionalized BIMs resulting in bundles of fillers and this bundling may create voids and will allow faster permeation, hence inclusion of carbon black will reduce the effectiveness of clay. This is also in accordance with our orientation measurements, as with inclusion of carbon black orientation of clays decreases. The decrease in orientation is higher in functionalized BIMS as association of carbon black is higher.

4.4 Flammability of EVA based nanocomposites.

In our previous work we have demonstrated that the TMI-modified organoclays can remain compatible with the polymer matrix and we used TGA, *in-situ* thermally resolved X-ray and rheological measurements to estimate properties of these nanocomposites at elevated temperatures. However, overall FR performance will depend on the whole spectrum of physio-chemical properties of tested composites. A series of nanocomposites based on un/modified organoclays was investigated in this study to elucidate the role of TMI on flammability of polymer nanocomposites. In this chapter a detailed study of the structure and morphology by SAXS and TEM followed by flame retardation tests is presented. We have used standard flame tests UL-94 and Limiting Oxygen Index (LOI) to establish how the flammability of polymer nanocomposites varies with various clays and TMI-modified clays.

4.4.1 TEM Examination of Clay Morphology

In polymer organoclay nanocomposites the status and morphology of organoclays plays a crucial role in deciding the effect on the final properties. It is thus very important that the inclusion of clay into the system takes place and we understand the mor-

phology of the resulting polymer nanocomposite thus formed, before estimating any property improvements. Even though X-ray analysis provides us with the details of variation in the layer structure and the changes in d-space values, to better assess the detailed morphology it is imperative to have photographic evidence of such polymer nanocomposites. TEM micrographs shown in Figure 4.54 reveal the distribution of organoclays (with and without TMI modification) dispersed in EVA nanocomposites. Excellent spatial resolution with a clear definition of the layered structure in intercalated organoclays (C20A and MMT-P) could be seen in these micrographs. The clay platelets are distributed parallel and dispersed evenly throughout the matrix, single exfoliated layers are also observed. In Figure 4.54, 2D TEM micrographs of EVA containing various unmodified and TMI modified organoclays as labeled are compared. Both systems exhibited a similar intercalated-exfoliated structure with uniform distribution of organoclays. As the organoclay loading is increased to 30 wt % no aggregates are observed. We observe strong local planar orientations in some locations. Based on the 2D images from EVA/TMI modified organoclays nanocomposites we again verify that there were no aggregates of TMI crystals present. Partially exfoliated morphology is revealed and the orientation of clay in the direction co planar to the film. This might be attributable to the increased melt viscosity of polymer nanocomposites and a higher number of network points may result in higher cross-linking. This kind of morphology may result in improved flammable property.

4.4.2 SAXS to Determine the Structure Variation

The effect of shearing on the morphology of polymer nanocomposite is very important, Figure 4.55 and Figure 4.56 illustrate the difference in morphology for two different shearing times. Figure 4.55 illustrates that shorter shearing time (3 min) in melt mixing results in formation of an intermediate layered structure with relatively sharp SAXS peaks located in between those in organoclays (or TMI-modified organoclays) and corresponding nanocomposites. This suggests that inefficient intercalation

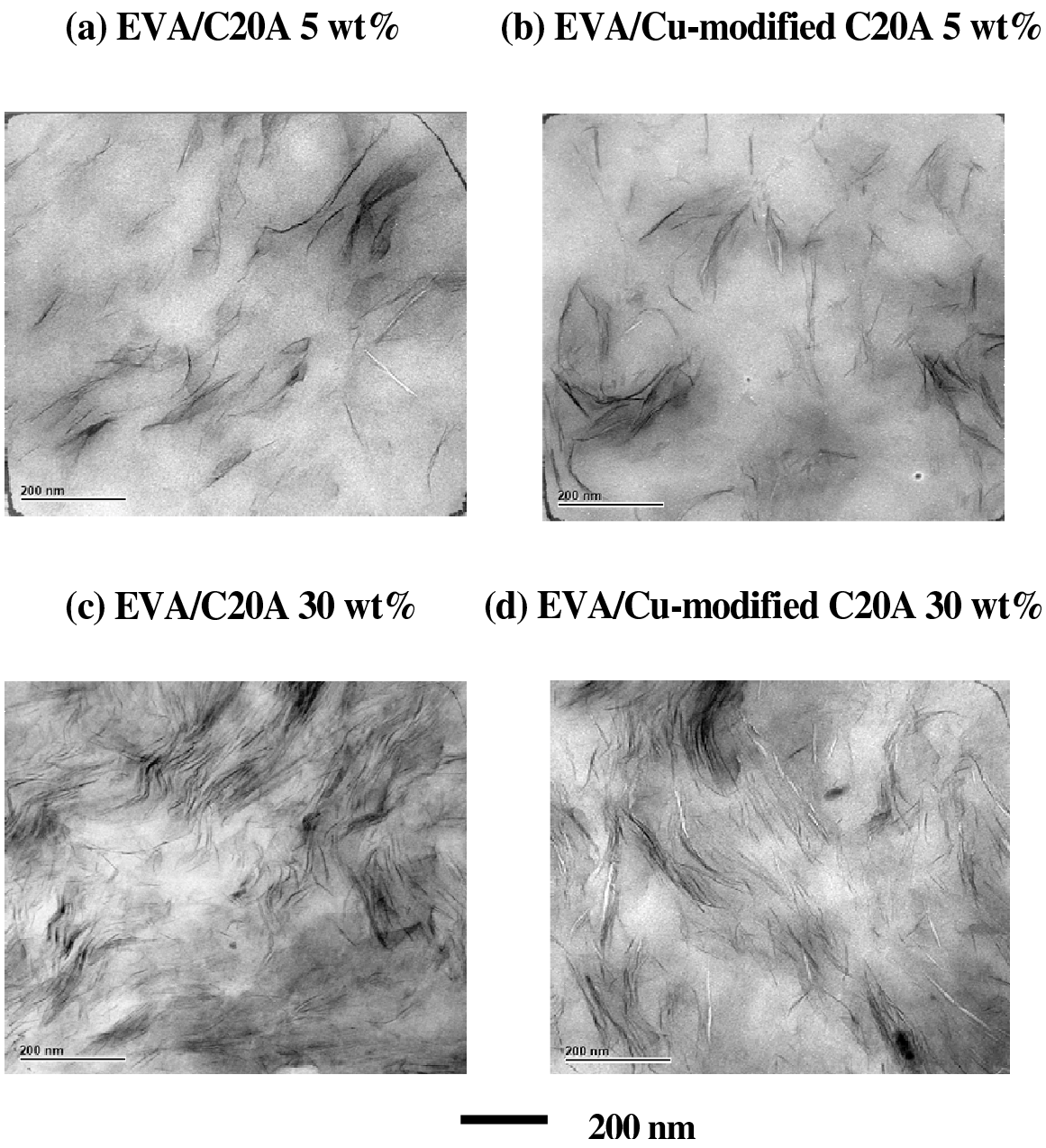

Figure 4.54: 2D TEM micrographs of EVA containing various unmodified and TMI modified organoclays.

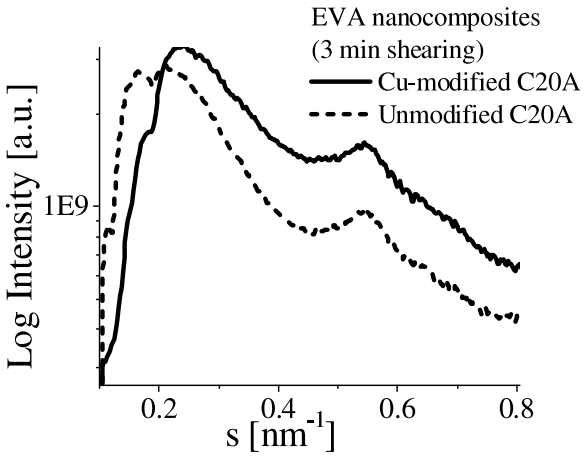

Figure 4.55: Integrated small angle X-ray profile of nanocomposites prepared by mixing for 3 minutes.

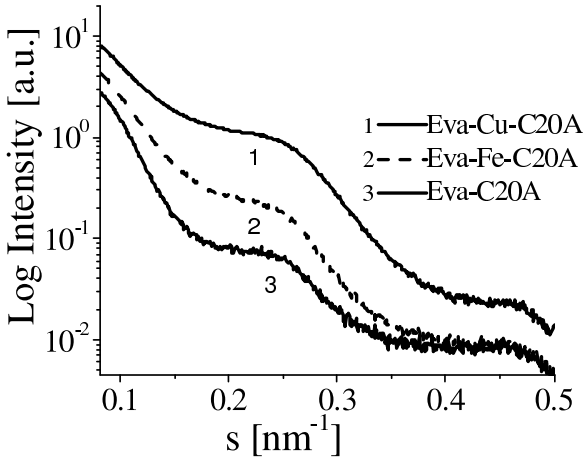

Figure 4.56: Integrated small angle X-ray profile of nanocomposites prepared by mixing for 10 minutes.

Sample	MMT	C20A	Cu- C20A	Fe- C20A	MMT-P	MMT-P/Cu
d-spacing (nm)	1.28	2.56	2.32	1.40	3.70	2.22

Figure 4.57: The *d*-spacing values of unmodified C20A and TMI-modified C20A.

and delamination of clay stacks took place in the matrix, resulting in formation of turbostratic structures. It is evident that the pillaring effect of TMI on the collapse of the layered structure, while notable in the pure filler form, can be overcome by sufficient shearing. We note that all of the following results were obtained from the shearing of 10 min. Figure 4.56 since longer time shearing did not affect the layer structure in TMI-modified clays. All the following results were obtained using 10 wt% of nanofillers unless specified otherwise. In our previous work [129], the TMI-modification of organoclays was shown to have a profound effect on the *d*-spacing of organoclay. The measured values of *d*-spacing for organoclays and TMI-modified organoclays used in this study are listed in Figure 4.57(Table). In $NaBH_4$-treated TMI-modified organoclays, we don't observe any clay peaks, possibly due to loss of periodicity upon reduction (shown in 2D SAXS images in Figure 4.58 and Figure 4.59. TMI can form pillar-like aggregates in the inter-layer gallery of the organoclays, whereby the structure enhances the binding of neighboring clay layers and decreases the *d*-spacing. This notion has raised the following concern that as some "weak" surfactant molecules are replaced by TMI, the modification process seems to impose an adverse effect on the resulting nanocomposite, i.e., the reduced concentration of surfactant molecules may hinder the intercalation and exfoliation of polymer molecules. To verify this, SAXS and measurements on nanocomposites based on TMI-modified organoclays were carried out and the results are as follows.

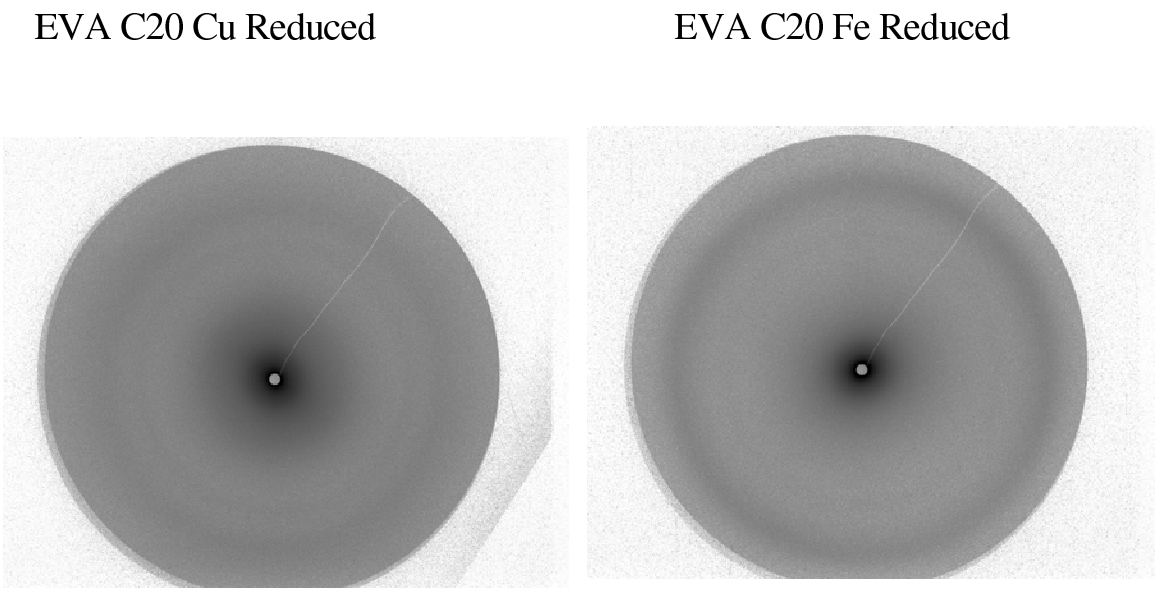

Figure 4.58: 2D SAXS images of EVA polymer nanocomposite containing reduced TMI in C20A organoclay.

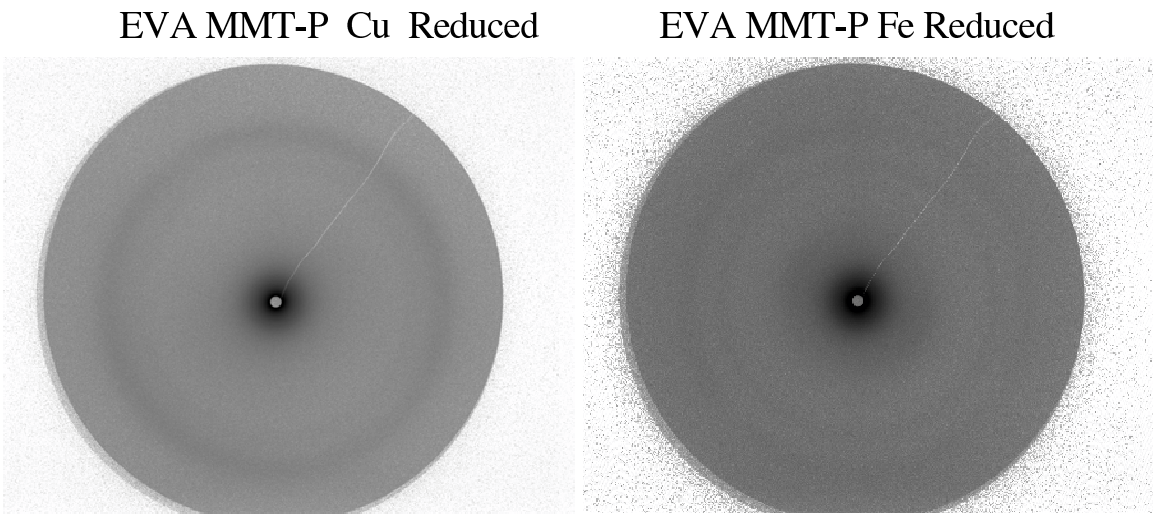

Figure 4.59: 2D SAXS images of EVA polymer nanocomposite containing reduced TMI in MMT-P organoclay.

Figure 4.60, Figure 4.61, Figure 4.62, Figure 4.63, and Figure 4.64, shows temperature resolved SAXS profiles of various nanocomposites (EVA/C20A, EVA/TMI-modified C20A, EVA/MMT-P, and EVA/TMI-modified MMT-P) prepared by melt mixing for 10 min. In EVA/C20A nanocomposites, the scattering peak at 0.24 nm_{-1} (d = 4.16 nm) and EVA/MMT-P peak at 0.27 nm_{-1} (d = 3.70 nm) represents the intercalated structure induced by EVA molecules, since the *d*-spacing of C20A is only 2.56 nm and that of MMT-P is only 2.22 nm Figure 4.57(Table). However, it is interesting to note that all the profiles in Figure 4.60, Figure 4.61, Figure 4.62, Figure 4.63, and Figure 4.64, (EVA/C20A, EVA/TMI-modified C20A) exhibit similar scattering features (i.e., peak shape and position), suggesting a nearly identical layered structure but in the case of EVA/MMT-P, and EVA/TMI-modified MMT-P the peak features and position changes drastically suggesting a drastic change in morphology of clay dispersed in polymer matrix. Broadening of SAXS peaks was found in scattering profiles of all nanocomposites, indicating that the average stack size was decreased due to partial delamination of organoclays and breaking up into small tactoids. The above results verify that there is a reasonable compatibility between TMI-modified organoclays and the EVA matrix.

The temperature dependence of nanostructure in nanocomposites was investigated using *in-situ* SAXS techniques. Our results indicate that the *d*-spacing in EVA nanocomposites always decreases with increasing temperature, which can be attributed to the reduced compatibility between polymers and organoclays (i.e., the LCST-like phase behavior) [7]. It is seen that as temperature increases from 80 to 200°C, the SAXS peaks in EVA nanocomposites Figure 4.60, all shifted towards higher s values (i.e., *d*-spacing decreased). From these results, it is evident that EVA nanocomposites exhibit the LCST-like polymer-clay phase segregation behavior. It is interesting to note that the loss of peak features in SAXS profiles after the heating-cooling cycle was less pronounced in EVA/TMI-modified C20A than that in

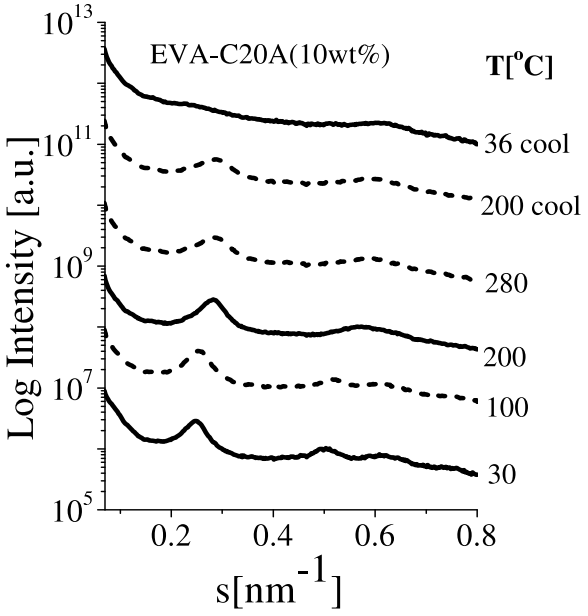

Figure 4.60: Temperature resolved integrated small angle profile for EVA C20A nanocomposite.

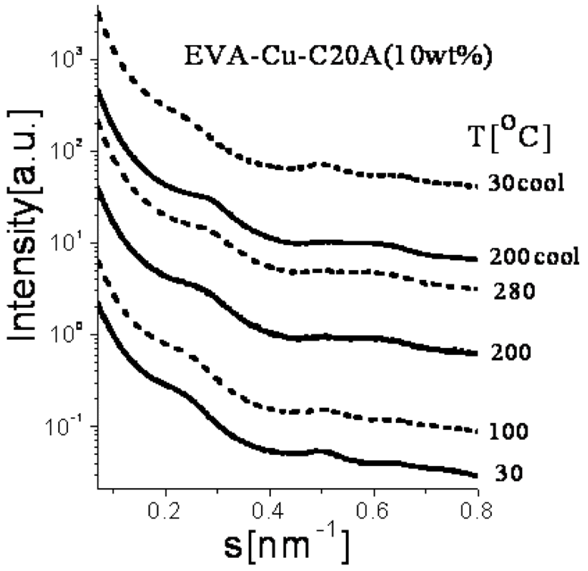

Figure 4.61: Temperature resolved integrated small angle profile for EVA C20A (Cu-modified) nanocomposite.

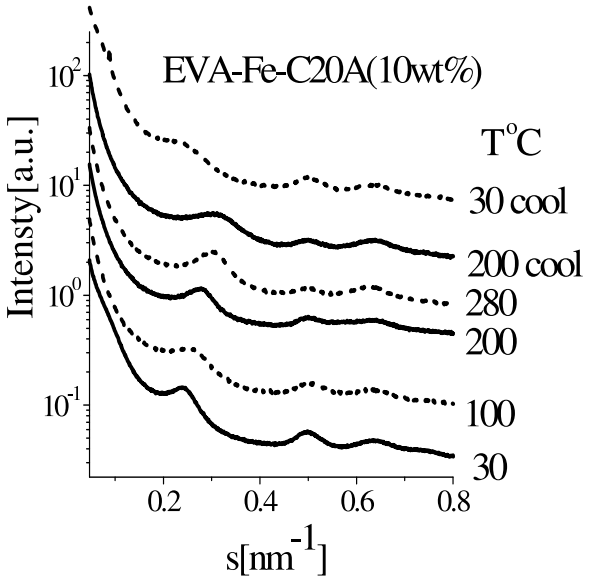

Figure 4.62: Temperature resolved integrated small angle profile for EVA C20A (Fe-modified) nanocomposite.

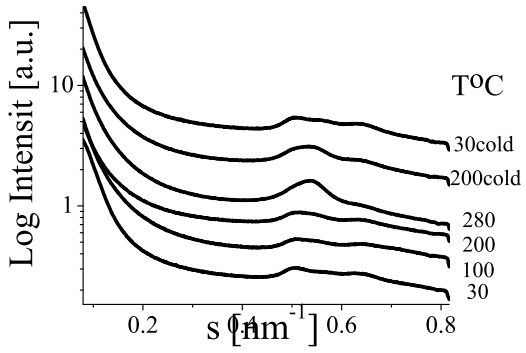

Figure 4.63: Temperature resolved integrated small angle profile for EVA MMT-P nanocomposite.

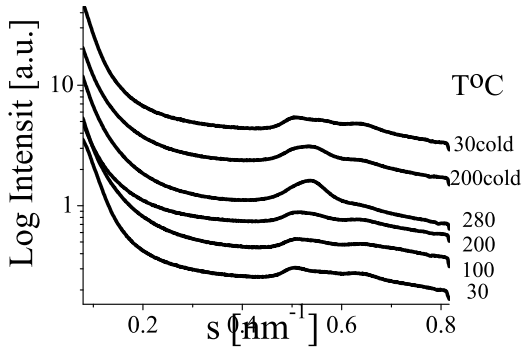

Figure 4.64: Temperature resolved integrated small angle profile for EVA MMT-P(cu-modified) nanocomposite.

EVA/C20A. It can be seen that broadening of SAXS peaks during the heating cycle within the temperature range of 120-280°C and consequent cooling cycle is more significant for a system containing un-modified organoclay than in its TMI-modified analogs. Moreover in EVA-C20A, after heating-cooling cycle SAXS peaks drastically broaden and the maxima positions do not recover upon cooling to 30°C conversely in EVA MMT-P nanocomposite the peak position is restored upon cooling which can be attributed to thermally stable phosphonium surfactants. The loss of scattering features in SAXS for EVA/C20A at temperatures above 200°C was attributed to thermal degradation of organic surfactants in organoclays. EVA nanocomposites undergo thermally reversible phase segregation upon heating above 180°C resulting in de-intercalation of organoclays and a decrease in average *d*-spacing. As the temperature decreases, compatibility between the organoclay and EVA increases, resulting in partial re-intercalation of clay layers by EVA. In the C20A-based system, because of surfactant loss during heating cycle and loss of periodicity during re-intercalation process, the original structure does not recover completely. In MMT-P, however, the recovery of structure takes place as evident from SAXS profile. This can be attributed to comparatively thermally weak C20A where desorption and degradation of surfactant component may cause complete collapse of organic layers, resulting in a loss of periodicity which causes the shifts and broadening of SAXS peaks observed in EVA8-C20A systems. Thus, the persistence of SAXS features in EVA/TMI-modified C20A nanocomposites and EVA/MMT-P nanocomposites as seen in thermally resolved integrated SAXS profiles indicates that TMI-modified organoclays and MMT-P organoclays have a higher thermal stability than unmodified C20A where the SAXS profile showed that scattering peaks moderately broadened and weakened at temperatures above 200°C (albeit to a lesser degree than in the EVA/C20A nanocomposite). In addition we suggest that the pillaring of the organoclays by TMI does not allow for complete collapse of organic layers even when surfactant loss is significant.

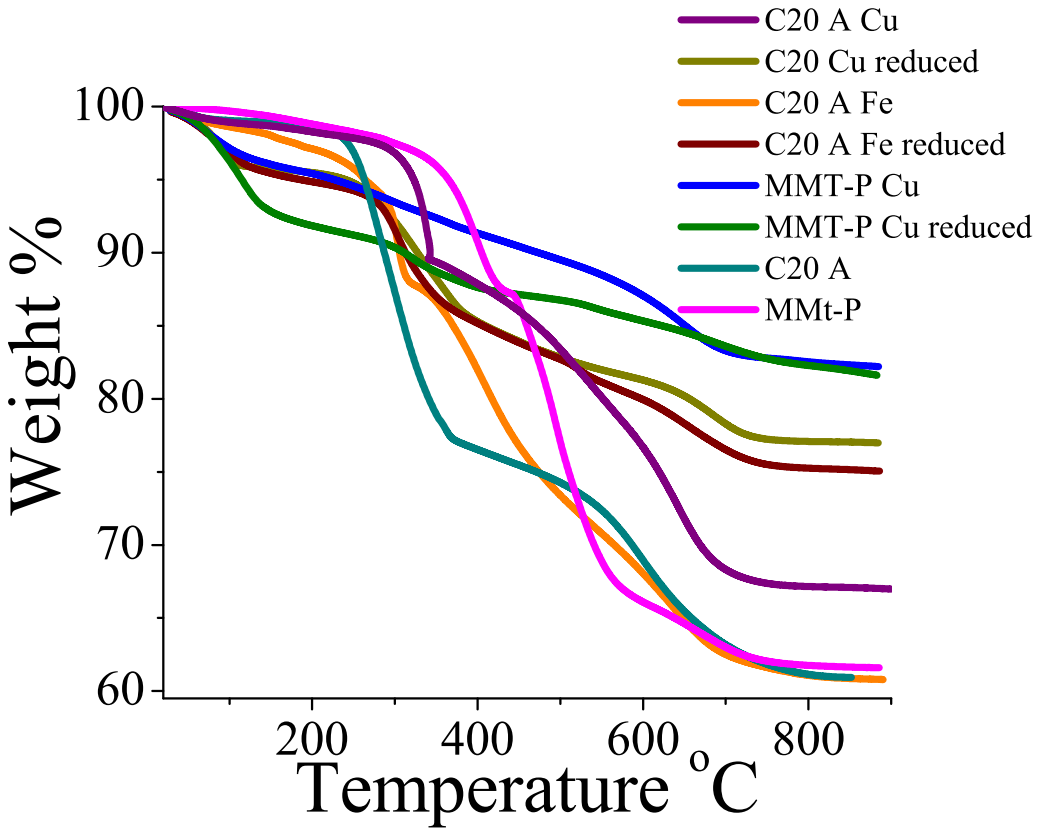

Figure 4.65: TGA thermograms of various organoclays and tranistion ion modified organoclays.

4.4.3 Thermo Gravimetric Analysis

In our previous study[129], the modification of TMI significantly increases the thermal stability of organoclays, i.e., the onset temperature of thermal degradation (in the region of 260-360°C) shifts towards a higher value (by 30°C) and the content of solid residue increases substantially. TGA thermograms of organoclays used and nanocomposites containing these organoclays (unmodified and TMI-modified organoclays) are illustrated in Figure 4.65 and Figure 4.66 respectively. It is seen that all nanocomposites exhibited the similar two-stage weight loss behavior. In the first stage of degra-

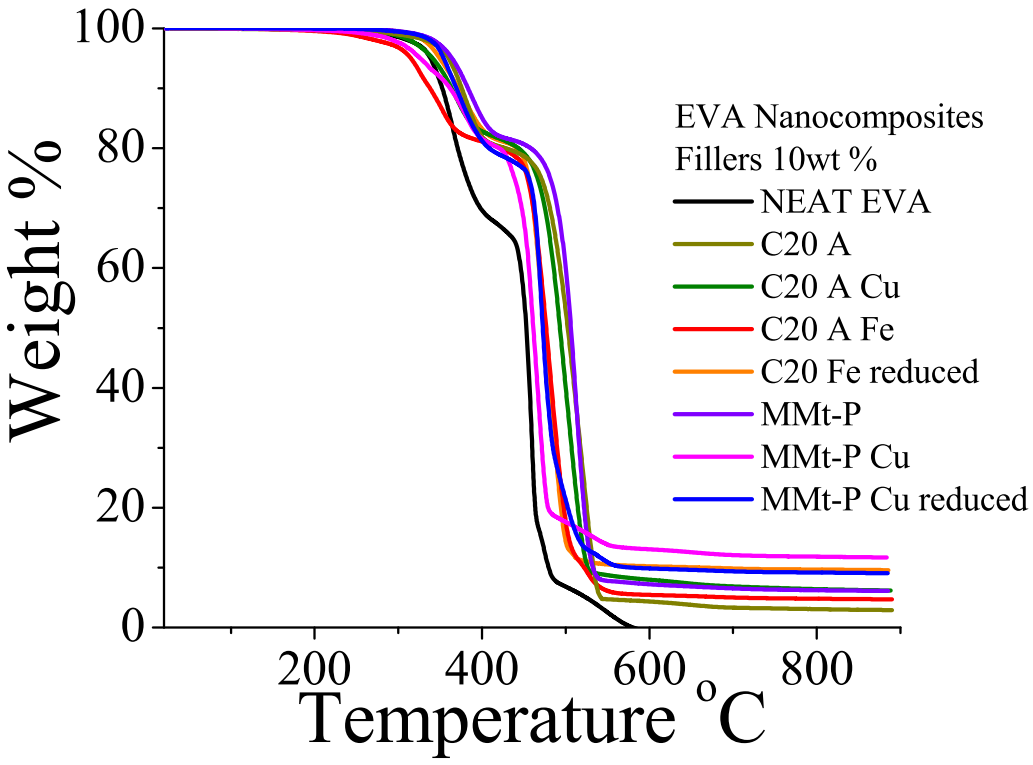

Figure 4.66: TGA thermograms of EVA polymer nanocomposites containing various organoclays and tranistion ion modified organoclays.

dation, only a moderate improvement in thermal stability was found in nanocomposites. For example, the onset temperature of degradation (between 260-360°C) for EVA/TMI-modified nanocomposites increased by about 15°C when compared to neat EVA. Even the organic content did not change much after the first stage of degradation; the formation of char significantly increased with the presence of TMI in the second stage of degradation. It is interesting to note that the maximum amount of char was formed when Cu was used in modification of C20A, while Fe-modified C20A produced char weighing less than that from Cu-modified C20A Figure 4.65. This difference can be attributed to the secondary effect, such as the catalytic activity of iron oxide on the combustion process. Of the two organoclays, TBHDP Br-MMT proved to be the more thermally stable, as indicated by its onset of degradation at a higher temperature (297°C, compared to approximately 250°C for C20A), which is as per our SAXS results. Also MMT-P based clays show less total loss of weight in TGA. This can be attributed to the fact that tetra alkyl-phosphonium salts like TBHDP Br can form more thermally stable phosphoryl (P=O) bonds with the aluminosilicate layers of montmorillonite, which enables (TBHDP Br)-MMT to undergo more reaction pathways, and thus can potentially produce more carbonaceous char when ignited. Alkylammonium salts, however, cannot degrade to form nitrosyl (N=O) bonds due to the lack of vacant d-orbitals of energy low enough to form a five-coordinate intermediate. Thus, it can be inferred that the internal chemistry of the clay plays more of a role in the thermal degradation of tetra alkyl phosphonium surfactants than in that of alkylammonium surfactants.

It was also observed that the organoclays modified with TMI and then treated with NaBH4 shows better therma properties. Even though $NaBH_4$ treated clay begins to degrade at approximately the same temperature (325°C) as the other two Cloisite 20A samples, it shows a much less total loss of weight, with a difference of approximately 25 wt%, thereby makes this clay sample the most thermally stable of the three. This

may be due to the catalytic activity of various oxidation states of TMI (Cu^{+}/Cu^{0} or $Fe^{2}+/Fe^{3}+$) that may increase the thermal stability of the organoclays in which they exist.

Figure 4.66 shows obtained thermograms for neat EVA polymer as well as EVA polymer-clay nanocomposites. The thermal degradation of EVA usually occurs in two steps: the initial loss of acetic acid, followed by the loss of the remaining partially unsaturated poly(ethylene-co-acetate). This process may be accelerated by the presence of clay. Specifically, it has been proposed that clay particles shield the polymer during degradation, which allows reactions in which some new side products are formed and also a change in the quantity in which they are formed. Also, the presence of hydroxyl groups on the clay edges may accelerate the initial loss of acetic acid. Upon combustion, a series of gases and hydrocarbons are released, including but not limited to carbon dioxide, methane, ethylene, and carbon monoxide. It is proposed that the most thermally stable nanocomposite will be intercalated with the most thermally stable organoclay. Figure 4.66 displays the thermograms of EVA polymer-clay nanocomposites of neat organoclays (Cloisite 20A and TBHDP-MMT) and those organoclays that had been modified with TMI and reduced TMI. Of all three thermograms displayed, the one of EVA with 10 wt% MMT-P modified with TMI and then treated with $NaBH_4$ displayed the greatest thermal stability with the least loss of weight, as predicted by the thermograms of its clay constituents. The onset of degradation temperatures of the two TMI-modified samples differ by approximately 35°C. This may indicate that $NaBH_4$ did indeed influence the chemical nature of the TMI ions, a pictorial representation indicating this is given in Figure 4.67.

4.4.4 Flammability by UL-94 and Limited Oxygen Index

SAXS and TGA results give us a good estimate of the structural changes that might occur at higher temperatures, but to elucidate the flammability of materials a series

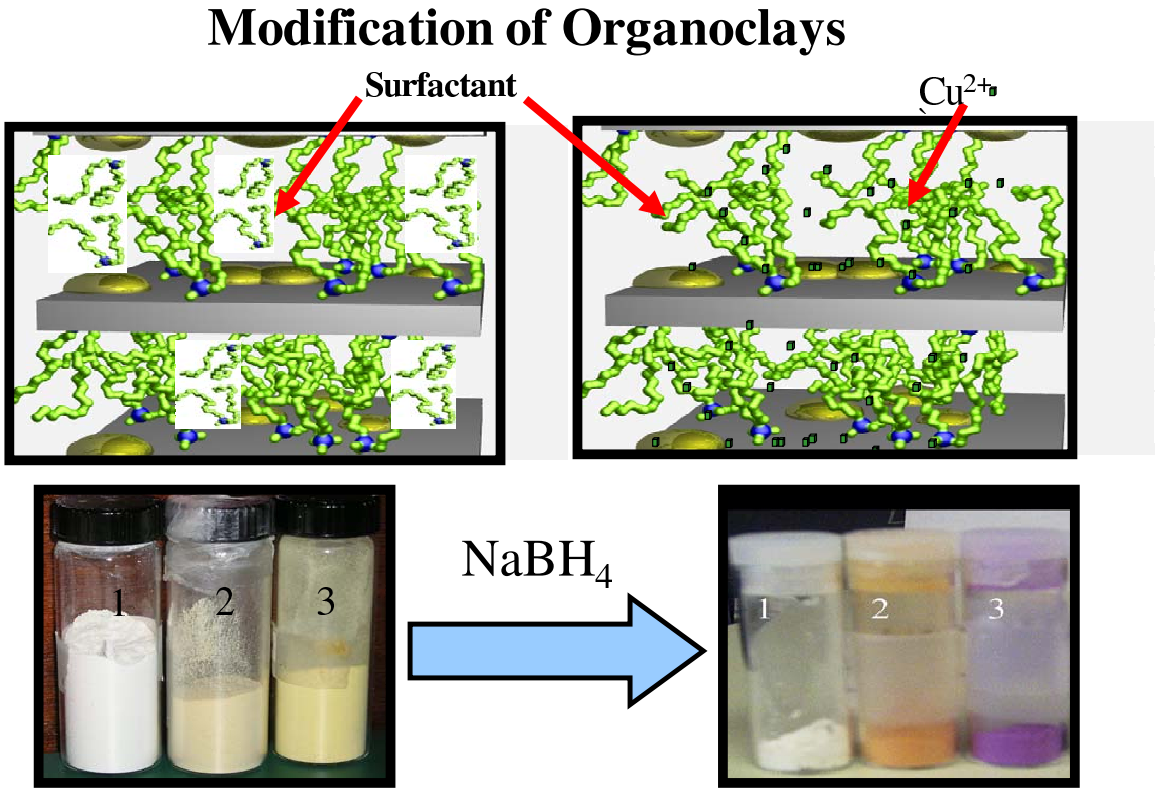

Figure 4.67: A pictorial representation showing introduction of TMI in the clay layers and visible effect of treatment of sodium borohydride on TMI modified C20A organoclays.

of flame tests is required. We have evaluated the flammability of polymer nanocomposites using standard UL 94 flame test and Limiting Oxygen index (LOI). These tests were used to measure the characteristics of plastic materials, in particular, to determine the tendency of a plastic material to self-extinguish or to spread flame after ignition. UL-94 follows the materials classification system for the vertical flame test, where materials are labeled as V-0, V-1, and V-2 materials and the basis of classification is given in Figure 4.68(Table) This classification is based on the ability of a vertically held sample subjected to flame, to self-extinguish within a certain time period after the flame source was removed. The samples are classified as per UL-94 standard as V-0 if for each sample the burning time does not exceed 10s, the sum for the five samples does not exceed 50s, and the surgical cotton below the specimen does not ignite during the test. The samples are classified as V-1 if for each sample the burning time does not exceed 30s, the sum for five samples does not exceed 250s and the surgical cotton below the specimen does not ignite during the test. If the surgical cotton below the specimen was ignited with the ignited dripping polymeric material, the sample is assigned as V-2. The time is counted only after the removal of flame upon ignition of sample. A series of nanocomposites based on organoclays and TMI-modified organoclays were tested for their flammability as per UL-94 standard by subjecting them to vertical flame test and are classified according to UL-94 standards. The results are tabulated in Figure 4.69(Table).

The limiting oxygen index determines the ability of material to burn in oxygen. Air is comprised of about 20.95% oxygen by volume and any material with a limiting oxygen index less than this will burn easily in air. Conversely, the burning behavior and tendency to propagate flame will be reduced if a polymer has a limiting oxygen index greater than 20.95 after removal of the igniting source. Self-sustaining combustion is not possible if LOI>100, such values are not physically meaningful. From the preceding lines, two obvious groupings are LOI<20.95 and LOI>100. We refer to

Criteria Conditions	V-0	V-1	V-2
Afterflame time for each individual specimen t_1 or t_2	≤ 10 s	≤ 30 s	≤ 30 s
Total afterflame time for any condition set ($t_1 + t_2$ for the 5 specimens)	≤ 50 s	≤ 250 s	≤ 250 s
Afterflame plus afterglow time for each individual specimen after the second flame application ($t_2 + t_3$)	≤ 30 s	≤ 60 s	≤ 60 s
Afterflame or afterglow of any specimen up to the holding clamp	No	No	No
Cotton indicator ignited by flaming particles or drops	No	No	Yes

Figure 4.68: UL-94 vertical flame test material classifications.

the materials satisfying these requirements as being "flammable" and "intrinsically non-flammable" respectively. Horrocks et. al. [181] suggested that the materials with a limiting oxygen index greater than 28 are generally self-extinguishing. Thus any material with LOI > 28.00 can be classified as "self-extinguishing". The threshold LOI=20.95 is of great practical interest and these materials can be referred to as marginally stable or "slow-burning". The tenet in the limiting oxygen index is that the higher the value of the LOI the 'safer' the material. A series of nanocomposites based on organoclays and TMI-modified organoclays were tested for their LOI values which are tabulated in Figure 4.69(Table). Increased oxygen consumption can be attributed to oxidation of volatile released upon combustion.

Sample	UL-94	LOI
Neat EVA	V2	19.19
EVA with C20A	V1	19.35
EVA with Cu-modified C20A	V1	19.25
EVA with C20A- Cu reduced	V1	19.25
EVA with C20A- Fe-modified	V1	19.72
EVA with C20A- Fe reduced	V1	19.78
EVA with MMT-P	V1	20.97
EVA with Cu-modified MMT-P	V0	21.65
EVA with Cu-reduced MMT-P	V0	21.64
EVA with Fe-modified MMT-P	V0	21.12
EVA with Fe reduced MMT-P	V0	21.12

Figure 4.69: Results as obtained from UL-94 and LOI flammability tests for various polymer nanocomposites.

4.4.5 Discussion

The morphology as observed from TEM showed that there are no large aggregates of clay in polymer nanocomposites, and intercalated and exfoliated morphologies coexist in all polymer nanocomposites. The presence of TMI ions may cause pillaring of mineral sheets in organoclays, thus decreasing the extent of clay exfoliation in EVA matrices and reducing the amount of tactoids available for the formation of tactoid networks. The relationships among the thermal properties, the amount of char formed during combustion of nanocomposites, and the corresponding organoclay structure are essential to the mechanism of FR activity. The EVA matrix without C20A burned and dripped, while nanocomposites with organoclay and TMI-modified organoclays showed visible FR activity, i.e., they formed char upon burning. The FR activity of nanocomposites with TMI-modified organoclays was notably better than that of nanocomposites containing unmodified organoclays. Also, the FR activity of MMT-P based polymer nanocomposite was better than C20A based nanocomposites. This can be attributed to higher thermal stability of phosphonium surfactants. As we move higher in temperature there is a slight shifting of peaks initially, and at higher temperatures, peak features are lost and this change in X-ray profiles suggest that there is reorganization of aluminum silicates layers that takes place at elevated temperature. Also the production of volatiles might result in the increase of the internal pressure within layer disorder resulting in lost of periodicity and stacking order. A possible loss of clay stacks might occur at very high temperature. This was shown in X-ray of char from polymer nanocomposites in our previous work. From the thermograms of EVA polymer-clay nanocomposites, these containing (TBHDP Br-MMT) and its TMI counterparts showed the highest onset of degradation and the least loss of weight when compared to its C20A equivalents, thus being the most thermally stable. The degradation of organoclays takes place via Hofmann elimination

or β-elimination as in the reaction scheme shown below in equation 4.7:

$$R_3N + -CH_2 - CH_2 - R' \rightarrow (Basex^-)R' - CH = CH_2 + R_3N + HX \qquad (4.7)$$

where R3N+-CH2-CH2-R' represents the tetra alkylammonium organic surfactants contained within organoclays such as Cloisite 20A and modified MMT, the nucleophilic base (X^-) is generally an anion from the external environment, such as a hydroxyl group from the aluminosilicate layer. In this reaction, the β-proton is abstracted by a basic molecule to generate a tertiary amine from the α-carbon. However, in the case of alkylammonium salts, other reactions, such as nucleophilic substitution, may also play a role in their degradation process at higher temperatures. This reaction is dependent on the basicity of the anion of the salt, thus making it self-catalyzed. The details of the nucleophilic subsititution reaction are given below in equation 4.8:

$$R_3N + -R' \rightarrow R_3N + R'X \qquad (4.8)$$

When intercalated into mineral clay such as montmorillonite, the basicity of the aluminosilicate layers paired with the Lewis base sites may also contribute to the thermal degradation of the salt, most likely favoring Hofmann elimination due to the onset of degradation of the ammonium organoclay at a lower temperature. The complete chemistry behind the thermal degradation of quaternary alkyl ammonium compounds is not yet fully understood. Like their quaternary alkyl ammonium counterparts, tetra alkyl phosphonium salts also degrade via Hofmann elimination and nucleophilic substitution reactions given above, but differ slightly in thermal degradation when intercalated into mineral clays such as montmorillonite. Unlike alkyl ammonium salts, tetra alkylphosphonium salts are much more sensitive to reactions with the acidic hydroxyl groups found in the aluminosilicate layers to yield highly stable phosphoryl bonds (P=O). This concept is illustrated in the following nucle-

ophilic substitution reaction, in equation 4.9:

$$R_3P+-CH_2-CH_2-R' \rightarrow (OH^-)R_3P+-CH_2-CH_2-R' \rightarrow R_3P=O+CH_3-CH_2-R' \tag{4.9}$$

Hofmann elimination reactions follow SN2 nucleophilic substitution route, and occur in the presence of basic anions such as hydroxide which extracts hydrogen from the β carbon of quaternary ammonium, yielding an olefinic and tertiary amino group. The proximity of the Lewis base sites and basic alluminosilicates surface to the intercalated alkyl quaternary ammonium molecule is conducive to enhancing of the Hofmann elimination reaction as seen by the lower onset temperature for organoclays and increased olefinic products. Confined within layers, the initial products undergo successive secondary reactions such as alkyl chain scission, free radical condensation, and addition of olefinic species. The presence of TMI in organoclays may serve as catalyst to oxidative cleavage of alkenes to produce aldehydes at elevated temperature The mechanism of thermal degradation for EVA involves two major steps: (1) the loss of vinyl acetate units via a de-acylation process resulting in the formation of double bonds, and (2) the degradation of resulting unsaturated material. It is conceivable that the presence of TMI-modified organoclays in the EVA matrix may promote cross-linking of unsaturated products formed during degradation, thus hindering the decomposition process. However, the Lewis acidity of clay surface in the presence of TMI may also facilitate the chain scission in EVA. As evidenced from TGA results, the content of char formed in the presence of TMI was substantially more than that unmodified organoclays. It is conceivable that in TMI-modified organoclays, TMI does not promote the combustion reaction, and instead, it forms a complex with the surfactant and results in more char. It is clear that the thorough understanding of the thermal degradation mechanism for polymer nanocomposites is rather complex as this material cross-links, forms char, and the degradation of material depends on the absorption characteristic of polymer nanocomposites when exposed to heat sources.

The presence of TMI promotes cross-linking in the polymer matrix during the combustion, and formation of tactoid network improving the FR activity is strongly pronounced over the entire range of tested temperatures. From our flammability tests we observed that the neat EVA matrix without organoclay burned and dripped, and due to the dripping behavior, material is removed from the pyrolysis zone. This decreases the fuel support rate, resulting in decrease of the size of flame during burning in case of neat polymer. On the other hand, upon inclusion of flame retardant additives there is an interconnected network formed which increases the melt viscosity of material and polymer is retained in molten state shielded by the inorganic silicates. Nanocomposites with unmodified organoclays and TMI-modified organoclays showed visible FR activity, i.e., they formed char upon burning. The FR activity of nanocomposites with TMI-modified organoclays was notably better than that of nanocomposites with unmodified organoclays. Also the oxidation of volatile products consumes oxygen and results in higher LOI values. During burning interconnected structure remained in material and influenced materials melt viscosity resulting in less dripping flowing and hindering the decomposition of volatiles feeding the flame. This percolated structure stabilized the pyrolysis zone and residue (stiff char was obtained). During flaming of materials bubbling is observed, which results in protective floccules shielding the polymer form external thermal radiation and heat feedback from the flame acting as thermally insulated layer for neat polymer.

Chapter 5

Conclusions

Detailed analysis of phase transitions, thermal stability, morphological, and structural changes in organoclays, under various conditions, are presented which were investigated by a combination of scattering, spectroscopic and thermal techniques. Results from this study show that feasible interpretation of SAXS data from organoclays must account for the complex character of layer thickness distribution in organoclays. It was concluded that the structures of cloisite organoclays have, a bimodal organic layer thickness distribution where the thinner organic layer contains a monolayer with surfactant molecules bound to the adjacent clay surfaces and the thicker layer contains two monolayers of surfactant with only about half of them being bound to the clay surface. The double layer content was found to increase with the overall surfactant loading. When the temperature is increased, organoclays undergo a melting-like order-disorder transition, resulting in the randomization of surfactant conformation followed by bimodal layer thickness distribution again.

Based on SAXS and SEM results, we suggest that the Somasif minerals contain a notable amount of 1:1 smectite clay in the form of a tubular (or scroll-like) structure, similar to that of chrysotile (the main component of asbestos). It is conceivable that the surface properties of alternating sides of the Somasif mineral sheets are different, resulting in "Peierls-distorted stacks" with AB-type periodicity in the corresponding organoclays, The AB-type periodicity was confirmed by SAXS, which profile exhibited a low intensity scattering maximum with its s value corresponding to the combined AB spacing. The temperature resolved SAXS results indicate that the Somasif-organoclays can result in structural rearrangements, causing the shifting

and splitting of SAXS peaks as the relative contributions of AA, AB and BB systems would change. It is clear that Somasif-based organoclays consist of two populations of organic layer thicknesses, which can undergo thermal transitions and desorption leading to different lamellar structures.

The exfoliation of organoclay was successfully achieved by microwave irradiation and solvent dispersion techniques. Surface energy plays a crucial role in exfoliation by dispersion of organoclays in various solvents, while the change in conformation of surfactants due to microwave irradiation is important to achieve successful exfoliation. Two organoclays with same surfactants were subjected to microwave irradiation, but the one which didn't contain any residual or very little amount of residual water was exfoliated. In other case hydrogen bonded water absorbed microwave radiation and exfoliation of such clays was not observed.

TEM investigation of polymer-layered silicate nanocomposites concludes that intercalated-exfoliated structures co-exist resulting in mixed morphology of polymer nanocomposites. There is a stack height distribution of tactoids and there is a finite fraction of tactoids with a stack height of one, i.e. single lamella. Due to the presence of the individual silicate layer, the total inner surface area and, thus, the average aspect ratio of the polymer nanocomposite increases, thereby decreasing its permeability. SAXS is used to quantify orientation distribution of dispersed organoclay particles in polymer matrix. The 2D analytical scheme also leads to the orientation distribution of the mineral stacks dispersed in polymer matrix. With the increase of the fraction of organoclay in polymer matrix the orientation increases. This is attributed to a decrease in available free volume for thermal fluctuation of organoclay particles.

Addition of carbon black and curing agent doesn't affect the morphology of polymer nanocomposites but induces a change in the orientation of clay platelets which conclusively affects the permeability of system. Orientation depends on the

free volume available for clays to move during compression and interaction of clay platelets with polymer matrix and other fillers. Association of clay with carbon black and polymer matrix play a crucial role in inducting orientation effects. The orientation of organoclays took place during compression and extrusion as samples from melt mixer did not exhibited orientation of clays. It was observed that cylindrically extruded samples have random orientation while orientation attributed to extrusion flow force and reorientation of clay can take place once flow force is removed. In compressed sheets, the preferential orientation of organoclays along the plane of film takes place upon compression, which can be attributed to squeeze flow force. In addition, orientation was higher for compressed sheets in comparison to cylindrically extruded samples, which could be explained by the difference in flow fields (i.e., squeeze flow versus extrusion flow). The oxygen permeability of polymer nanocomposites film decreases with increase of orientation of organoclays which creates a tortous path for the permeating molecule. Even in highly compressed films, organoclays had relatively poor in-plane orientation. This is because the organoclays can rotate and bend in the melt; thus, they are very difficult to completely align along the direction of plane even under extensive flow conditions.

Effective fire retardant fillers were developed using TMI modification of commercially available organoclays C20A and organoclay synthesized using thermally stable surfactant tri-butyl-hexadecyl-phosphonium bromide (TBHDPB) for thermoplastic polymers to form nanocomposites with all expected characteristics and enhanced FR properties. TEM and SAXS results indicate that TMI-modified organoclays exhibited strong pillaring effects, which decreased the interlayer d-spacing. However, the shearing force during melt mixing could overcome the pillaring effect of TMI such that polymer chains would penetrate the TMI-modified organoclay stacks. Polymer nanocomposites containing TMI-modified organoclays were found to possess better flame retardant properties than their counterparts containing unmod-

ified organoclays. The physico-chemicalmechanism behind these phenomena is not yet completely understood, yet we hypothesize that crosslinking of non-saturated products of thermal degradation, as well as oxidative dehydrogenation processes that would result in aromatization, may be catalyzed by TMI. The catalytic effect may play a role in the increased flammability of nanocomposites. Organoclays synthesized from inorganic mineral clays (montmorillonite) using organic surfactant TBHDP Br were superior in comparison to C20A, and this may be attributed to the formation of thermally stable phosphoryl (P=O) bonds whereas the tetraalkylammonium surfactants in C20A organoclay are not capable of forming similar bonds. Further TMI-modified samples were then treated with NaBH4 in ethanol to reduce the TMI within them. It was proposed that the synergistic effect of TMI and thermally stable surfactant are helpful in developing FR agents for improved flammability of polymers.

Bibliography

[1] E.P. Giannelis, Polymer layered silicate nanocomposites, Advanced Materials., **1996**, 8 (1), 29.

[2] A. Blumstein *Journal of Polymer Science Part A*, **1964**, 3(7), 2665.

[3] Y.Kojima, A. Usuki , M. Kawasumi, A. Okada, T. Karauchi and O. Kamigaito, *J Polym. Sc. Part A*, **1993**, 49, 1259.

[4] E.P. Giannelis , *JOM*, **1992**, 44, 28.

[5] H. Gleiter. *Advanced Materials*, **1992**, 4(7-8), 474.

[6] B. M..Novak, *Advanced Materials*, **1993**, 5(6), 422.

[7] M. Gelfer, C. Burger, A. Fadeev, I. Sics, B. Chu, B. S. Hsiao, A. Heintz, K. Kojo, S-L. Hsu, M. Si, and M. Rafailovich, *Langmuir*, **2004**, 20 (9), 3746.

[8] M. Biswas and S. S. Ray in *New Polymerization Techniques and Synthetic Methodologies*, **2001**, 155, 167.

[9] E. P. Giannelis, R. Krishnamoorti and E. Manias. *Advances in Polymer Science*, **1999**, 138, 108.

[10] R. A. Vaia, G. Price, P. N. Ruth, H. T. Nguyen and J. Lichtenhan. *Applied Clay Science*, **1999**, 15(1-2), 67.

[11] R. A. Vaia, H. Ishii and E. P. Giannelis. *Chemistry of Materials*, **1993**, 5(12), 1694.

[12] R. K. Bharadwaj. *Macromolecules*, **2001**, 34(26), 9189.

[13] R. Xu, E. Manias, A. J. Snyder and J. Runt. *Macromolecules*, **2001**, 34(2): 337.

[14] K. Yano, A. Usuki, A. Okada, T. Kurauchi and O. Kamigaito. *Journal of Polymer Science, Part A: Polymer Chemistry*, **1993**, 31(10): 2493.

[15] J. W. Gilman. *Applied Clay Science*, **1999**, 15(1-2), 31.

[16] J. W. Gilman, C. L. Jackson, A. B. Morgan, R. Harris Jr, E. Manias, E. P. Giannelis, M. Wuthenow, D. Hilton and S. H. Phillips. *Chemistry of Materials*, **2000**, 12(7), 1866.

[17] T. Liu , W. C.Tjiu, C.He, S.S.Na, T.S.Chung, *Polymer International*, **2004**, 53(4), 392.

[18] Lee A, J.D. Lichtenhan, *J, Appl. Polym. Sc.,* **1999,** 73(10), **1993**, 2001.

[19] G.M. Kim, D.H. Lee, B. Hoffmann, J. Kressler, and G. Stppelmann, *Polymer*, **2001**, 42, 1095.

[20] F. Hussain, M. Hojjati, M. Okamoto, R. E. Gorga, *Journal of Composite Materials*, **2006**, 40(17), 1511.

[21] R. E. Gorga. and R. E. Cohen, *J. Polym. Sci., Part B: Polym. Phys.,* **2002**, 42(14), 2690.

[22] S. S. Ray, K. Yamada, M. Okamoto, Y. Fujimoto, A. Ogami, and K. Ueda, *Polymer*, **2003**, 44, 6631.

[23] Y. Halpern, D.M. Mott and R.H. Niswander, *Ind. Eng. Chem. Prod. Res.Dev.,* **1984**, 23, 233.

[24] J. W. Cho and D. R. Paul, *Polymer*, **2001**, 42(3), 1083.

[25] E. Thostenson, C. Li, and T. Chou, *Journal of Composites Science and Technology*, **2005**, 65, 491.

[26] D. Schmidt, D. Shah, and E.P. Giannelis, *Solid State and Materials Science,* **2002**, 6(3): 205.

[27] J.J. Luo, and I.M. Daniel, *Compos. Sci. Technol.*, **2003**, 63(11): 1607.

[28] J. W. Lee, Y.T. Lim, and O.O.Park, *Polym. Bull.* **2000**, 45, 191.

[29] W. Xie, Z.M. Gao, W.P. Pan, D. Hunter, A. Singh, and R Vaia, *Chem. Mater.* **2001**, 13, 2979.

[30] P.K. Ghosh and A.J. bard, *J. Am. Chem. Soc.*, **1983**, 105, 5691.

[31] H.Y. Liu and F.C. Anson, *J. Electroanal. Chem.,* **1985**, 184, 411.

[32] R.D. king, G.D. Nocera and T.J. Pinnavaia, *J. Electroanal. Chem.,* **1987**, 236, 43.

[33] D. Rong, Y.I. Kim, and E.T. Mallouk, *Inorg. Chem.,* **1990**, 29, 1531.

[34] T.J. Pinnavaia, *Science,* **1983**, 220, 365.

[35] A. Kadkhodayan and T.J. Pinnavaia, *J. Mol Catal,* **1983,** 21, 109.

[36] A. Blumenstein, *J. Polym. Sci.,* **1965**, 3,2653-2665.

[37] S.F. Xavier and Y. N. Sharma, *Polymer Composite,* **1986**, 7, 42.

[38] G.F. Walker, G. F. *Clay Miner. ,***1967**, 7, 129-143.

[39] W.D. Johns, P.K.S. Gupta, *Am. Mineral.,* **1967**, 52, 1706-1724.

[40] W. U. Malik, S. K. Srivastava, and D.Gupta, *Clay Miner.,* **1972**, 9, 369.

[41] G. Lagaly, S. Fitz, and A. Weiss, *Clays and Clay Miner.,* **1975**, 23, 45.

[42] W. L. Ijdo, and T.J. Pinnavaia, *J. Solid State Chem.,* **1998**, 139, 281.

[43] G. Lagaly,. *Solid State Ionics,* **1986**, 22, 43.

[44] W. L. Ijdo, and T.J.Pinnavaia, *Chem. Mater.,* **1999**, 11, 3227.

[45] R. A. Vaia, R.K. Teukolsky,and E.P. Giannelis, *Chem. Mater.,* **1994**, 6, 1017.

[46] E. Hackett, E. Manias, and E.P.Giannelis, *J. Chem. Phys.,* **1998**, 108, 7410.

[47] F. Villieras, L.J. Michot, J.M. Cases, I. Berend, F. Bardot, M. Francois, G. Gerard, and J. Yvon, J. *Static and dynamic studies of the energetic surface heterogeneity of clay minerals,* Rudzinski, W. A. S. G. Z., Ed.; Elsevier: Amsterdam, **1997**, 104, 573.

[48] J. M. Cases, I. Berend, G. Besson, M. Francois, J.P. Uriot, F. Thomas, J.E. Poirier, *Langmuir,* **1992**, 11, 2730.

[49] V. A. Drits, and C.Tchoubar, . *X-ray Diffraction by Disordered Lamellar Structures; Theory and Application to Microdivided Silicates and Carbons; Springer-Verlag:* New York, **1990**.

[50] S. H. Xu,; S.A. Boyd, *Environ. Sci. Technol.,* **1995**, 29, 3022.

[51] H. J. M. Hanley, C. D. Muzny, and B. D. Butler, *Langmuir,* **1997**, 13, 5276.

[52] A. Patzko, and I. Dekany, *Colloid Surf. A,* **1993**, 71, 299.

[53] T. Yui,; H. Yoshida, H. Tachibana, D.A. Tryk, D. H. Inoue, *Langmuir,* **2002**, 18, 891.

[54] L.-Q. Wang, J. Liu, G. J. Exarhos, K. Y. Flanigan, R. Bordia, *J. Phys. Chem. B,* **2000**, 104, 2810.

[55] D. Kubies; R. Jerome; J. Grandjean, *Langmuir,* **2002**, 18, 6159.

[56] K. Suga,; F. Rusling, *Langmuir,* **1993**, 9, 3649.

[57] A. Tahani,; M. Karroua, H.V. Damme, P. Levitz, F. Bergaya, J. Colloid Interface Sci. **1999**, 216, 242.

[58] S. H Xu, and S.A.Boyd, *Langmuir,* **1995**, 11, 2508.

[59] R.C. Reynolds, *Interstratified Clay Minerals,* Brindley, G. W., Brown, G., Eds.; Mineralgical Society: London, **1980**, 249.

[60] G. W. Brindley, *Order-Disorder in Clay Mineral Structures,* Brindley, G. W., Brown, G., Eds.; Mineralgical Society: London, **1980**, 125.

[61] R. Krishnamoorti, R. A. Vaia, and E.P. Giannelis, *Chem. Mater.,* **1996**, 8, 1728.

[62] R. A. Vaia, and E.P. Giannelis, *Macromolecules,* **1997**, 30, 8000.

[63] P. C. LeBaron, Z. Wang and T.J. Pinnavaia, *Appl. Clay Sci.,* **1999**, 15, 11.

[64] M. Alexandre, and P. Dubois, *Mater. Sci. Eng.,* **2000**, 28, 1.

[65] G. Pfirrman, G. Lagaly, and A. Weiss. *Clays and Clay Minerals,* **1973**, 21, 239.

[66] G. W. Brindley, and S.Ray, *Am. Mineral.,* **1964**, 49, 106.

[67] Y. Okahata, and A. Shimuzi, *Langmuir,* **1989**, 5, 954.

[68] W. Xie, Z. M. Gao, K. L. Liu, W. P Pan, R. Vaia, D. Hunter, A. Singh, *Thermochim. Acta.,* **2001**, 367, 339.

[69] Y. Kojima , A. Usuki , M. Kawasumi, A. Okada, Y. Fukushima, T. Karauchi T. and O. Kamigaito, *J. Mater. Res.,* **1993**, 8, 1185.

[70] Y.Kojima , K. Fukumori, A. Usuki, A. Okada and T. Karauchi, *J. Mater. Sc. Lett.,***1993**,12,889.

[71] J. Zhu , F.M. Uhl, A. B. Morgan and C.A.Wilikie, *Chem. Mater.,* **2001**, 13,4649.

[72] L. W. Carter, JG Hendricks, DS Bolley. *United States Patent No. 2,531,396,* **1950** (assigned to National Lead Co).

[73] M. Kawasumi, N. Hasegawa, M. Kato, A. Usuki., and A. Okada., *Macromolecules,* **1997**, 30, 6333.

[74] M. Alexandre, P. Dubois, T. Sun, J. M. Garces and R. Jerome , *Polymer,* **2002**, 43, 2123.

[75] Y. T. Vu, J. E. Mark , L. H. Pham, and M. Englehardt, *J. Appl. Poly. Sci.,* **2001**, 82, 1391.

[76] S. Sadhu and A.K. Bhowmick, *J. Appl. Poly. Sci.,* **2004**, 92, 698.

[77] A. Usuki, A. Tukigase and M. Kato, *Polymer,* **2002**, 43, 2185.

[78] R. Krishnamoorti and E. P. Giannelis, *Macromolecules,* **1997**, 30, 4097.

[79] N. Hasegawa, H. Okamoto, M. Kawasumi and A. Usuki, *J. of Appl. Poly. Sci.,* **1999**, 74 (14), 3359.

[80] J. Zhu and C. Wilkie, *Polymer International,* **2000**, 49 (10) 1158.

[81] A.S. Moet and A. Akelah, *Mat. Lett.,* **1993**, 18, 97.

[82] Y. Kojima, A. Usuki, M. Kawasumi, A. Okada, T. Kurauchi and O. Kamigaito, *J. Polym. Sci. Part A: Polym. Chem.,* **1993**, 31, 983.

[83] K. Yano, A Usuki, A Okada, T Karauchi and O Kamigaito, *J. Polym. Sci. Part A: Polym. Chem.,* **1993**, 31, 2493.

[84] D. C. Lee and L. W. Jang, *J Appl Polym Sci,* **1996**, 61, 1117.

[85] G. M. Whitesides, J. P. Mathias, and C. T. Seto, *Science*, **1991**, 254, 1312.

[86] T. Lan, P. D. Kaviratna, and T.J. Pinnavaia, *Chem. Mater.,* **1995**, 7, 2144.

[87] T. Lan and T. J. Pinnavaia, *Chem. Mater.,* **1994**,6, 2216.

[88] P. Hajji, L. David, J. F. Gerard, J. P. Pascault and G. Vigier. *J. Polym. Sci., Part B: Polym. Phy.,* **1999**, 37(22), 3172.

[89] J. Liu, W. J. Boo, A. Clearfield and H. J. Sue, *Materials and Manufacturing Processes,* **2006**, 21(2), 143.

[90] Y. Fukushima, A. Okada, M. Kawasumi, T. Kurauchi and O. Kamigaito, *Clay Minerals,* **1988**, 23(1), 27.

[91] D.H. Solomon and D.G. Hawthorne. *In: Chemistry of Pigments and Fillers* , Wiley, New York, **1983**, 8.

[92] E. L. Cussler, S. E. Hughes, W. J. Ward, III, and R. Aris, *J. Membr. Sci.,* **1988**, 38, 161.

[93] R. A. Vaia, K. D. Jandt, E. J. Kramer, and E. P. Giannelis, *Macromolecules,* **1995**, 28, 8080.

[94] A. Mousa and J. Krager-Kocsis, *Macromol. Mater. Eng.,* **2001**, 286,260.

[95] E. Wang , T. J Pinnavaia, *Chem. Mater.,* **1998**, 10, 3769.

[96] Y. Z Wang, L. Q. Zhang, C. H. Tang and D. S. Yu, *J. Appl.Polym.Sci,* ,**2000**, 78, 1879.

[97] P. J. Flory and R. Rehner, *J. Chem. Phys.,* 1943, 11521.

[98] Y. Konishi M Cakamk, *Polymer,* **2006**, 47, 5371.

[99] P. J. Flory, *Principles of Polymer Chemistry* , Ithaca Ny, Cornell Univ Press, **1953**.

[100] G. Tansley, *Ecology ,* **1933**, 16, 284-307.

[101] D. Stauffer and A. Aharony, *Introduction to percolation Theory,* Washington DC, Taylor and Francis **1992**.

[102] K. Miyasaka, K. Watanbe, E. Jojima, H. Aida, M. Sumita, and K. Ishikawan, *J. Mater. Sci.,* **1982**, 17, 1610.

[103] J. C. Huang, C. L. Wu, and S. J. Grossman, *J. Polym. Eng.,* **2000**,20,213.

[104] A. R. Hopkins, and J. R. Reynolds, *Macromolecules,* **2000**,33,5221.

[105] *ASTDM 2516* Carbon Black Particle Size Classification.

[106] G.R. Hamed, *Rubber Chem. Tech. ,* **2000**, 73, 524.

[107] V. M. Lobe, and J. L. White, *Polymer Engineering and Science,* **2004**, 19(9), 617.

[108] J. B. Donnet, Composite Science and Technology, 2003, 63, 1085.

[109] M. C. Lonergan, E.J. Severin, B.J. Doleman, S.A. Beaber,R.H. Grubbs, N.S. Lewis, *Chem. Mater.,* **1996**, 8(9), 2298.

[110] D. Li and G. Sun, *Dyes and Pigments,* **2007**, 72(2), 144.

[111] R. Richner, S. Miller and A. Wokaun, *Carbon ,* **2002**, 40(3), 307.

[112] C. Brosseau, *Recent Res. Dev. in Polymer Sci.* 1998, 2.

[113] A. R. Payne, *Journal of Applied Polymer Science,* **2003**, 6(19), 57.

[114] J. B. Donnet, R.C. Bansal, M. Wang, *J. Carbon Black Science and Technology,* Second ed Marcel Dekker NY **1993**

[115] J. Le Bras, and E. Papirer, *Journal of Applied Polymer Science,* **2003**, 22(20, 525.

[116] K. Lakdawala and R. Salovey, *Polym. Eng. Sci.,* **1987**, 27,1035

[117] A. B. Morgan, and J. W. Gilman, *J. of Appl Poly Sci,* **2003**, 87, 1329.

[118] X. Fu and S. Qutubuddin, *Polymer,* **2001**, 42(2),807.

[119] M. Maiti, S. Sadhu, and A. K. Bhowmick, *Journal of Appl Polymer Sc.,* **2005**, 96, 443.

[120] Z. Mencik, and A.J. Chompff, *J. Polym Sci Part B, Polym Phys.,* **1974**, 12,977.

[121] A. R. Horrocks, *Fire Retardant Materials* (Price, D.; Ed.) Woodhead, Cambridge, **2001**.

[122] J. W. Gilman, T. Kashiwagi, S. Lomakin, E. Giannelis, E. Manias, J. Lichtenhan, and P. Jones, *The Royal. Soc. Chem*: Cambridge, **1998**, 203.

[123] A. Cornelis, P. Laszlo, *NATO ASI Series, Series C:* Mathematical and Physical Sciences, **1986**, 165, 213.

[124] J. M. Thomas, J. M. Adams, S. H. Graham, and T.B. Tennakoon, *Chemical Conversion Using Sheet-Silicate Intercalates, in Solid State* Chemistry of Energy Conversion and Storage Goodenough, J. B. and Whittingham, M. S., Ed., ACS: Washington D.C. **1977**, 163, 298.

[125] J. M. Thomas, *Sheet Silicate Intercalates:* New Agents for Unusual Chemical Conversions, in Intercalation Chemistry Whittingham, M. S. and Jacobson, A. J., Ed., Academic Press: NY, **1982**, 1, 55.

[126] T. J. Pinnavaia, M. S. Tzou, and S. D. Landau, *J. Am. Chem. Soc.,* **1985**, 107, 4783.

[127] M. Lewin , and M. Endo, *Polym. Adv. Tech.,* **2001**, 12, 215.

[128] E. D. Weil, and N. G. Patel, *Polym. Degradation and Stability,* **2003**, 82, 291.

[129] P. Nawani, M. Y. Gelfer, B. S. Hsiao, A. Frenkel, J. W. Gilman and S. Khalid, *Langmuir,* **2007**, 9808.

[130] G. Beyer, *Fire and Materials,* **2001**, 25(5), 193.

[131] G. Beyer, *Fire and Materials,* **2005**, 29, 61.

[132] S. Peeterbroeck, et al., *Compos. Sci. Technol.* **2004**, 64, 2317.

[133] P. Nawani, P. Desai, M. Lundwall, M. Y. Gelfer, B. S. Hsiao, M. Rafailovich, A. Frenkel, A. H. Tsou, J. W. Gilman and S. Khalid. *Polymer*, **2007**, 48(3), 827.

[134] M. Y. Gelfer, C. Burger, B. Chu, B. S. Hsiao, A. D. Drozdov, M. Si, M. Rafailovich, B. B. Sauer, and J. W. Gilman, *Macromolecules,* **2005**, 38(9), 3765.

[135] G. Galgali, S. Agarwal, and A. Lele *Polymer*, **2004**, 45(17), 6059.

[136] A. Bafna, G Beaucage, F. Mirabella, and S. Mehta, *Polymer,* **2003**, 44(40), 1103.

[137] K. Hongladarom, V. M. Ugaz, D. K. Cinader, W. R. Burghardt, J. P. Quintana, B. S. Hsiao, M. D. Dadmun, W. A. Hamilton and P. D. Butler, *Macromolecules*, **1996**, 29 (16), 5346.

[138] M.D. Dadmun, and C. C. Han, *Macromolecules,* **1994**, 27, 7522.

[139] M. M. Malwitz, S. Lin-Gibson, E. K. Hobbie, P. D. Butler, and G. Schmidt, *Journal of Polymer Science Part B,* **2003**, 41(24), 3237.

[140] J. Lee, T. Takekoshi and E. P. Giannelis, *Mat. Res. Soc. Symp. Proc.,* **1997**, 457, 513.

[141] Z. Wang, J. Massam, and T. J. Pinnavaia, *Epoxy-Clay Nanocomposites,* in Pinnavaia, T. J. and Beall, G. W. (eds.), Polymer-Clay Nanocomposites. John Wiley and Sons, Ltd., New York: **2000**, 127.

[142] G. Beson, C. T. Mitsud and J. Mering, *Clays and Clay Miner.,* **1974**, 22, 379.

[143] M. A. Osman, and U. W. Suter, *Journal of Colloid and Interface Science,* **2000**,224, 112.

[144] M. A. Osman, C. Moor, W. R. Caseri, and U. W. Suter, *Journal of Colloid and Interface Science,* **1999**, 209, 232.

[145] M. A. Osman, and U. W. Suter, *Journal of Colloid and Interface Science,* **1999**,214, 400.

[146] L. Perez-Rodriguez, A. Weiss and G. Lagaly, *Clay Miner.,* **1977**, 25, 243.

[147] M. Ogawa, K. Kuroda and C. Kato, *Chem. Lett.* **1989**, 1659.

[148] W. F. Jaynes, and S. A. Boyd, *Soil Science Society of America Journal,* **1991**, 55(1), 43.

[149] Z. Wang and T. J. Pinnavaia, *Chem. Mater.,* **1998**, 10, 1820.

[150] X. Kornmann, L. A. Berglund, J. Sterte and E. P. Giannelis, *Polym. Eng. Sci.,* **1998**, 38 (8), 1351.

[151] P. Chu, F. G. Dwyer, and J. C. Vartuli, *U. S. Patent, 4778666*, **1988**.

[152] B. L. Newalkar and S.Komarneni, *Chem. Mater.,* **2001**, 13 (12), 4573.

[153] C. G. Wu and T. Bein, *Chem. Commun.,* **1996**, 925.

[154] C. S. Gundy, R.J. Plaisted,and J.P. Zhao, *Chem. Commun.,* **1998**, 1465.

[155] J. Berlam, *Radiat Phys Chem,* **1995**, 45, 501.

[156] J. Zhu, O. Polchik, S. Chen and A. Gedanken, *J. Phys. Chem. B,* **2000**, 104(31), 7344..

[157] L. Liu, Z. Qi and X. Zhu. *Journal of Applied Polymer Science*, **1999**, 71(7), 1133.

[158] D. Porter, E. Metcalfe and M. J. K. Thomas, *Fire Mater.,* **2000**, 24.

[159] M. Zanetti, and L. Costa, *Polymer,* **2004**, 45, 4367.

[160] L. E. Nielsen, *Journal of Macromolecular Science,* **1967**, A1, 929.

[161] A. A. Gusev, and H. R. Lusti, *Advanced Materials*, **2001**, 13, 1641.

[162] R. Aris, *Archive for Rational Mechanics and Analysis,* **1986**, 95, 83.

[163] G. H. Fredrickson, and J. Bicerano, *Journal of Chemical Physics,* **1999**, 110, 2181.

[164] M. Y. Gelfer, A. Waddon, K. Schmidt-Rohr, R. Gale, L. Kleiner, and R. Berggren, *Journal of Polymer Science Part B: Polymer Physics,* **2001**, 39 (22), 2774.

[165] D. J. Brennnan, A. P. Haag, J. E. White and C. N. Brown, *Macromolecules*, **1998**, 31, 2622.

[166] K. Takaya, C. Itoh, and Y. Uunno, *Journal of Polymer Science: Part A: Polymer Chemistry,* **1998**, 36, 889.

[167] G. J. Fredrickson and J. Bicerano, *J. Chem. Phys.,* **1999**, 110, 2181.

[168] E. L. Cussler, S. E. Hughes, W. J. Ward, III, and R. Aris, *J. Membr. Sci.,* **1988**, 38, 161.

[169] M. A. Osman, V. Mittal, and H. R. Lusti, *Macromol. Rapid Commun,* **2004**, 25,1145.

[170] M. A. Osman, V. Mittal, M. Morbidelli, and U. W. Suter, *Macromolecules*, **2003**, 36 9851.

[171] G. J. Fredrickson and J. Bicerano, *J. Chem. Phys.,* **1999**, 110, 2181.

[172] A. Gusev and H. R. Lusti, *Adv. Mater.,* **2001**, 13, 1641.

[173] Koros, W. J. and G. K. Fleming, *J. of Membr. Sci,* **1993**, 83, 1.

[174] M. Kay, A. F. Price and I. Lavery, *J. Fire Retard. Chem.,* **1979**, 6, 69.

[175] C. E. Anderson Jr, J. Dziuk Jr, W. A. Mallow and J. Buckmaster, *J. Fire Sci.,* **1985**, 3, 151

[176] D. E. Cagliostro, S. R. Riccitiello, K. J. Clark and A. B. Shimizu, *J. Fire Flamm.,* **1975**, 6, 205

[177] R. Delobel, M. Le Bras, N. Quassou and F. Alistigsa, *J. Fire Sci.,* **1990**, 8, 85.

[178] R. Delobel, M. Le Bras, N. Quassou and R. Descressain, *Polym. Degrad. Stab.,* **1990**, 30, 41

[179] G. Camino, L. Costa and L. Trossarelli, *Polym. Degrad. Stab.,* **1984**, 7, 25.

[180] R. D. Davis, J. W. Gilman, T. E. Sutto, J. H. Callahan, P. C. Trulove, De Long, and C. Hugh, *Clays and Clay Minerals,* **2004**, 52(2), 171.

[181] A. R. Horrocks, M. Tunc, and D. Price, *Textile Progress,* **1989**, 18(1-3) 1.

[182] K. Yasue, S. Katahira, M. Yoshikawa, and K. Fujimoto, *Polymer-Clay Nanocomposites.* John Wiley and Sons, Ltd., New York: **2000**, 111.

[183] M. Y.Gelfer, C. Burger, P. Nawani, B. S. Hsiao, B. Chu, M. Si, M. Rafailovich, G. Panek, G. Jeschke, A. Fadeev, Y. Alexander, and J. W. Gilman, *Clays and Clay Minerals*, **2007**, 55(2), 140.